Theory and modelling of energy transport in quantum nanostructures

Amir Fruchtman

Linacre College

University of Oxford

A thesis submitted for the degree of

Doctor of Philosophy

Trinity 2016

To my late father,

Moshe Fruchtman

(1951-1996)

Abstract

Theory and modelling of energy transport in quantum nanostructures

Amir Fruchtman

Linacre College
University of Oxford

A thesis submitted for the degree of
Doctor of Philosophy
Trinity term 2016

This thesis is concerned with quantum properties of excitonic energy transport in nanostructures that are embedded in a noisy environment. Of principal interests are ways to exploit this environment to facilitate the transport of energetic excitations.

The first research chapter deals with an extension to the 'standard' open quantum system picture, where the Hilbert space is split into three: system, environment, and a wider universe. This division is natural for many biological and artificial nanostructures. A new analytical method, based on a phase space representation of the density matrix, is developed for studying such division. The effects of the wider universe are shown to be captured by a simple correction of the environmental response function.

The second research chapter addresses the question: when do second-order perturbative approaches to open quantum systems, which are intuitive and simple to compute, provide adequate accuracy? A simple analytical criterion is developed, and its validity is verified for the case of the much-studied FMO dynamics as well as the canonical spin-boson model.

In the third research chapter, an intuitive model of a photocell is studied. The model comprises two light-absorbing molecules coupled to an idealised reaction centre, showing asymmetric dimers are capable of providing a significant enhancement of light-to-current conversion under ambient conditions. This is done by 'parking' the energy of an absorbed photon in a dark state which neither absorbs nor emits light.

In the final research chapter, a basic model for what can be thought as a "quantum brachistochrone" problem is investigated. Exotic energy configurations are found to yield considerable enhancement to the exciton's transfer probability, due to similar mechanisms studied in the previous chapter.

Acknowledgements

I have had the pleasure of many stimulating discussions over the last few years, and I feel privileged to have worked with so many talented individuals.

First, I would like to thank my group members and Leverhulme colleagues (in alphabetical order): Andrea Rocchetto, Elinor Irish, Felix Pollock, George Knee, Joe O'Gorman, Kieran Higgins, Naomi Nickerson, Stefan Zohren, and Ying Li.

I would also want to thank my research collaborators Neill Lambert, Rafael Gmez-Bombarelli, and especially Brendon Lovett.

Most of all I thank my supervisors, Simon Benjamin and Erik Gauger, for their advice and guidance, and for inspiring me with ideas and insights.

Finally, I thank my wife Michal, for her support, partnership and help during these years in Oxford, while pursuing her own doctorate.

Publication List

This thesis is based, in part, on the following publications:

1. A. Fruchtman, B. W. Lovett, S. C. Benjamin, and E. M. Gauger, "Quantum dynamics in a tiered non-Markovian environment," *New Journal of Physics*, vol. 17, p. 023063, feb 2015.

2. A. Fruchtman, N. Lambert, and E. M. Gauger, "When do perturbative approaches accurately capture the dynamics of complex quantum systems?," *Scientific Reports*, vol. 6, p. 28204, jun 2016.

3. A. Fruchtman, R. Gómez-Bombarelli, B. W. Lovett, and E. M. Gauger, "Photocell optimization using dark state protection," *Physical Review Letters*, vol 117, p. 203603, nov 2016.

Contents

Chapter 1

Introduction

Many technological advances come from our ability to manipulate and control matter at increasingly smaller scales. Examples include the latest computer processors manufactured with an accuracy of several nanometers, 2D materials such as carbon nanotubes and graphene, and cutting edge experiments demonstrating accurate control of individual atoms leading towards building a quantum computer. We are at the stage where advances must be accompanied by quantum engineering, taking into account properties like superposition, uncertainty, and entanglement.

The early formulation of quantum mechanics by Schrödinger, Heisenberg, Dirac, and many others, considered systems which are completely isolated from their environment. However in reality, it is formidably difficult to completely suppress environmental effects. This offers a challenge, but also an opportunity to incorporate these effects into the design of new technologies. This is because an isolated system, according to quantum theory, evolves unitarily, *i.e.* has reversible dynamics. With the inclusion of an environment, unidirectional processes emerge. This way it is possible for a noisy environment to direct the system into a desired state. One of the goals of this Thesis is to better understand and utilise environmental noise that resides in every system, in the context of energy transport.

A prime example where energy transport is important is photosynthesis. When light is absorbed in a photosynthetic apparatus, it excites electronic states of the underlying molecular aggregate, where the resulting excitations are called excitons.

These excitons are then shuttled, in a very efficient manner, to the reaction centre where they undergo charge separation to produce energy. Recent experiments indicated that the transfer is done in a wave-like manner, which is most likely as a result of a quantum phenomena. Inspired by natural photosynthesis, new possibilities for engineering enhanced light absorption devices arise. These have the potential to improve a wide range of technologies from solar cells to cameras and scientific instruments.

The first chapter of this Thesis starts with a general introduction to open quantum systems. It serves as a brief introduction to the concepts, and to the notation employed. This is followed by a description of a model for energy transport in the presence of an environment, and a review of some mathematical techniques that are used in later chapters. Next, four original research chapters are presented. The first two are focused on better understanding, and further developing, the mathematical techniques used to study the evolution of open quantum systems, while the last two are concerned with optimising energy transport in realistic and simplistic models.

Chapter 2 is the first research chapter. It introduces a new analytical method for studying the open quantum systems problem of a discrete system weakly coupled to a tiered environment. This chapter is based on Ref. [1].

Chapter 3 addresses the question: when do more intuitive and simpler-to-compute second-order perturbative approaches provide reliable results? These approaches include the familiar time-convolutionless (TCL) expansion, and the method introduced in Chapter 2. A simple analytical criterion to test if a system lies in the perturbative regime is developed and verified. This chapter is based on Ref. [2].

The Thesis proceeds by studying two related models for energy transport. Starting in Chapter 4, which studies a model photocell comprised of two different light-absorbing molecules coupled to an idealised reaction centre. It shows that some pairs of molecules exhibit a 'dark state', which neither absorbs nor emits light, due to interference effects arising from dipole-dipole interactions. Having a dark state provides a significant enhancement of light-to-current conversion under ambient conditions. This

chapter is based on Ref. [3], which also provides additional calculations performed by a theoretical chemistry collaborator showing how to find such pairs in practice.

Chapter 5 studies a basic model for a problem which could be called the "quantum brachistochrone" problem. This model is based on the model presented in Chapter 4, but instead of two different molecules we now have a chain of many. A similar 'dark state' mechanism provides enhancement of light-to-current conversion in this case as well. Chapter 6 concludes the Thesis and provides a future outlook.

1.1 Basic Concepts in Open quantum systems

In this section we introduce some basic concepts and definitions in the theory of open quantum systems. This includes the density operator which is a generalisation of the quantum state vector for an open system with uncertainties. We discuss the physically allowed evolution of the density operator, introducing completely-positive maps and the dynamical semi-group, and show how the Lindblad master equation is naturally derived from these general concepts. We also discuss the interaction picture which is the starting point of many perturbative master equation derivations, discussed later in section 1.3. These are basic ideas that are introduced in standard textbooks such as Ref. [4].

1.1.1 The Density Operator

In a perfectly isolated system, a quantum system's state can be described by a vector $|\psi\rangle$ in a complex Hilbert space $\mathscr{H}$. $|\psi\rangle$ contains all the information about the system, that is the expectation values of any physical observable – represented by Hermitian operators on $\mathscr{H}$. The dynamics of the state is determined by its Hamiltonian $\mathcal{H}$, through the Schrödinger equation

$$\mathrm{i}\hbar\frac{\partial}{\partial t}|\psi\rangle = \mathcal{H}|\psi\rangle \ . \tag{1.1}$$

The solution of this equation is given by $|\psi(t)\rangle = U(t,t_0)|\psi(t_0)\rangle$, where $U(t,t_0)$ is the time-evolution operator, which is unitary[§]. The expectation-value, or quantum-

[§]If the Hamiltonian is constant in time, then $U(t,t_0) = e^{-\mathrm{i}\mathcal{H}(t-t_0)}$.

mechanical average of any operator A is given by

$$\langle A \rangle = \langle \psi | \, A \, | \psi \rangle \ . \tag{1.2}$$

In a real-life experiment, it might not be possible to describe the system of interest using a state vector alone. This could happen for two reasons. First, the system might be a part of a larger system – for example, think of two spins, each of them can be in the "up" ($|\uparrow\rangle$) or "down" ($|\downarrow\rangle$) state. The state vector of these two spins can be written as

$$a_1 \, |\uparrow\rangle_1 \, |\uparrow\rangle_2 + a_2 \, |\uparrow\rangle_1 \, |\downarrow\rangle_2 + a_3 \, |\downarrow\rangle_1 \, |\uparrow\rangle_2 + a_4 \, |\downarrow\rangle_1 \, |\downarrow\rangle_2 \ , \tag{1.3}$$

where a_n are some complex amplitudes satisfying $\sum_n |a_n|^2 = 1$, and $|\bullet\rangle_k$ is the k^{th} spin's state. Say we are interested only in the first spin, we cannot in general express its state using a state vector alone.

The second reason is a classical one: perhaps one might not know exactly which state the system is in, but one may have some (classical) statistical knowledge of it. Let us assume a case where according to our subjective knowledge, the system is in state $|\psi_n\rangle$ with probability p_n. How can we incorporate this knowledge into the state vector?

In 1927, the great physicists John von Neumann[5] and Lev Landau[6] independently found that one can use a matrix to represent the knowledge (or lack thereof) of a state of a system, even when it is a part of a larger system. This is known as the *density matrix*, which is defined as the average of the projector onto the state of the system:

$$\rho \equiv \left\langle \, |\psi\rangle \, \langle\psi| \, \right\rangle_{\mathrm{avg}} \ . \tag{1.4}$$

The average in the above equation is not the standard expectation value, but instead it is both a statistical average over our knowledge of the system[7,8], and a partial trace, as explained below, in the case where the system is not isolated. The density matrix allows us to calculate any expectation value of a system's operator,

using the trace operator

$$\langle A \rangle = \mathrm{Tr}\{A\rho\} \ . \tag{1.5}$$

Below we explain why the above formula holds. In the first case, assume we have some statistical knowledge of the system, *i.e.* that the system is in state $|\psi_n\rangle$ with probability p_n. This is known as a *proper mixture*. The expectation value of any operator A is the average expectation value over the different possible states, *i.e.*

$$\langle A \rangle = \sum_n p_n \langle A \rangle_n = \sum_n p_n \langle \psi_n | A | \psi_n \rangle \ . \tag{1.6}$$

In density matrix language, the density matrix is given by

$$\rho = \sum_n p_n |\psi_n\rangle \langle \psi_n| \ . \tag{1.7}$$

The trace operation yields exactly the expectation value

$$\mathrm{Tr}\{A\rho\} = \mathrm{Tr}\{A \sum_n p_n |\psi_n\rangle \langle \psi_n|\} = \sum_n p_n \mathrm{Tr}\{A |\psi_n\rangle \langle \psi_n|\} \tag{1.8}$$

$$= \sum_n p_n \sum_k \langle k| A |\psi_n\rangle \langle \psi_n | k\rangle \tag{1.9}$$

$$= \sum_n p_n \sum_k \langle \psi_n | k\rangle \langle k| A |\psi_n\rangle \tag{1.10}$$

$$= \sum_n p_n \langle \psi_n | A |\psi_n\rangle = \langle A \rangle \,, \tag{1.11}$$

where $\{|k\rangle\}$ are some orthonormal basis vectors. An alternative but equivalent picture to uncertainty of the state of the system, is that we can think of an ensemble of identical systems, with p_n being the portion of the ensemble in state $|\psi_n\rangle$, and the average is an ensemble average.

Now let us examine the case where the system is not isolated: say we have two systems S and E, with Hilbert spaces $\mathscr{H}_S$ and $\mathscr{H}_E$, respectively. The Hilbert space of the joint system $\mathscr{H}_S \otimes \mathscr{H}_E$ is spanned by $|s_k\rangle |e_j\rangle$, where $|s_k\rangle$ are in $\mathscr{H}_S$, and $|e_j\rangle$ are in $\mathscr{H}_E$. Moreover we assume we are not interested in the state of the entire system, but only on the state of S. This is known as an *improper mixture*.

We denote the density matrix of the joint system by W. The expectation value of any operator A is then given by

$$\langle A \rangle = \mathrm{Tr}\{AW\} \ , \tag{1.12}$$

and in particular, if the operator A acts on system S, we have

$$\begin{aligned}
\langle A \rangle = \mathrm{Tr}\{AW\} &= \sum_{k,j} \langle s_k | \langle e_j | AW | s_k \rangle | e_j \rangle & (1.13)\\
&= \sum_{k} \langle s_k | A \underbrace{\left(\sum_{j} \langle e_j | W | e_j \rangle \right)}_{=\rho_S} | s_k \rangle & (1.14)\\
&= \sum_{k} \langle s_k | A\rho_S | s_k \rangle & (1.15)\\
&= \mathrm{Tr}\{A\rho_S\} \ , & (1.16)
\end{aligned}$$

where $\rho_S = \sum_j \langle e_j | W | e_j \rangle$ is known as the *reduced density matrix* for system S, which is given by the *partial trace* of the full density matrix over system E's degrees of freedom. Thus the reduced density matrix contains all the information needed to calculate any expectation value of an operator that works on system S, using the trace operation.

Quite different forms of knowledge about a physical system can lead to the same density matrix. As an example, think of a spin system which can be in state $|\uparrow\rangle$ or $|\downarrow\rangle$ (or any linear combination of them). The density matrix of a system that was prepared in state $|\downarrow\rangle$ with 50% probability, and in state $|\uparrow\rangle$ with 50% probability, will be exactly the same as the reduced density matrix of a spin system which is a part of a two-spin system prepared at the state $(|\uparrow\rangle|\uparrow\rangle + |\downarrow\rangle|\downarrow\rangle)/\sqrt{2}$, and also the same as a density matrix of a spin system that we have no prior knowledge about!

Given that the density matrix is an average of a projector (Eqn. 1.4), several properties follow immediately:

- $\rho^\dagger = \rho$ (Hermitian).
- $0 \leq \lambda_k \leq 1$, where λ_k are the eigenvalues of ρ. This is because the eigenvalues of a projection operator are either 0 or 1.

- $\mathrm{Tr}\{\rho\} = 1$, because the expectation value of the identity is 1.
- $\mathrm{Tr}\{\rho^2\} \leq 1$, which follows directly from the previous two points. This is known as the *purity* of the state. The equality occurs when the density matrix can be written as $\rho = |\psi\rangle\langle\psi|$ for some state $|\psi\rangle$, which is known as a *pure state*. Note that it is possible to have a pure state for a reduced density matrix, while the full density matrix (*i.e.* before the partial trace) is not in a pure state[§].

Now we examine the time evolution of the density matrix. For the case where the system is isolated, instead of the Schrödinger equation for the state vector, we have the von Neumann equation for the density matrix

$$\mathrm{i}\hbar\frac{\partial}{\partial t}\rho = [\mathcal{H}, \rho] \ . \tag{1.17}$$

This follows directly from the Schrödinger equation and Eqn. (1.7). The solution to this equation is

$$\rho(t) = U(t, t_0)\rho(t_0)U^\dagger(t, t_0) \ . \tag{1.18}$$

Throughout this Thesis we refer to the diagonal elements of the density matrix in the system's Hamiltonian eigenbasis as *populations*, and the off-diagonal elements as *coherences*. The populations remain static under unitary evolution[§§], while the coherences oscillate according to

$$\langle i|\,\rho(t)\,|j\rangle = e^{-\mathrm{i}\Delta_{ij}(t-t_0)}\,\langle i|\,\rho(t_0)\,|j\rangle \ , \tag{1.19}$$

where $\Delta_{ij} = (\lambda_i - \lambda_j)/\hbar$ is the transition frequency between the two eigenstates. Sometimes in the literature there is a confusion about the definition of coherences and populations, and the position basis is used instead of the eigenbasis.

The equivalent of the von Neumann equation for the reduced density matrix is known as a master equation. In general finding a solution for a master equation is as involved as solving the von Neumann equation for the whole system, but there are several tricks and approximations that can be made in order to simplify them. This is the subject of the next sections, and two research chapters in this Thesis.

[§]This is when the density matrix can be factorised into $\rho = \rho_S \otimes \rho_E$, with ρ_S a pure state of S, and ρ_E a non-pure state of E.

[§§]That is the evolution of the system alone, without an interaction with a wider environment.

1.1.2 CP maps and the Dynamical semi-group

A density matrix of a closed system must always have unitary evolution (Eqn. 1.18). For a reduced density matrix, the evolution map $\rho_S(t) \mapsto \Phi(t,0)\rho_S(0)$ must take density matrices to density matrices (i.e positive, Hermitian and have unit trace). An important subclass of such transformations are linear and completely-positive (CP) maps. Linear means that $\Phi(t,0)(\lambda\rho_1+(1-\lambda)\rho_2) = \lambda\Phi(t,0)\rho_1+(1-\lambda)\Phi(t,0)\rho_2$, while CP means that even if the system is a subset of a larger system, the map will yield a physical density matrix. Mathematically it means that if Φ operates on the Hilbert space $\mathscr{H}_A$, and $W = \sum_n A_n \otimes B_n$ is a density matrix in the Hilbert space $\mathscr{H}_A \otimes \mathscr{H}_B$, so is $\Big(\Phi(t,0)\otimes \mathbb{1}\Big)W = \sum_n \Big(\Phi(t,0)A_n\Big)\otimes B_n$, for any size of $\mathscr{H}_B$. A standard counter-example for CP is that of a transpose: Take a density matrix of a spin system. The map $|\uparrow\rangle\langle\downarrow| \leftrightarrow |\downarrow\rangle\langle\uparrow|$ is a valid map when thinking of an isolated system, but applying it to one spin of the density matrix $(|\downarrow\rangle|\downarrow\rangle + |\uparrow\rangle|\uparrow\rangle)(\langle\downarrow|\langle\downarrow| + \langle\uparrow|\langle\uparrow|)/2$ results in a non-physical density matrix (which has a negative eigenvalue).

The most general linear CP map form is due to Kraus[9,10], and given by

$$\Phi(t,t_0)\rho(t_0) = \rho(t) = \sum_n K_n \rho(t_0) K_n^\dagger \ , \tag{1.20}$$

where K_n are called *Kraus operators*, which satisfy $\sum_n K_n^\dagger K_n = \mathbb{1}$, and are a function of t_0 and t. From this Kraus map, we can derive the corresponding generator of the map $\mathcal{L}$, defined by $\frac{\partial}{\partial t}\rho(t) = \mathcal{L}(t)\rho(t)$. First, for a small enough dt, we assume we can expand $\Phi(t+dt,t) \approx \mathbb{1} + \mathcal{L}(t)dt$. If $K_n = K_n(t+dt,t)$ are the Kraus operators mapping from $t \mapsto t+dt$, then one[§] of them (say K_0) is close to the identity (up to a dt correction), while all the others are proportional to $\sqrt{dt}$. That is $K_0(t+dt,t) \approx \mathbb{1} - (A_0 + \mathrm{i}H)dt$, and $K_{n>0}(t+dt,t) \approx A_n\sqrt{\gamma_n dt}$, with H and A_0 Hermitian, and $\gamma_n > 0$. Thus we get

$$\Phi(t+dt,t)\rho = \rho - (A_0+\mathrm{i}H)\rho dt - \rho(A_0 - \mathrm{i}H)dt + \sum_{n>0} A_n\rho A_n^\dagger \gamma_n dt + O(dt^2) \ . \tag{1.21}$$

[§]It could be that several operators are finite for $dt \to 0$, summing up to unity. The generalisation to this case is trivial and gives the same results up to a different summation index.

Now we make use of $\sum_n K_n^\dagger K_n = \mathbb{1}$ to find that $A_0 = \frac{1}{2}\sum_{n>0}\gamma_n A_n^\dagger A_n$, and conclude that

$$\frac{\partial}{\partial t}\rho(t) = \mathcal{L}\rho(t) \tag{1.22}$$

$$= -\,\mathrm{i}[H(t),\rho(t)] + \sum_{n>0}\gamma_n(t)\left(A_n(t)\rho(t)A_n^\dagger(t) - \frac{1}{2}A_n^\dagger(t)A_n(t)\rho(t) - \frac{1}{2}\rho(t)A_n^\dagger(t)A_n(t)\right). \tag{1.23}$$

This is known as the *Lindblad master equation*[§]. The operators A_n are known as *Lindblad operators*, and γ_k are referred to as rates, both in general are time-dependent, as the Kraus operators $K_n(t+dt,t)$ are time-dependent. Any completely positive evolution can be represented in this general form. The first line in Eqn. (1.23) generates unitary dynamics, while the second line is known as the *dissipator* and introduces irreversibility.

If the generator $\mathcal{L}$ in the Lindblad equation is constant in time, *i.e.* all the Lindblad operators A_n, rates γ_n, and unitary H are constant, then the time evolution map takes the form

$$\Phi(t,0) = e^{\mathcal{L}t}\ , \tag{1.24}$$

which creates a *dynamical semi-group* with the property

$$\Phi(t,0)\Phi(s,0) = \Phi(t+s,0)\ . \tag{1.25}$$

It has been proven by Gorini, Kossakowski, and Sudarshan in 1976[11] that Eqn. (1.23) with a constant generator $\mathcal{L}$ is the most general form of a quantum-dynamical semi-group for a linear CP evolution, in the case of a finite Hilbert space. At the same time Linblad[12] has proven the same thing (also) for an infinite dimensional Hilbert space.

Physically, having a dynamical semi-group for the evolution of a system means that the dynamics are *Markovian*, that is, there is no concept of a memory of the map,

[§]Using the same procedure one can derive the *adjoint master equation*, corresponding to the evolution of the Heisenberg operator $X_H(t)$ defined by $Tr\{X\rho(t)\} = Tr\{X_H(t)\rho(t_0)\}$. This gives $X_H(t) = \sum_n K_n^\dagger X K_n$ and $\frac{\partial}{\partial t}X_H = +\mathrm{i}[H,X_H] + \sum_{n>0}\gamma_n\left(A_n^\dagger X_H A_n - \frac{1}{2}A_n^\dagger A_n X_H - \frac{1}{2}X_H A_n^\dagger A_n\right)$.

and the evolution of future times depends only on the current state of the system, and not its history. For this reason Eqn. (1.23) with a constant generator is also known as the *Markovian master equation*.

Suppose we have two systems S and E, where the system S and environment E are statistically independent at initial time, *i.e.* the initial density matrix at time $t = 0$ is $W(0) = \rho_S(0) \otimes \rho_E(0)$. It is fairly simple to show that the time evolution of the reduced matrix $\rho_S(t)$ will be a Kraus map (Eqn. 1.20) and hence CP. The key is that the evolution of the combined system-environment is unitary with propagator $U(t, t')$. We use the spectral decomposition of the density matrix ρ_E of the environment, $\rho_E(0) = \sum_i \lambda_i |\phi_i\rangle \langle\phi_i|$, where $|\phi_i\rangle$ form an orthonormal basis in the Hilbert space of E, and get

$$\rho_S(t) = \mathrm{Tr}_E \left[U(t,0)\rho_S(0) \otimes \rho_E(0)U^\dagger(t,0)\right] \tag{1.26}$$

$$= \sum_{i,j} \langle\phi_i| U(t,0) |\phi_j\rangle \langle\phi_j| \rho_S(0) \otimes \rho_E(0)U^\dagger(t,0) |\phi_i\rangle \tag{1.27}$$

$$= \sum_{i,j} \lambda_j \langle\phi_i| U(t,0) |\phi_j\rangle \rho_S(0) \langle\phi_j| U^\dagger(t,0) |\phi_i\rangle \tag{1.28}$$

$$= \sum_{i,j} K_{ij}\rho_S(0)K_{ij}^\dagger \ , \tag{1.29}$$

where in the last step we identified $K_{ij} = \sqrt{\lambda_j} \langle\phi_i| U(t,0) |\phi_j\rangle$ as the Kraus operators. Note that $0 \leq \lambda_j \leq 1$ and $\sum_j \lambda_j = 1$, which makes $\sum_{i,j} K_{ij}^\dagger K_{ij} = \mathbb{1}$. Interestingly, if the initial state of the full system cannot be written in a factorised form, *i.e.* there are some correlations between the S and E, then the evolution of the reduced matrix ρ_S is not guaranteed to be positive[13,14] or even linear[15].

1.1.3 Schrödinger, Heisenberg, and interaction pictures

In the Schrödinger picture the time dependence of the density matrix $\rho(t)$ is governed by the von Neumann equation (1.17). An equivalent description of the system is obtained by transferring the time dependence from the density matrix to the operators in the Hilbert space $\mathscr{H}$, which is known as the Heisenberg picture. In this picture the density matrix ρ_H remains constant, while the operators evolve in time. Here and in

the following Heisenberg picture operators are indicated by a subscript H. Crucially, the expectation values of the observables are the same in both pictures,

$$\langle A(t)\rangle = tr\{A\rho(t)\} = tr\{A_H(t)\rho_H(t)\} \ . \tag{1.30}$$

For a closed system, given the evolution (1.18), this means that the evolution of a Heisenberg operator $A_H(t)$ is given by

$$A_H(t) = U^\dagger(t,t_0)AU(t,t_0) \ . \tag{1.31}$$

The Schrödinger and Heisenberg pictures are two limiting cases of a more general picture, which is called the interaction picture. Let us write the Hamiltonian of the system as a sum of two parts

$$\mathcal{H} = \mathcal{H}_0 + \eta\mathcal{H}_I \ . \tag{1.32}$$

The precise choice of the splitting can be arbitrary, and the constant η will be used later to define the parameter of perturbation in the perturbative treatment, but for now it should be simply viewed as a constant. Again, the evolution operator of the system is $U(t,t_0)$, but now we define two extra evolution operators: $U_0(t,t_0)$, which is the evolution operator we get by setting $\mathcal{H} = \mathcal{H}_0$, and $U_I(t,t_0)$ defined by $U_I(t,t_0) = U_0^\dagger(t,t_0)U(t,t_0)$.

This defines the interaction picture density matrix $\rho_I(t)$ and operator $A_I(t)$ as

$$\rho_I(t) = U_I(t,t_0)\rho(t_0)U_I^\dagger(t,t_0) \ , \tag{1.33}$$

$$A_I(t) = U_0^\dagger(t,t_0)AU_0(t,t_0) \ . \tag{1.34}$$

If we choose a splitting $\eta\mathcal{H}_I = 0$ and $\mathcal{H}_0 = \mathcal{H}$, we get the Heisenberg picture. On the other hand if $\eta\mathcal{H}_I = \mathcal{H}$ and $\mathcal{H}_0 = 0$ then we get the Schrödinger picture. Thus the interaction picture interpolates between the two.

In the interaction picture, the von Neumann equation takes the form

$$\frac{\partial}{\partial t}\rho_I(t) = -\mathrm{i}\eta[\tilde{\mathcal{H}}_I(t),\rho_I(t)] = \eta\mathcal{L}(t)\rho_I(t) \ , \tag{1.35}$$

where $\tilde{\mathcal{H}}_I(t) = U_0^\dagger(t,t_0)\mathcal{H}_I(t)U_0(t,t_0)$ is $\mathcal{H}_I$ in the interaction picture, and we have defined the Liouville super-operator $\mathcal{L}(t)\square = -\mathrm{i}\mathcal{H}_I^\times(t)\square = -\mathrm{i}[\mathcal{H}_I(t),\square]$.

The above is frequently useful as a starting point for perturbative approaches, discussed in section 1.3.

1.1.4 P-representation

In this section we describe the *P-representation* or *coherent state representation*, which is a phase-space method to represent the density operator of a harmonic oscillator as an analytical function, instead of an infinite matrix. The coherent state is defined as the eigenstate of the annihilation operator a, that is

$$a\,|\alpha\rangle = \alpha\,|\alpha\rangle \quad . \tag{1.36}$$

Because a is not Hermitian, its eigenvalues can be (and in fact are) complex[§]. It is easy to show that the only solution to (1.36) which also satisfies $\langle\alpha|\alpha\rangle = 1$ is (up to a phase)

$$|\alpha\rangle = e^{-|\alpha|^2/2}\sum_{n=0}^{\infty}\frac{\alpha^n}{\sqrt{n!}}\,|n\rangle \tag{1.37}$$

$$= e^{-|\alpha|^2/2}e^{\alpha a^\dagger}\,|0\rangle \tag{1.38}$$

$$= e^{\alpha a^\dagger - \alpha^* a}\,|0\rangle \quad . \tag{1.39}$$

The number α can be any complex number, and in the last equality we used the Baker-Campbell-Hausdorff formula which states that for any two operators A and B such that $[A,B]$ commutes with both of them, one can write $e^{A+B} = e^Ae^Be^{-\frac{1}{2}[A,B]}$[§§] Some important properties of the coherent states are:

- The coherent states are not orthogonal, and have the scalar product $\langle\alpha|\beta\rangle = e^{\alpha^*\beta - \frac{1}{2}|\alpha|^2 - \frac{1}{2}|\beta|^2}$, which means the overlap between two states exponentially decays as $\left|\,\langle\alpha|\beta\rangle\,\right|^2 = e^{-|\alpha-\beta|^2}$.

[§]In fact there is no guarantee that there exists an eigenstate to a non-Hermitian operator, and indeed simple algebra shows that there is no eigenstate to the raising operator $a^\dagger$.

[§§]More precisely, this is the dual of the Baker-Campbell-Hausdorff formula, known as the Zassenhaus Formula, which gives a decomposition $e^{A+B} = e^Ae^B\prod_{n=2}^{\infty}e^{C_n(A,B)}$ which for this case terminates at $n = 2$.

- The closure formula:

$$\frac{1}{\pi}\int d^2\alpha\,|\alpha\rangle\langle\alpha| = \mathbb{1}\,, \tag{1.40}$$

  where $d^2\alpha = d\mathrm{Re}\{\alpha\}d\mathrm{Im}\{\alpha\}$.

- Over-completeness: Since the coherent states are not orthogonal, we call them *overcomplete*. In fact, any convergent sequence of complex numbers α_n forms a complete basis $\{|\alpha_n\rangle\}$.[16]

- $a\,|\alpha\rangle = \alpha\,|\alpha\rangle$, $\quad a^\dagger\,|\alpha\rangle = (\frac{1}{2}\alpha^* + \frac{\partial}{\partial\alpha})\,|\alpha\rangle$.

- Expansion of arbitrary states in terms of coherent states: For any state $|f\rangle$, the function $f(\alpha^*) = e^{|\alpha|^2/2}\langle\alpha|f\rangle$ is *an analytic function* of α^*.

- Any operator T is determined by its expectation in all coherent states, that is we have

$$\langle n|\,T\,|m\rangle = \frac{1}{\sqrt{n!m!}}\frac{\partial^n}{\partial\alpha^{*n}}\frac{\partial^m}{\partial\alpha^m}e^{|\alpha|^2}\langle\alpha|\,T\,|\alpha\rangle\Big|_{\alpha=0}\,. \tag{1.41}$$

- Poissonian number distribution of coherent states: The probability of observing n oscillator quanta in a coherent state $|\alpha\rangle$ is given by a Poisson distribution $|\langle n|\alpha\rangle|^2 = e^{-|\alpha|^2}|\alpha|^{2n}/n!$, which has the mean

$$\langle\alpha|\,a^\dagger a\,|\alpha\rangle = |\alpha|^2\,. \tag{1.42}$$

Other interesting properties can be found in Ref. [17].

Most importantly for our discussion, is that Glauber[18] and Sudarshan[19] have shown that a large class of density matrices of a harmonic oscillator can be written as

$$\rho = \int d^2\alpha P(\alpha,\alpha^*)\,|\alpha\rangle\langle\alpha|\ , \tag{1.43}$$

which is known as the P representation. Klauder *et al*[20] showed that, provided $P(\alpha,\alpha^*)$ is allowed to be a sufficiently singular generalised function, such a representation exists for any density operator ρ. Thus, instead of dealing with the matrix ρ,

we use the function $P(\alpha, \alpha^*)$. Note that the Hermiticity of the density matrix implies that P is real, and the unit-trace property corresponds to

$$\int d^2\alpha P(\alpha, \alpha^*) = 1 \ . \tag{1.44}$$

The thermal state of an oscillator at equilibrium with inverse temperature β, $\rho = \frac{1}{N_\omega(\beta)} e^{-\beta\omega(a^\dagger a+1)}$, corresponds to a Gaussian P function

$$P_{\text{thermal}}(\alpha, \alpha^*) = \frac{1}{\pi N_\omega(\beta)} e^{-|\alpha|^2/N_\omega(\beta)} \ , \tag{1.45}$$

where $N_\omega(\beta) = (e^{\beta\omega} - 1)^{-1}$ is the average occupancy number. A number state of the oscillator $\rho = |n\rangle \langle n|$ does not have a functional form of the equivalent P-function, but instead corresponds to the generalised distribution

$$P_n(\alpha, \alpha^*) = \frac{1}{n!} e^{|\alpha|^2} \left(\frac{\partial^2}{\partial\alpha\partial\alpha^*} \right)^n \delta^2(\alpha) \ . \tag{1.46}$$

The mapping between the density operator and the P function yields the following operator correspondence[17]:

$$a\rho \leftrightarrow \alpha P \ , \tag{1.47}$$

$$\rho a^\dagger \leftrightarrow \alpha^* P \ , \tag{1.48}$$

$$a^\dagger \rho \leftrightarrow \left(\alpha^* - \frac{\partial}{\partial\alpha} \right) P \ , \tag{1.49}$$

$$\rho a \leftrightarrow \left(\alpha - \frac{\partial}{\partial\alpha^*} \right) P \ . \tag{1.50}$$

This way the master equation for the evolution of the density matrix of a harmonic oscillator, turns into a differential equation, where analytical techniques are available for solving complex equations. This mapping between infinite matrices and differential equations has been used extensively in the field of quantum optics, and in Chapter 2 we show how we used it for the case of a finite system coupled to a bath of harmonic oscillators.

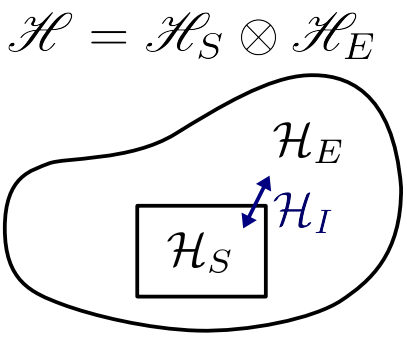

Figure 1.1: An illustration of the open system model. The system of interest is coupled to an environment, via an interaction Hamiltonian $\mathcal{H}_I$. Hamiltonians $\mathcal{H}_S$ and $\mathcal{H}_E$ each operate on their respective Hilbert space.

1.1.5 Open System Hamiltonian

The standard and generic model of an open quantum system is the following: We have some system of interest S, which interacts with a (possibly very large) number of degrees of freedom E, called the environment. These are either inaccessible or not interesting in the experiment. Therefore we are interested in the reduced density matrix of the system of interest. The Hilbert space of the system is given by $\mathscr{H} = \mathscr{H}_S \otimes \mathscr{H}_E$, where the subscript denotes the respective system. The Hamiltonian for this model can be split into

$$\mathcal{H} = \mathcal{H}_S \otimes \mathbb{1}_E + \mathbb{1}_S \otimes \mathcal{H}_E + \mathcal{H}_I \ , \tag{1.51}$$

Where $\mathcal{H}_S$ and $\mathcal{H}_E$ each operate on their respective Hilbert space, and the interaction Hamiltonian $\mathcal{H}_I$ operates in the full Hilbert space. The interaction Hamiltonian can always be written as

$$\mathcal{H}_I = \sum_\nu S_\nu \otimes E_\nu \ , \tag{1.52}$$

with S_ν and E_ν being Hermitian. An illustration of this model is given in Fig. 1.1.

In Chapter 2 we show how to further split the environment to an immediate environment that we would like to solve more accurately, and a further 'universe' that is coupled only to the immediate environment, which will be treated approximately.

A very important quantity in the theory of open quantum systems is the *response function*, $\alpha_{\nu\mu}(t)$, which is defined by

$$\alpha_{\nu\mu}(t) = \langle E_\nu(0)E_\mu(t)\rangle_E \tag{1.53}$$

$$= Tr\{E_\nu(0)U_E(t)E_\mu(0)U_E^\dagger(t)\rho_E(0)\} \ . \tag{1.54}$$

Here $U_E(t)$ is the evolution operator of the environment alone, *i.e.* for the Hamiltonian $\mathcal{H}_E$ ($U_E(t) = T_{\leftarrow}e^{-\mathrm{i}\int_0^t \mathcal{H}_E(\tau)d\tau}$[§]), and $\rho_E(0) = tr_S\{W(0)\}$ is the initial state of the environment. In many cases the real and imaginary parts of the response function appear separately from each other, so it is useful to define

$$\alpha_{\nu\mu}(t) \equiv D_{\nu\mu}(t) + \mathrm{i}D_{1,\nu\mu}(t) \ , \tag{1.55}$$

with D and D_1 being real, sometimes being referred to as the *dissipation* and *noise* kernels, respectively.

The response function is the main quantity that characterises the environment, and it appears in all the open systems methods introduced below. For large environments with infinite degrees of freedom it decays with a characteristic time τ_E which is known as the memory time of the environment.

In this Thesis we are concerned in the case where the environment is modelled by a set of harmonic oscillators,

$$\mathcal{H}_E = \sum_k \omega_k a_k^\dagger a_k, \tag{1.56}$$

where $\omega_k > 0$ are the frequencies, and $a^\dagger$ (a) are the usual creation (annihilation) operators, obeying $[a_i, a_j^\dagger] = \delta_{ij}$. Furthermore, we will restrict ourselves to the case of *linear coupling* between the system and environment, where

$$E_\nu = \sum_k g_{\nu k}(a_{\nu_k} + a_{\nu_k}^\dagger). \tag{1.57}$$

This form is justified by weak-coupling arguments: even if the original Hamiltonian does not hold this linear form, in the weak-coupling regime the system behaves as

[§]Here, the time-ordering operator $T_{\leftarrow}$ orders the time arguments of the equation chronologically, and is defined as $T_{\leftarrow}e^{-\mathrm{i}\int_0^t \mathcal{H}_E(\tau)d\tau} \equiv \lim_{\delta\tau\to 0} e^{-\mathrm{i}\mathcal{H}_E(t)\delta\tau}e^{-\mathrm{i}\mathcal{H}_E(t-\delta\tau)\delta\tau}\ldots e^{-\mathrm{i}\mathcal{H}_E(2\delta\tau)\delta\tau}e^{-\mathrm{i}\mathcal{H}_E(\delta\tau)\delta\tau}e^{-\mathrm{i}\mathcal{H}_E(0)\delta\tau}$.

if it is evolving under a fictitious interaction given by Eqn. (1.57). In this case, the effective coupling constants $g_{\nu k}$ are temperature-dependent[21,22]. Given this linear form, we can define the *spectral density* of the environment, via

$$J_\nu(\omega) = \sum_k g_{\nu k}^2 \delta(\omega - \omega_{\nu_k}). \tag{1.58}$$

In most physical systems, where the environment is modelled using an infinite number of oscillators, we take the spectral density to be a continuous function of ω, and require it to vanish for very small and very large values of ω. That is, for small values we have $J(\omega) \sim \omega^s$, where for $s = 1$ it is called an *Ohmic* spectral density[§]. When $s > 1$ or $s < 1$ we call the spectral density *sub-Ohmic* or *super-Ohmic*, respectively.

If the initial state of the environment $\rho_E(0)$ is diagonal in the excitation number basis, we can write the (diagonal of the) response function of the environment as

$$\alpha_{\nu\nu}(t) = \int_0^\infty d\omega J_\nu(\omega) \left[2N_\nu(\omega)\cos\omega t + e^{-\mathrm{i}\omega t}\right], \tag{1.59}$$

where $N_\nu(\omega) = Tr\{\sum_k a^\dagger_{\nu_k} a_{\nu_k} \rho_E(0)\}$ is the average excitation number. If moreover initially the environment is in thermal equilibrium with inverse temperature β, *i.e.* $\rho_E(0) \sim e^{-\beta \mathcal{H}_E}$, we have the usual $N(\omega) = (e^{\beta\omega} - 1)^{-1}$, and the response function is given by

$$\alpha_{\nu\nu}(t) = \int_0^\infty d\omega J_\nu(\omega) \left[\coth(\beta\omega/2)\cos\omega t - \mathrm{i}\sin\omega t\right] \tag{1.60}$$

$$= \int_0^\infty d\omega \frac{J_\nu(\omega)}{\sinh(\beta\omega/2)} \cosh(\beta\omega/2 - \mathrm{i}\omega t)\ . \tag{1.61}$$

Finally, for mathematical simplicity, we assume that initially the system and environment are statistically independent, hence the density matrix of the joint system at time 0 can be written as $W(0) = \rho_S(0) \otimes \rho_E(0)$.

In section 1.3 we discuss some of the different techniques used in the literature to calculate the exact or approximated evolution of the reduced density matrix $\rho_S = Tr_E W$.

[§]This is because when applied to the case of an electron flowing through a wire, $J(\omega) = \eta\omega$ will generate Ohmic dissipation, *i.e.* proportional to the velocity of the particle, see the Caldeira–Leggett model[23]

1.2 A Model for Energy Transport

In this Thesis we will be interested in modelling the dynamics of electronic excitations in a molecular structure. When a molecule absorbs a quantum of energy that corresponds to a transition from one molecular orbital to another molecular orbital, the result is an electronic excited state, which is described as an exciton.

There is a major difference that exist between excited-state properties of a *single* molecule, and those of complexes of molecules. Many, but not all, spectral properties of small aggregates of molecules are directly traceable to properties of individual molecules. However, the energy of interaction between the molecules, weak as it may be, imposes a communal response upon the molecular behaviour in the aggregate. The collective response is embodied in an entity called an exciton[24,25], whose wave-function is well described by a linear combination of wave-functions of excited (electronic) states of the individual molecules. This quasi-particle was initially introduced by Frenkel in 1931[26], and later generalised by Wannier[27].

The molecules also have vibrational degrees of freedom, which can be perturbed by the existence of an electronic excitation. If we are concerned with energy transport as part of a photosynthetic process, these molecules are chromophores, but in general they can differ from system to system, and within the system itself. Each molecule can have several electronically excited states in general, but for simplicity we will be concerned with cases where only the lowest excited state is of interest. The excitonic state of each molecule, or 'site', in our system is thus either 'excited' ($|e\rangle$) or 'in the ground state' ($|g\rangle$). Furthermore, we will be concerned with systems which have a very low probability of an excitation, so we can restrict ourselves to no more than one exciton in the entire structure. Thus the excitonic Hamiltonian is spanned by the ground state of the system, $|g\rangle$, where there is no excitation in the system, and states $|n\rangle$, which means that all of the molecules are in the ground state, apart from molecule n which is excited. The individual excited states are coupled through an exchange Hamiltonian $\mathcal{H}_{nm} = V_{nm} |n\rangle \langle m| + V^*_{nm} |m\rangle \langle n|$, which arises due to spatial overlap of the two wave-functions of the excited states, or the dipole-dipole interaction[28], and

accounts for the span of an exciton to several molecules. The excitonic Hamiltonian is thus given by

$$\mathcal{H}_S = \epsilon_g |g\rangle \langle g| + \sum_n \epsilon_n |n\rangle \langle n| + \sum_{n<m} \left(V_{nm} |n\rangle \langle m| + V_{nm}^* |m\rangle \langle n| \right) \ . \tag{1.62}$$

As mentioned above, the different molecules also have vibrational degrees of freedom. In many cases these are very large molecules with many vibrational degrees. We will assume that each molecule vibrates independently from its neighbours, which for the model means that each 'site' has its *local bath* made of a set of harmonic oscillators, *i.e.*

$$\mathcal{H}_E = \sum_n \sum_k \omega_{n,k} a_{n,k}^\dagger a_{n,k} \ , \tag{1.63}$$

with $[a_{n,k} \ , \ a_{n',k'}^\dagger] = \delta_{nn'}\delta_{kk'}$, where the subscript n is the number of the molecule. The coupling between the excitons and the oscillators is taken to be linear, as discussed in section (1.1.5). The way it is modelled is by a displacement of the environmental oscillators in the presence of an excitation $a_{n,k} \to a_{n,k} + \frac{g_{n,k}}{\omega_{n,k}}$, for the total Hamiltonian to be given by

$$\mathcal{H} = \mathcal{H}_S + \sum_{n,k} \omega_{n,k} \left(a_{n,k}^\dagger + \frac{g_{n,k}^*}{\omega_{n,k}} |n\rangle \langle n| \right) \left(a_{n,k} + \frac{g_{n,k}}{\omega_{n,k}} |n\rangle \langle n| \right) \ . \tag{1.64}$$

Below we take the coupling constants $g_{n,k}$ to be real, which is always possible in the case of independent local environments. Expanding the brackets in the above equation reveals the interaction Hamiltonian as

$$\mathcal{H}_I = \sum_n \sum_k g_{n,k} |n\rangle \langle n| \left(a_{n,k} + a_{n,k}^\dagger \right) \ . \tag{1.65}$$

The displacement also gives rise to an energy counter term $\mathcal{H}_c = \sum_n \sum_k \frac{g_{n,k}^2}{\omega_{n,k}} |n\rangle \langle n| = \sum_n \lambda_n |n\rangle \langle n|$, where λ_n is known as the reorganisation energy

$$\lambda_n = \sum_k \frac{g_{n,k}^2}{\omega_{n,k}} = \int_0^\infty d\omega J_n(\omega)/\omega \ . \tag{1.66}$$

The reorganisation energy is the extra energy needed in order to excite an electron due to the presence of coupling to an environment. Here $J_n(\omega)$ is given by Eqn. (1.58).

The total Hamiltonian is thus given by

$$\mathcal{H} = \mathcal{H}_S + \mathcal{H}_I + \mathcal{H}_E + \mathcal{H}_c \ , \tag{1.67}$$

where normally the reorganisation energies are absorbed into the system's Hamiltonian via $\mathcal{H}_S \to \mathcal{H}_S + \mathcal{H}_c$. This is the energy transport model. Variations of this model have had great success in modelling excitation dynamics of microscopic biological systems. Example include: Molecular complexes involved in photosynthesis, such as the *Fenna-Matthews-Olsen* (FMO) complex in green sulphur bacteria[29–35], and the light harvesting photosystems in green plants[36]; electron transport in metalloproteins[37]; magnetoreception in birds[38], and models for olfaction[39]. Perhaps the simplest case of such a model is when we only have two sites in the system. This is equivalent to the famous spin-boson model, which has been used to study energy transport in numerous systems. A very comprehensive review was written about the spin-boson model by Leggett *et al* in 1987[40].

1.3 Perturbative techniques

In this section we derive the time-convolutionless (TCL) perturbative master equation, which is based on a projection operator technique. We also discuss some common approximations employed in order to simplify the (second order) TCL generator – the Markov and the secular approximations. We show how the Markov approximation leads to the Redfield equations, and how the secular approximation leads to the Pauli master equation, and to a Lindblad form. Missing from this derivation is the famous Born approximation, which is not needed if one derives the equations via the TCL master equation. For a different approach which includes a discussion about the Born approximation, see Chapter 3 of Ref. [4].

1.3.1 TCL expansion

The time-convolutionless (TCL) projection operator technique is a time-local master equation. The basic idea underlying the projection operator is to regard the operation

of tracing over the environment as a formal projection $\rho \mapsto \mathcal{P}\rho$. The super-operator $\mathcal{P}$ is a projection operator with the property $\mathcal{P}^2 = \mathcal{P}$, and the density matrix $\rho_r = \mathcal{P}\rho$ is called the *relevant* part of the density matrix. Complementarily, one defines the projector $\mathcal{Q} = \mathbb{1} - \mathcal{P}$ which projects the density matrix into the *irrelevant* part $\rho_{irr} = \mathcal{Q}\rho$. The TCL technique leads to an exact equation of motion for the relevant part ρ_r, at least for some Hamiltonians and initial conditions. We start by defining the super-operator $\mathcal{P}$ according to

$$\rho \mapsto \mathcal{P}\rho = \mathrm{Tr}_E\{\rho\} \otimes \rho_E \ , \tag{1.68}$$

where ρ_E is some (physical) state of the environment, which is called the reference state. Note that ρ_E can be any state, not necessarily the initial state of the environment, it can even be time-dependent. It is chosen according to mathematical/physical convenience, typically taken to be the (static) thermal state of the environment. In many cases it may be assumed that the odd moments of the interaction Hamiltonian with respect to the reference vanish, *i.e.* $tr_E\{\mathcal{H}_I(t_1)\mathcal{H}_I(t_2)\cdots\mathcal{H}_I(t_{2n+1})\rho_E\} = 0$, which leads to the relation

$$\mathcal{P}\mathcal{L}(t_1)\mathcal{L}(t_2)\cdots\mathcal{L}(t_{2n+1})\mathcal{P} = 0 \ . \tag{1.69}$$

Here $\mathcal{L}(t)$ is given in Eqn. (1.35). When this relation holds, all the odd terms of the TCL expansion vanish (see below). In the interaction picture, the von Neumann equation takes the form of (1.35), which is written here again for ease of reading

$$\frac{\partial}{\partial t}\rho_I(t) = -\mathrm{i}\eta[\tilde{\mathcal{H}}_I(t), \rho_I(t)] = \eta\mathcal{L}(t)\rho_I(t) \ . \tag{1.70}$$

Hereafter, we discard the I subscript, but nevertheless continue to work in the interaction picture. Equation (1.70) can be split into

$$\frac{\partial}{\partial t}\rho_r(t) = \eta\mathcal{P}\mathcal{L}(t)\rho_r(t) + \eta\mathcal{P}\mathcal{L}(t)\rho_{irr}(t) \ , \tag{1.71}$$

$$\frac{\partial}{\partial t}\rho_{irr}(t) = \eta\mathcal{Q}\mathcal{L}(t)\rho_r(t) + \eta\mathcal{Q}\mathcal{L}(t)\rho_{irr}(t) \ . \tag{1.72}$$

The idea is to formally solve the equation for the irrelevant part, and plug it into the equation for the relevant part, to get a solution. The formal solution to (1.72) is

$$\rho_{irr}(t) = \mathcal{G}(t,t_0)\rho_{irr}(0) + \eta \int_{t_0}^{t} d\tau \mathcal{G}(t,\tau)\mathcal{QL}(\tau)\rho_r(\tau) \ , \tag{1.73}$$

where we defined the propagator $\mathcal{G}(t,\tau)$ which satisfies the differential equation

$$\frac{\partial}{\partial t}\mathcal{G}(t,\tau) = \eta\mathcal{QL}(t)\mathcal{G}(t,\tau) \ , \tag{1.74}$$

with the initial condition $\mathcal{G}(\tau,\tau) = 1$. The density matrix of the joint system evolves unitarily according to (1.33), hence the time-reversed propagator exists as well

$$\rho(s) = U_I^\dagger(t,s)\rho(t)U_I(t,s) \equiv G(t,s)\rho(t) \ . \tag{1.75}$$

With the use of the reversed propagator $G(t,s)$, we get an expression for the irrelevant part through

$$[1-\Sigma(t,t_0)]\rho_{irr}(t) = \mathcal{G}(t,t_0)\rho_{irr}(t_0) + \Sigma(t,t_0)\rho_r(t) \ , \tag{1.76}$$

where $\Sigma(t,t_0) = \eta\int_{t_0}^{t} d\tau\mathcal{G}(t,\tau)\mathcal{QL}(\tau)\mathcal{P}G(t,\tau)$. $\Sigma(t,t_0)$ has the properties of $\Sigma(t_0,t_0) = 0$ and $\Sigma(t,t_0)|_{\eta=0} = 0$, hence $1-\Sigma(t,t_0)$ may be inverted for small $t-t_0$, and for weak-coupling. Assuming $[1-\Sigma(t,t_0)]^{-1}$ exists, we can write down an equation for the relevant part of the density matrix:

$$\frac{\partial}{\partial t}\rho_r = \mathcal{K}(t)\rho_r(t) + \mathcal{I}(t)\underbrace{\rho_{irr}(t_0)}_{=0} \ , \tag{1.77}$$

with the time-local generator, called the TCL generator

$$\mathcal{K}(t) = \eta\mathcal{PL}(t)[1-\Sigma(t,t_0)]^{-1} \ , \tag{1.78}$$

and the inhomogeneity $\mathcal{I}(t) = \mathcal{K}(t)\mathcal{G}(t,t_0)$. Note that for factorised initial conditions, if the reference state is the initial state of the environment, we get $\rho_{irr}(t_0) = 0$. In this Thesis this is the only case we consider, so we can ignore the inhomogeneity from now on.

Let us assume the following geometric series converges:

$$[1-\Sigma(t,t_0)]^{-1}=\sum_{n=0}^{\infty}[\Sigma(t,t_0)]^n\ . \tag{1.79}$$

In this case, we get the following perturbative expansion for the TCL generator

$$\mathcal{K}(t)=\eta\mathcal{P}\mathcal{L}(t)\sum_{n=0}^{\infty}[\Sigma(t,t_0)]^n=\sum_{n=1}^{\infty}\eta^n\mathcal{K}_n(t)\ . \tag{1.80}$$

Of course, the super-operator $\Sigma(t,t_0)$ itself can be written as a power series in η. Since $\mathcal{K}\rho_r$ operates on $\mathscr{H}_S$, we can use ρ_S instead of ρ_r in Eqn. (1.77), and get the TCL equation

$$\frac{\partial}{\partial t}\rho_S(t)=\mathcal{K}(t)\rho_S(t)=\sum_{n=1}^{\infty}\eta^n\mathcal{K}_n(t)\rho_S(t)\ . \tag{1.81}$$

Assuming (1.69) holds, it is possible to prove that all the odd terms in the series vanish[4], and the first two non-vanishing terms are then given by (setting $\eta=1$):

$$\mathcal{K}_2(t)=\mathcal{P}\mathcal{L}(t)\int_0^t dt_1\mathcal{L}(t_1), \tag{1.82}$$

$$\begin{aligned}\mathcal{K}_4(t)=&\mathcal{P}\mathcal{L}(t)\int_0^t dt_1\int_0^{t_1}dt_2\int_0^{t_2}dt_3\int_0^{t_3}dt_4\Big(\mathcal{L}(t_1)\mathcal{L}(t_2)\mathcal{L}(t_3)\\&-\mathcal{L}(t_1)\mathcal{P}\mathcal{L}(t_2)\mathcal{L}(t_3)-\mathcal{L}(t_2)\mathcal{P}\mathcal{L}(t_1)\mathcal{L}(t_3)-\mathcal{L}(t_3)\mathcal{P}\mathcal{L}(t_1)\mathcal{L}(t_2)\Big)\ .\end{aligned} \tag{1.83}$$

If we write the interaction as (1.52), the second and fourth terms are explicitly given by[4,41]:

$$\mathcal{K}_2(t)=-\sum_{\nu_0,\nu_1}\int_0^t dt_1 S^{\times}_{\nu_0}(t)R_{\nu_0,\nu_1}(t,t_1)\ , \tag{1.84}$$

$$\begin{aligned}\mathcal{K}_4(t)=&\sum_{\nu_0,\nu_1,\nu_2,\nu_3}\int_0^t dt_1\int_0^{t_1}dt_2\int_0^{t_2}dt_3\Big\{\\&S^{\times}_{\nu_0}(t)\left[S^{\times}_{\nu_1}(t_1),R_{\nu_0,\nu_2}(t,t_2)\right]R_{\nu_1,\nu_3}(t_1,t_3)\\&+S^{\times}_{\nu_0}(t)\left[S^{\times}_{\nu_1}(t_1)R_{\nu_1,\nu_2}(t_1,t_2),R_{\nu_0,\nu_3}(t,t_3)\right]\Big\}\ .\end{aligned} \tag{1.85}$$

Here we defined

$$S^{\times}_{\nu}(t)\square \equiv [S_{\nu}(t), \square] \ , \tag{1.86}$$

$$S^{\circ}_{\nu}(t)\square \equiv \{S_{\nu}(t), \square\} \ , \tag{1.87}$$

$$\begin{aligned} R_{\nu_a,\nu_b}(t_a, t_b) \equiv & D_{\nu_a\nu_b}(t_a - t_b) S^{\times}_{\nu_b}(t_b) \\ & + \mathrm{i} D_{1,\nu_a\nu_b}(t_a - t_b) S^{\circ}_{\nu_b}(t_b) \ . \end{aligned} \tag{1.88}$$

$D_{\nu_a,\nu_b}(t)$, $D_{1,\nu_a,\nu_b}(t)$ are the real and imaginary part of the response function (see 1.55).

As we show in the next section, it is useful to write $\mathcal{K}$ in Liouville space, with $|i\rangle\langle j| \to |ij\rangle$. Note that $\mathcal{K}$, and thus each term in the TCL expansion, obeys

$$\langle ij| \mathcal{K} |rs\rangle = \Big(\langle ji| \mathcal{K} |sr\rangle \Big)^* \ , \tag{1.89}$$

$$\sum_k \langle kk| \mathcal{K} |rs\rangle = 0 \ , \tag{1.90}$$

which follows from the Hermiticity of the density matrix, and the trace preservation of the density matrix, respectively.

In practice we cut off the series at some order, typically the second order, though in Chapter 3 we go to up to the fourth order. The strength of the TCL perturbation technique is in the numerical and analytical simplicity of the first terms. Going to higher orders gets exponentially more demanding with every term, so for cases where higher-order contributions are important, *i.e.* strong-coupling, this method is not recommended. In Chapter 3 we discuss when it is justified to cut off this series, by comparing second to fourth order terms, and introduce a simple measure of when it is valid to cut the TCL expansion.

1.3.2 Redfield equations, Pauli ME, and Lindblad ME

The second order of the TCL expansion, Eqn. (1.84), is the starting point of several very common approximations which, depending on the level of approximations, result in the famous Redfield equations, or in a Lindblad form for the master equation, and the Pauli master equation. For simplicity we assume a single interaction term

$\mathcal{H}_I = V \otimes E$. In the system's eigenbasis, the elements of $\mathcal{K}_2$ are given by (written in Liouville space):

$$\begin{aligned}\langle ij|\mathcal{K}_2\,|rs\rangle = -e^{-\mathrm{i}(\Delta_{rs}-\Delta_{ij})t}\int_0^t d\tau\Big\{ \\ \sum_k\Big[\delta_{js}e^{-\mathrm{i}\Delta_{kr}\tau}V_{ik}V_{kr}\alpha(\tau)+\delta_{ir}e^{+\mathrm{i}\Delta_{ks}\tau}V_{sk}V_{kj}\alpha^*(\tau)\Big] \\ -V_{ir}V_{sj}\Big[e^{-\mathrm{i}\Delta_{ir}\tau}\alpha(\tau)+e^{+\mathrm{i}\Delta_{js}\tau}\alpha^*(\tau)\Big]\Big\}\,,\end{aligned} \tag{1.91}$$

where $\Delta_{ij} = \epsilon_i - \epsilon_j$ is the energy difference between two sites i, j, $V_{ij} = \langle i|\,V\,|j\rangle$, δ_{ij} is the Kronecker delta function, and $\alpha(t)$ is the response function (see Eqn. 1.53). The master equation takes the explicit form

$$\frac{\partial}{\partial t}\rho_{ij}(t) = \sum_{rs}\langle ij|\,\mathcal{K}_2\,|rs\rangle\,\rho_{rs}(t)\,, \tag{1.92}$$

where $\rho_{ij}(t) = \langle i|\,\rho_S(t)\,|j\rangle$. At this point one can make the *Markov approximation* in order to simplify the equations. The Markov approximation assumes that the response function of the environment decays on a faster time-scale than the coherent evolution of the system, thus we can extend the limit of the integral in Eqn. (1.91) to infinity. This means that the 'memory' of the environment is very short, and the only time dependence in the TCL2 generator is the leading exponent. Now one can rewrite the TCL2 generator as

$$\langle ij|\,\mathcal{K}_2\,|rs\rangle = e^{-\mathrm{i}(\Delta_{rs}-\Delta_{ij})t}\,\langle ij|\,\tilde{\mathcal{K}}_2\,|rs\rangle\,, \tag{1.93}$$

where $\tilde{\mathcal{K}}_2$ has no time-dependence. Remember that Eqn. (1.92) is written in the interaction picture. Transforming back to the Schrödinger picture, we get

$$\frac{\partial}{\partial t}\tilde{\rho}_{ij}(t) = -\mathrm{i}\Delta_{ij}\tilde{\rho}_{ij}(t) + \sum_{rs}\langle ij|\,\tilde{\mathcal{K}}_2\,|rs\rangle\,\tilde{\rho}_{rs}(t)\,. \tag{1.94}$$

This is known in the literature as the *Bloch-Redfield equation*.

The Bloch-Redfield equations are not in, and cannot be cast into, Lindblad form. This causes them to yield unphysical results for some initial conditions. A way of circumventing this is to introduce a *slippage of initial conditions*[42,43], which means

changing the initial state of the density matrix to account for any non-physical evolution that occurs from making the Markov approximation. This is discussed in more detail in Chapter 3.

Another way of proceeding is, instead of transforming back to the Schrödinger picture, we can make another approximation that removes the time-dependence from the RHS of Eqn. (1.93) and brings the equation to Lindblad form. This is known as the *secular approximation*, which is to take the time average of the TCL2 kernel instead of its instantaneous time. This means that the terms rotating as $\sim e^{-\mathrm{i}(\Delta_{rs}-\Delta_{ij})t}$ in the TCL2 kernel average out to zero unless $\Delta_{rs} = \Delta_{ij}$. The justification for this approximation comes from the assumption that the coupling to the environment is relatively weak, such that the time scale it introduces is long relative to the coherent dynamics, so that these terms oscillate rapidly and can be averaged out. This is obviously not a good approximation when we have two transition frequencies in the system that are very close to each other, but otherwise we show in Chapter 4 that for the cases discussed in this Thesis, this is a very good approximation. Thus we obtain

$$\langle ij|\, \mathcal{K}_2^{\mathrm{sec}}\, |rs\rangle = \delta_{\Delta_{rs}-\Delta_{ij}}\, \langle ij|\, \tilde{\mathcal{K}}_2\, |rs\rangle\,, \tag{1.95}$$

where the delta function is the Kronecker delta function. If we denote

$$\int_0^\infty d\tau e^{-\mathrm{i}\omega\tau}\alpha(\tau) = \frac{1}{2}\gamma(\omega) + \mathrm{i}S(\omega)\ , \tag{1.96}$$

with real $\gamma(\omega)$ and $S(\omega)$, we find that

$$\begin{aligned}\langle ij|\, \mathcal{K}_2^{\mathrm{sec}}\, |rs\rangle =& \delta_{\Delta_{rs}-\Delta_{ij}} V_{ir}V_{sj}\gamma_{ir} \\ &- \frac{1}{2}\delta_{js}\delta_{\Delta_{ir}}\sum_k V_{ik}V_{kr}\gamma(\Delta_{kr}) - \frac{1}{2}\delta_{ir}\delta_{\Delta_{js}}\sum_k V_{sk}V_{kj}\gamma(\Delta_{ks}) \\ &- \mathrm{i}\sum_k \Big(\delta_{js}\delta_{\Delta_{ir}}V_{ik}V_{kr}S(\Delta_{kr}) - \delta_{ir}\delta_{\Delta_{js}}V_{sk}V_{kj}S(\Delta_{ks})\Big).\end{aligned} \tag{1.97}$$

Direct comparison confirms that the first two lines of the above equation are equivalent to a Lindblad dissipator, with rates $\gamma(\omega)$ and Linblad operators

$$A(\omega) = \sum_{ij}\delta_{\Delta_{ij}-\omega}V_{ij}\,|i\rangle\,\langle j|\ . \tag{1.98}$$

That is, $A(\omega)$ is the part of V that couples states with energy difference ω, and we have the relation $\sum_\omega A(\omega) = V$, where the sum is over all the eigenfrequencies of the system. The last line of Eqn. (1.97) is generating coherent dynamics, through the so called *Lamb shift* Hamiltonian

$$\mathcal{H}_{LS} = \sum_\omega A^\dagger(\omega) A(\omega) S(\omega) \ , \tag{1.99}$$

which commutes with the unperturbed system Hamiltonian $\mathcal{H}_S$. In most cases the Lamb shift is extremely small and can be ignored[44]. The master equation thus can be written in a Lindblad form, as

$$\frac{\partial}{\partial t}\rho(t) = -\mathrm{i}[\mathcal{H}_{LS}, \rho(t)] + \sum_\omega \gamma(\omega) \left(A(\omega)\rho(t)A^\dagger(\omega) - \frac{1}{2}\left\{A^\dagger(\omega)A(\omega), \rho(t)\right\}\right) \ . \tag{1.100}$$

For a response function given by Eqn. (1.59), the Lindblad rates are given by[§]

$$\gamma(\omega) = \begin{cases} 2\pi J(\omega)N(\omega), & \text{if } \omega > 0 \\ 2\pi J(|\omega|)[N(|\omega|)+1], & \text{otherwise} \ , \end{cases} \tag{1.101}$$

$$S(\omega) = -\int_0^\infty d\omega' J(\omega') \left[\frac{N(\omega')}{\omega - \omega'} + \frac{N(\omega')+1}{\omega + \omega'}\right] \ . \tag{1.102}$$

An important observation is the following: before the secular approximation, the expression for the populations is

$$\frac{\partial}{\partial t}\rho_{ii}(t) = \sum_{rs} e^{-\mathrm{i}\Delta_{rs}t} \langle ii| \tilde{\mathcal{K}}_2 |rs\rangle \rho_{rs}(t) \ . \tag{1.103}$$

Thus, performing the secular approximation *decouples the coherences from the populations*, and one gets for the populations

$$\frac{\partial}{\partial t}\rho_{ii}(t) = \sum_j |V_{ij}|^2 [\gamma(\Delta_{ij})\rho_{jj}(t) - \gamma(-\Delta_{ij})\rho_{ii}(t)] \ . \tag{1.104}$$

This is known as the Pauli master equation, and in the case of a thermal state of the environment, the Pauli master equation leads to a thermal or Gibbs state of the system, in the long time limit.

[§]To get this result we used the identity $\int_0^\infty d\tau e^{-\mathrm{i}\omega\tau} = \pi\delta(\omega) - \mathrm{i}P\frac{1}{\omega}$, where P denotes the Cauchy principal value, and $\delta(\omega)$ is the Dirac delta function.

1.4 Numerically exact techniques

In this section we present a survey of the numerically-exact techniques used throughout this Thesis. This includes the Hierarchical Equations Of Motion (HEOM), and the Quasi-Adiabatic Path Integral approach (QUAPI). Both are based on the Feynman-Vernon influence functional, which is introduced below. These techniques are used only as a benchmark to the perturbative approaches which are the main interest in this work, so here we only include a short introduction to the methods.

1.4.1 Feynman-Vernon Influence Functional

Many numerical methods for having an exact solution to an open system problem are based on the seminal work of Feynman and Vernon[8] dating back to 1963, which is briefly described below.

Using Feynman's path integral representation of non-relativistic quantum mechanics, we can derive a formally exact form of the effect of an environment on a system coupled to it. This is the famous *Influence Functional*. Using Feynman's path integral formalism, the time evolution operator $U(t,t_0)$ from time t_0 to time t, in the position basis of a particle is given by

$$\langle x_t|\, U(t,t_0)\, |x_0\rangle = \int D[x(\tau)] e^{\mathrm{i}S[x]} \ , \tag{1.105}$$

where $D[x(\tau)]$ is an integration over all the different paths for which $x(t_0) = x_0$ and $x(t) = x_t$, and $S[x] = \int_{t_0}^{t} L[\dot{x}(\tau), x(\tau), \tau] d\tau$ is the classical action for each path. If $|\psi_n\rangle, |\psi_m\rangle$ are two states of the system, then the transition amplitude A_{mn} between $|\psi_n\rangle$ and $|\psi_m\rangle$ is given by

$$\begin{aligned} A_{mn} = \langle \psi_m|\, U(t,t_0)\, |\psi_n\rangle &= \int dx_t dx_0 \, \langle \psi_m|x_t\rangle \, \langle x_t|\, U(t,t_0)\, |x_0\rangle \, \langle x_0|\psi_n\rangle \\ &= \int dx_t dx_0 \int D[x] \psi_m^*(x_t) e^{\mathrm{i}S[x]} \psi_n(x_0) \ . \end{aligned} \tag{1.106}$$

Now let us think about an open system, where we have system coordinates q and environment coordinates x which are abstract and could consist of many independent

coordinates $q_1, ..., q_n, x_1, ..., x_N$. The dynamics is governed by the Hamiltonian

$$\mathcal{H} = \mathcal{H}_S(q) + \mathcal{H}_E(x) + \mathcal{H}_I(q, x) \ . \tag{1.107}$$

Now, similar to (1.105), the time evolution operator $U(t, t_0)$ in the position basis is

$$\langle q_t, x_t | \, U(t, t_0) \, | q_0, x_0 \rangle = \int D[q] D[x] e^{\mathrm{i}\{S_S[q] + S_E[x] + S_I[q,x]\}} \ , \tag{1.108}$$

with obvious notation. To get the expression for the reduced density matrix, we integrate over all of the bath variables, assuming the initial state was *factorized* $\rho_0 = \rho_S(0) \otimes \rho_B$:

$$\begin{aligned}
\langle q_t | \, \rho_S(t) \, | q_t' \rangle &= \int dx_t \, \langle q_t, x_t | \, U(t, t_0) \rho_S(0) U^\dagger(t, t_0) \, | q_t', x_t \rangle \\
&= \int D[\tilde{q}] D[\tilde{\tilde{q}}] dq' dq'' \Big\{ e^{\mathrm{i}\{S_S[\tilde{q}] - S_S[\tilde{\tilde{q}}]\}} \\
&\qquad \times \int e^{\mathrm{i}\{S_E[\tilde{x}] - S_E[\tilde{\tilde{x}}] + S_I[\tilde{q}, \tilde{x}] - S_I[\tilde{\tilde{q}}, \tilde{\tilde{x}}]\}} \, \langle x' | \, \rho_E \, | x'' \rangle \, D[\tilde{x}] D[\tilde{\tilde{x}}] dx' dx'' dx_t \Big\} \\
&\equiv \int D[\tilde{q}] D[\tilde{\tilde{q}}] dq' dq'' \Big\{ F[\tilde{q}, \tilde{\tilde{q}}] e^{\mathrm{i}\{S_S[\tilde{q}] - S_S[\tilde{\tilde{q}}]\}} \Big\} \ ,
\end{aligned} \tag{1.109}$$

with the path integral boundary conditions $\tilde{q}(0) = q', \tilde{q}(t) = q_t, \tilde{x}(0) = x', \tilde{x}(t) = x_t, \tilde{\tilde{q}}(0) = q'', \tilde{\tilde{q}}(t) = q_t', \tilde{\tilde{x}}(0) = x'', \tilde{\tilde{q}}(t) = x_t$. $F[\tilde{q}, \tilde{\tilde{q}}]$ is the *influence functional*, which would be equal to unity if no environment coupling existed, and describes the exact influence of the bath on the system. Frequently it is written in an exponential form,

$$F[\tilde{q}, \tilde{\tilde{q}}] \equiv e^{\mathrm{i}\Phi[\tilde{q}, \tilde{\tilde{q}}]} \ , \tag{1.110}$$

$$\langle q_t | \, \rho_S(t) \, | q_t' \rangle = \int D[\tilde{q}] D[\tilde{\tilde{q}}] dq' dq'' \Big\{ e^{\mathrm{i}\{S_S[\tilde{q}] - S_S[\tilde{\tilde{q}}] + \Phi[\tilde{q}, \tilde{\tilde{q}}]\}} \Big\} \ , \tag{1.111}$$

with the influence phase functional $\Phi[\tilde{q}, \tilde{\tilde{q}}]$ being the phase induced by the environment for each path in the path integral. The common way to represent the bath is by a large number of harmonic oscillators, which make the bath Hamiltonian quadratic. Furthermore, we normally assume a linear coupling in the interaction Hamiltonian, which makes it possible to perform the path integral over the bath coordinates analytically, yielding the following expression for the phase functional, for the case of an initial thermal state for the bath:

$$\Phi[\tilde{q}, \tilde{\tilde{q}}] = S_c[\tilde{q}] - S_c[\tilde{\tilde{q}}] + \frac{1}{2} \int_0^t dt' \int_0^{t'} dt'' \Big\{ D(t' - t'') \tilde{q}(t) \tilde{\tilde{q}}(t'') + \mathrm{i} D_1(t' - t'') \tilde{q}(t') \tilde{q}(t'') \Big\} \ . \tag{1.112}$$

Here S_c is the counter-term action, and $D(t'-t'')$, $D_1(t'-t'')$ are the dissipation and noise kernel, respectively (see Eqn. 1.55).

A generalized method for the case of a correlated (*i.e.* not factorised) initial state is discussed in Refs. [45,46].

This was a (very) short introduction to the idea behind the path integral approach. In practice, in order to actually calculate transition rates and system dynamics, some numerically converging methods have been developed. Two of them, namely HEOM and QUAPI, are discussed below.

1.4.2 HEOM

The Hierarchical Equations Of Motion (HEOM) approach, sometimes referred to as the hierarchical second-order cumulant expansion approach, was originally proposed by Tanimura and Kubo[47] in the late 80's, and is based on the path-integral formalism. Tanimura and Kubo showed that if the response function of the environment is given by an exponential decay,

$$\alpha(t) \sim e^{-\mu t} \ , \tag{1.113}$$

where μ is some (possibly) complex decay constant with a positive real part, the reduced density matrix can be written as a continued-fraction of operators acting on the initial reduced density matrix $\rho_S(0)$. This is equivalent to a hierarchy of coupled auxiliary density operators (ADOs) $\rho^0, \rho^1, \rho^2, \cdots$ where $\rho^0 = \rho_S$ is the reduced density matrix of the system, and $\rho^{n>0}$ are the ADOs, which are to be solved simultaneously. Each ADO is coupled to its two nearest neighbours (ρ^n is coupled to $\rho^{n\pm1}$). For the factorized initial state, at time $t = 0$ all of the ADOs are set to zero (except of course for ρ_0), while a correlated initial state can be accounted for by choosing nonzero elements of $\rho^n(0)$[48,49].

In 2009 Ishizaki and Fleming[32,34] showed how HEOM can also be used when we have multiple independent environments, as in the energy transport model (section 1.2), and when the response functions are a sum of exponents rather than a single

one,

$$D(t) = \sum_{k=1}^{N_R} c_k^R e^{-\mu_k^R t} \ , \qquad D_1(t) = \sum_{k=1}^{N_I} c_k^I e^{-\mu_k^I t} \ . \tag{1.114}$$

In this case, the ADO index n becomes a vector, $\vec{n} = (\vec{n}_{\nu R}, \vec{n}_{\nu I})$. Below we use $\vec{n}_{\nu j} = (n_{\nu j1}, n_{\nu j2}, .., n_{\nu j N_j})$, $n_{\nu jk}$ are integers $n_{\nu jk} \in \{0, .., N_c\}$, up to the cut-off tier of the hierarchy N_c, and where $\nu \in \{0, .., N\}$ labels the different independent baths, up to their number N. For notational simplicity we assume all baths have the same correlation functions, but again generalisation is straightforward. The HEOM (with renormalized coupling between hierarchies[50]) then takes the form

$$\begin{aligned}
\dot{\rho}^n(t) \ = \ & -\left(\mathrm{i}H_S^\times + \sum_{\nu=1}^{N} \sum_{j=R,I} \sum_{k=1}^{N_j} n_{\nu jk} \mu_k^j \right) \rho^n(t) - \mathrm{i} \sum_{\nu=1}^{N} \sum_{k=1}^{N_R} \sqrt{\frac{n_{\alpha Rk}}{|c_k^R|}} c_k^R V_\nu^\times \rho^{n^-_{\nu Rk}}(t) \\
& + \sum_{\nu=1}^{N} \sum_{k=1}^{N_I} \sqrt{\frac{n_{\nu Ik}}{|c_k^I|}} c_k^I V_\nu^\circ \rho^{n^-_{\nu Ik}}(t) \\
& - \mathrm{i} \sum_{\nu=1}^{N} \sum_{j=R,I} \sum_{k=1}^{N_j} \sqrt{(n_{\nu jk}+1)|c_k^j|} V_\nu^\times \rho^{n^+_{\nu jk}}(t) \ .
\end{aligned} \tag{1.115}$$

The notation $\rho^{n^\pm_{\nu jk}}$ indicates an increase/decrease of just the νjk'th element of the hierarchy index by 1. One then solves these coupled equations numerically, setting all the ancillary ($\vec{n} \neq (0, 0, ..., 0)$) density matrices to zero at $t = 0$.

The form of the response function (1.114) is analytically exact for some spectral densities, including the Drude-Lorentz spectral density[47], a Lorentzian spectral density[51] and an underdamped Brownian oscillator[52–55]. For other cases, it is possible to extend the treatment to cases of arbitrary spectral density with the help of the Meier-Tannor numerical decomposition scheme[56], or, as we show in Chapter 3, we can approximate different response functions into form (1.114) by a simple fit procedure.

HEOM is non-pertubative in the coupling strength, but instead it is an expansion in bath-correlations, where we can discard $\rho_{k>N}$ for μN large enough compared with the characteristic frequency of the system[49]. It thus provides an exact numerical solution to the problem that scales exponentially with the size of the system, and is

very numerically demanding, especially in the strong-coupling and low-temperature regime[50]. In 2006 Tanimura wrote a review article[57] summarizing some of the successes of the method.

Because this method is so computationally expensive, in recent years some methods have been applied in order to optimize the algorithms. These include automatic filtering of ADOs[50] (2009), utilizing open software to integrate the HEOM on parallel computers[58,59] (2012), and even GPU-accelerated algorithms[60] (2011).

Though HEOM is in principal numerical, for some cases it is possible to derive analytical results or map the problem to a stochastic problem[57].

To summerize, the HEOM gives a way of exactly computing the dynamics of an open system, at all temperatures and coupling strengths. The limitations of this method are: it is numerically expensive, and scales very badly with the size of the system[61].

1.4.3 QUAPI

Another method based on the Feynman path integral representation is the quasi-adiabatic propagator path-integral (QUAPI) originated by Makri in the 90's[62–64]. The idea behind this is to preform the path integral from Eqn. (1.109) in the eigenbasis of the system Hamiltonian, instead of in the position basis q[62]. The memory kernel of the bath $\alpha(\tau) = D(\tau) + \mathrm{i}D_1(\tau)$ is assumed to be a smooth function that decays rapidly, so that it can be discretised with only a few points K required to adequately capture the behaviour of the kernel[63]. Using this discretisation, two tensors are constructed: a propagator tensor $\mathcal{K}(t+\delta t, t)$ of rank $2K$ that propagates the reduced density tensor, a tensor of rank K, from time t to $t+\delta t$, where δt should be small compared to the characteristic timescales of the system. The density tensor represents K past instances of the density matrix, enough for any non-Markovian effects to be captured reliably. For $\delta t \to 0$ and $K \to \infty$ this method is exact, yet in practice one needs to find the right balance $K\delta t > \tau_{\mathrm{memory}}$ where τ_{memory} is the time after which the memory kernel vanishes $\alpha(\tau_{\mathrm{memory}}) \to 0$, and aiming for the desired accuracy

and computation resources. Reducing δt results in fewer errors but requires K to be bigger, which makes the computation more demanding and requires more memory.

When the short-time propagator tensor $\mathcal{K}(t+\delta t, t)$ has been calculated, the density matrix can be propagated to an arbitrarily long time using standard tensor multiplication techniques.

An interesting property of this method, as Makri showed in Ref. [63], is that the eigenvalues of $\mathcal{K}(t+\delta t, t)$ give the decay-rate of the reduced system, so to calculate these one does not need to propagate the density matrix to long times.

As discussed above, for energy-transfer models we usually model each site to have its own bath. For that case, in 2010 Nalbach, Eckel and Thorwart[65] generalized the QUAPI method to include multiple heat baths, which allows for correlations between the different baths as well. QUAPI has been recently extensively used in order to study energy transfer[66].

As to scaling, this method scales as $\sim M^{2K+2} \times t$ where t is the simulated time period, M is the number of sites, and typically $K \sim 12 - 14$[35]. For extremely low temperatures, K needs to be increased in order to capture the longer bath memory time.

Calculating a typical result of a time-dependent occupation with $M = 2$ using the QUAPI code on a standard Inter Xenon Processor (2.66 GHz), takes a few hours[35]. This exponential scaling property limits the applicability of this method to small systems at finite temperature.

In 2011, Ishizaki and Fleming (the authors of the HEOM generalization[34]), wrote with Nalbach and Thorwart (the authors of the QUAPI generalization[65]) an interesting paper comparing the two methods for the study of energy transfer[35], where they show that the two methods yield coinciding results, yet both are numerically expensive. In 2012, Marki[67] introduced a method to further optimize the algorithm, capturing long memory effects via renormalization of the path integrals, and in another paper from 2012 Lambert and Makri[68] use filtering procedures that select and store only statistically significant path segments of low-frequency modes that span the memory kernel, thus reducing the memory needed for the computation. In 2014,

Makri[69] introduced a procedure based on a blip decomposition of the path integral, which allows for an exponential decrease in the number of paths needed for the calculations, for cases where the memory of the environment is very long and so the number K must be large.

Chapter 2

Quantum dynamics in a tiered non-Markovian environment

2.1 Introduction

In this chapter we introduce a technique that, in contrast to conventional open quantum system approaches, considers a hierarchical environment consisting of two tiers. The outer tier represents a heat bath that acts on an inner tier constituting the immediate environment of the system. The inner tier may consist of a single harmonic oscillator, a continuous bath of oscillator modes, or any additive combination thereof. An illustration of this model is given in Fig. 2.1 (to be compared with Fig. 1.1). This unique setup makes this technique eminently suitable for modelling several of today's most intensely studied experimental systems. This includes many examples of discrete quantum systems interacting with an optical or mechanical resonator, such as, e.g., NV^- centres on diamond cantilevers[70], nanomechanical resonators coupled to superconducting qubits[71], superconducting circuit QED[72,73], and quantum dots on carbon nanotubes[74,75], for which our technique has been very recently applied[76]. Each of these systems features a high quality resonator, some with extremely high – though of course finite – Q factors, as well as a discrete system whose interaction with the environment will in general not be entirely restricted to the resonator.

Beyond these artificial systems, this technique is also very relevant to the research into energy transfer mechanisms within living systems. The motivation to research

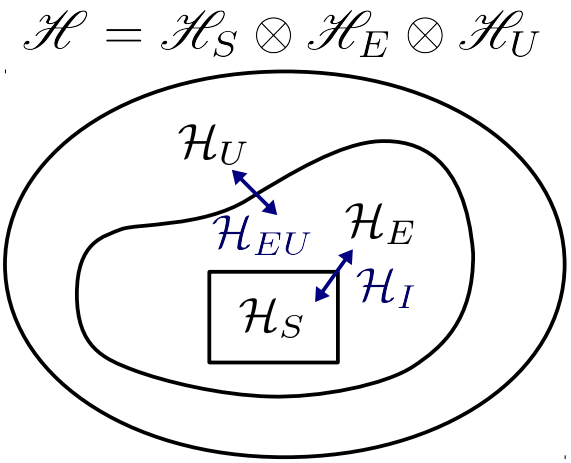

Figure 2.1: An illustration of the model under study. The system of interest is coupled to an immediate environment, which is in turn coupled to the wider 'universe'. The environment is modelled as a set of harmonic oscillators, whereas the 'universe' weakly dampens each of these oscillators to a thermal state. To be compared with Fig. 1.1.

this system actually came from thinking about the FMO complex, where each BChl molecule has internal vibrations, but is also coupled to a wider protein environment, which damps those internal vibrations.

The interplay of vibrational modes and the excitonic states in molecular structures are thought to be key to fully understanding photosynthesis[77]. Indeed, a dominant coupling of an energy transfer complex to a small number of discrete vibrational modes may be responsible for efficient energy transfer[78], and previous work has shown how a continuous spectrum of modes can be mapped onto a bath plus one or more coupled and discrete oscillator modes.[79,80] However, new theoretical developments, and further experiments, are needed to understand the functional role of discrete modes in energy transfer systems. The theoretical framework we describe here is ideal for studying this kind of system-discrete mode-bath system and is applicable across a wide range of parameter space.

Previous works such as Refs. [81–83] consider similarly tiered environments for a different conceptual reason: in those cases a single environmental tier is subdivided with the purpose of capturing more accurate, non-Markovian dynamics. By contrast, our approach here is not motivated by 'mathematical' convenience but is rather de-

signed to capture a commonly occurring 'physical reality'. This latter motivation had already been applied to some specific models such as the damped Jaynes-Cummings model[84,85] and fictitious harmonic oscillators[82], and the idea has led to the theory of pseudo-modes[86] (intrinsically restricted to zero temperature). A similar idea underlies the so-called 'reaction coordinate' method, where the inner tier is a single harmonic oscillator that is coupled to a wider environment[87–89], an approach that is often referred to as a 'structured environment' in the literature[90–93]. It employs a mapping between the original environment and a spin boson model with an effective spectral density[87].

We call our method the P-mat method, since it was originally based on the phase-space representation, or P representation, of the full density matrix (See Chapter 1.1.4). In retrospect it is possible to get the same results without using a phase-space approach, but we find it is easier to use the P representation. Our approach is intuitive, intrinsically non-Markovian, and works for general spectral densities. It is also perturbative in the system-environment coupling parameter.

In most perturbative approaches, the expansion or approximations are made on the master equation. In contrast, most exact numerical approaches are methods to get the time evolution of the density matrix, and not the master equation. This is because the exact methods are normally based on the Feynman-Vernon influence functional approach (see Chapter 1.4). The P-mat approach is an exception to this rule of thumb: it is a perturbative method that approximates the evolution operator for the reduced density matrix.

P-mat applies to a general choice of system and bosonic environment at finite temperature, and the two environmental tiers typically represent different environmental influences. It also remains applicable when there is no natural division into separate tiers, and only a single environment is considered (or when both tiers arise from the same environment). In this case we still obtain non-Markovian contributions to the dynamics, and when applied to canonical cases, we recover known results from the literature. We show that if we cut the series in second-order, we gain a very simple relation to the TCL2 generator, where interestingly the P-mat method

naturally employs the secular approximation in long times. This method is, however, more distinctive when two different environmental influences are present.

To illustrate the P-mat method, we show that it delivers a highly accurate description of the ubiquitous Rabi model, even when the oscillator is damped by a larger environment. As a second example, we take the spin boson model, showing how our method reduces to the weak-coupling results in the appropriate limit, and comparing it with exact QUAPI calculations. We also explore the case where the bath oscillators are themselves coupled to a larger environment, and derive analytical expressions for the decoherence and dephasing rates for this case.

This chapter is organized as follows: in Sec. 2.2 we define our model, and introduce the influence functional. Section 2.3 introduces the perturbative solution to the case where the environment is a single damped vibrational mode. In Sec. 2.4 we examine the case of a more complex environment which is defined via a general spectral density, and show that up to second order in perturbation, each mode contributes independently to the dynamics. Sec. 2.4.1 studies the spin-boson model, comparing P-mat to other approaches. In Sec. 2.5 we show how to calculate higher order terms, and finally, in Sec. 2.6 we summarize the results and discuss the validity of our technique.

2.2 Coherent state representation and Model

2.2.1 Model

As explained, the Hilbert space of this model is given by $\mathscr{H}_S \otimes \mathscr{H}_E \otimes \mathscr{H}_U$, where the subscript S denotes the system, E denotes the environment, and U denotes the 'universe'. We start with the Hamiltonian

$$\mathcal{H} = \mathcal{H}_S + \mathcal{H}_E + \mathcal{H}_I + \mathcal{H}_U + \mathcal{H}_{EU}, \tag{2.1}$$

depicted in Fig. 2.1. Here $\mathcal{H}_S$ is the Hamiltonian governing the system of interest. We shall take the "system Hamiltonian" to be defined on a discrete, finite-dimensional Hilbert space, on which measurements can be performed. No other assumptions are

necessary, and in particular $\mathcal{H}_S$ does not need to be time-independent. The term $\mathcal{H}_E = \sum_k \omega_k a_k^\dagger a_k$ represents an environment consisting of harmonic oscillators, where $a_k^\dagger$ (a_k) is the creation (annihilation) operator for a mode with angular frequency ω_k. We assume linear coupling between the system and environment via interaction Hamiltonian $\mathcal{H}_I = V \sum_k g_k(a_k^\dagger + a_k)$, where V is an arbitrary system operator. We consider here a single environmental bath, but show in Section 2.4 how to generalise this method to several independent environments, *i.e.* for $\mathcal{H}_E = \sum_{\nu,k} \omega_{\nu,k} a_{\nu,k}^\dagger a_{\nu,k}$ and $\mathcal{H}_I = \sum_\nu S_\nu \sum_k g_{\nu,k}(a_{\nu,k}^\dagger + a_{\nu,k})$.

Eqn. (2.1) also includes terms that allow our environment to be coupled to the rest of the universe denoted by $\mathcal{H}_U$. When such a wider environment is present, we assume that it is well approximated by an infinite heat bath with no memory. The oscillator modes of the immediate environment are then dynamically driven towards a thermal state by virtue of the environment-to-universe coupling term $\mathcal{H}_{EU}$. We shall show the effect of the 'universe' is completely captured by introducing an exponential cut-off to the response function. Fig. 2.1 gives an illustration of our model.

Instead of explicitly treating the coupling between the environment and the rest of the universe with a microscopic derivation, we make the simplifying assumption that $\mathcal{H}_{EU}$ is small enough that each mode ω_k of the environment simply experiences damping with rate γ_k via standard Lindblad operators (for a derivation see, e.g., Ref. [4]). More accurately, we use two Lindblad operators for each mode, a_k with rate $\gamma_k(N_k + 1)$, and $a_k^\dagger$ with rate $\gamma_k N_k$, where $N_k = N(\omega_k)$ is the thermal occupancy of mode k.

For this to be consistent, two conditions must be satisfied: Firstly, the damping rate $\gamma_k \ll \omega_k$ must be small for each mode, because this is the parameter regime assumed in the derivation of the damped harmonic oscillator master equation. Secondly, the system-environment coupling described by $\mathcal{H}_I$ may not become too large either, otherwise the damping Lindblad operators acting on each mode are influenced by the presence of the system and our simple independent choice ceases to be a good approximation[94] (also see Ref. [84] for a discussion of this approximation in the context of the resonant damped Jaynes-Cummings model). Remember that the Lindblad equation is

derived using the secular approximation, which is done in the energy eigenbasis of the system. The derivation dictates that the Lindblad operators satisfy $[A, \mathcal{H}] - \omega A = 0$ where A is the Lindblad operator that changes the energy of a state by ω. In our case for, e.g., the Lindblad operator $A = \sqrt{\gamma_k(N_k+1)}a_k$ (we have included the rate into the operator), we get $[A, \mathcal{H}_S + \mathcal{H}_E + \mathcal{H}_I] - \omega_k A = [A, \mathcal{H}_I] = \sqrt{\gamma_k(N_k+1)}g_k V \neq 0$[§]. Thus this is only a good approximation for $\sqrt{\gamma_k g_k^2} \ll 1$.

Finally, we assume that the initial density matrix can be factorized as $\rho(0) = \rho_s(0) \otimes \rho_E^{th}$ with the initial thermal state of the environment being $\rho_E^{th} = \mathcal{N}^{-1} \exp(-\beta \mathcal{H}_E)$ (where $\mathcal{N}$ is the appropriate normalization factor).

2.2.2 The P-Matrix

To represent the density matrix of a single harmonic oscillator we use the *coherent state* or *P representation* (see Chapter 1.1.4 or Ref. [17]), which has been extensively studied in quantum optics. The coherent state representation maps between the density matrix of a harmonic oscillator ρ and a function of two continuous variables $P(\alpha, \alpha^*)$ via

$$\rho = \int d^2\alpha P(\alpha, \alpha^*) \left|\alpha\right\rangle \left\langle\alpha\right| \ , \tag{2.2}$$

where $\left|\alpha\right\rangle$ is the coherent state defined as $\left|\alpha\right\rangle = e^{\alpha a^\dagger - \alpha^* a} \left|0\right\rangle$ or alternatively $a \left|\alpha\right\rangle = \alpha \left|\alpha\right\rangle$, and $d^2\alpha \equiv d\mathrm{Re}(\alpha) d\mathrm{Im}(\alpha)$. For a system with states $\left|i\right\rangle$ coupled to an oscillator, instead of a P function we now need a P matrix to represent the density matrix,

$$\rho = \sum_{i,j} \int d^2\alpha P_{i,j}(\alpha, \alpha^*) \left|i, \alpha\right\rangle \left\langle j, \alpha\right| \ . \tag{2.3}$$

Generalizing from a single mode to a set of modes is straightforward, with the corresponding set of variables $\{a_k, a_k^\dagger\} \leftrightarrow \{\alpha_k, \alpha_k^*\}$ and

$$\rho = \sum_{i,j} \left(\prod_k \int d^2\alpha_k \right) P_{i,j}(\{\alpha_k, \alpha_k^*\}) \left|i, \{\alpha_k\}\right\rangle \left\langle j, \{\alpha_k\}\right| \ . \tag{2.4}$$

[§]For the $\sqrt{\gamma_k N_k} a_k^\dagger$ operator we get $-\sqrt{\gamma_k N_k} g_k V$.

A partial trace over the oscillator space is given by

$$\mathrm{Tr}_{\mathrm{osc}}(\rho) = \sum_{i,j} \left(\prod_k \int d^2\alpha_k \right) P_{i,j}(\{\alpha_k, \alpha_k^*\}) \left|i\right\rangle \left\langle j\right| \ . \tag{2.5}$$

For notational ease, from hereon we switch to a vectorized form of the density matrix and operators, *i.e.* Liouville space, mapping $\left|i\right\rangle \left\langle j\right| \mapsto \left|ij\right\rangle$. Thus the P matrix can be written as a vector $\vec{P} = \sum_{ij} P_{ij} \left|ij\right\rangle$, and the density matrix is given as

$$\rho = \sum_{ij} \int_\alpha P_{ij} \left|ij\right\rangle \left|\{\alpha_k\}\right\rangle \left\langle\{\alpha_k\}\right| \ , \tag{2.6}$$

where for convenience we denote $\int_\alpha \equiv \prod_k \int d^2\alpha_k$, and $P = P(\{\alpha_k, \alpha_k^*\})$. We are interested in the partial trace over the environment

$$\rho^S = \sum_{ij} \int_\alpha P_{ij} \left|ij\right\rangle \ . \tag{2.7}$$

The condition $Tr\rho = 1$ implies $\sum_i \int d^2\alpha P_{ii}(\alpha, \alpha^*) = 1$.

2.2.3 The Influence Functional

At this stage, we use the following form for writing down the full dynamics of the reduced system:

$$\rho^S(t) = U(t) e^{\Theta(t)} \rho^S(0) \ , \tag{2.8}$$

where $U(t)$ is the propagator (in the vectorized representation) of the system without the environment, and the influence of the rest of the world on the system is encoded in the influence functional $\Theta(t)$. The motivation for this form comes from the Feynman-Vernon influence functional[8] of the same form (see also Chapter 1.4). Further, we anticipate that this form will be convenient for recovering the known exponential decay in the weak-coupling limit. The main result of this chapter is that it is possible to write $\Theta(t) = \sum_n \Theta_n(t)$ as a perturbation series with respect to the interaction $\mathcal{H}_I$, and find exact expressions for each term. Expansion up to second order has the simple relation to the TCL2 generator $\Theta_2(t) = \int_0^t d\tau \mathcal{K}_2(\tau)$ (see Chapter 1.3) in the special case where only one tier is present. It thus recovers the known dephasing and

relaxation rates given by the standard TCL expansion, but with an added explicit non-Markovian contribution related to the so-called 'slippage of initial condition', discussed below.

2.3 A Single Mode

Let us first examine the case where the environment $\mathcal{H}_E = \omega a^\dagger a$ consists of only a single mode. When taking a two-level system (2LS) as the system (a limitation which is not required in the following), then this constitutes the well-known Rabi model.

In its vectorized form, the system-environment part of Hamiltonian (2.1) can be decomposed into

$$\mathcal{H}_S(t) = \sum_{ij} H_{ij}(t)\,|ij\rangle\rangle \ , \tag{2.9}$$

$$\mathcal{H}_E = \omega a^\dagger a \ , \tag{2.10}$$

$$\mathcal{H}_I(t) = gV(t)(a + a^\dagger) \ , \tag{2.11}$$

$$V(t) = \sum_{ij} V_{ij}(t)\,|ij\rangle\rangle \ . \tag{2.12}$$

Then the operator correspondence between ρ and $\vec{P}$ (Eqns. 1.47-1.50) yields:

$$\begin{aligned} \frac{\partial}{\partial t}\rho = -\mathrm{i}[\mathcal{H}_S + \mathcal{H}_E + \mathcal{H}_I, \rho] + D(\rho) \leftrightarrow \\ \frac{\partial}{\partial t}\vec{P} = -\mathrm{i}(\mathcal{H}_S^\times + L)\vec{P} + gA_g\vec{P} \ . \end{aligned} \tag{2.13}$$

Here $D(\rho)$ is the Lindblad dissipator induced by $\mathcal{H}_U + \mathcal{H}_{EU}$, which consists of two Lindblad operators, a with rate $\gamma(N+1)$, and $a^\dagger$ with rate γN, where $N = [\exp(\beta\omega) - 1]^{-1}$ is the mean oscillator occupation number at thermal equilibrium with inverse temperature $\beta = (k_\mathrm{B}T)^{-1}$. The operator

$$\begin{aligned} L = &\Big(-\omega + \frac{\mathrm{i}}{2}\gamma\Big)\frac{\partial}{\partial\alpha}\alpha + \Big(\omega + \frac{\mathrm{i}}{2}\gamma\Big)\frac{\partial}{\partial\alpha^*}\alpha^* \\ &+ \mathrm{i}\gamma N\frac{\partial^2}{\partial\alpha\partial\alpha^*} \end{aligned} \tag{2.14}$$

is simply the corresponding P representation Fokker-Plank operator[4], *i.e.* for a single damped oscillator the master equation would read $\frac{\partial}{\partial t}P = -\mathrm{i}LP$. In the vectorized

representation, the terms $-\mathrm{i}\mathcal{H}_S^\times P$ and gA_gP take the place of $-\mathrm{i}[\mathcal{H}_S,\rho]$ and $-\mathrm{i}[\mathcal{H}_I,\rho]$, respectively. We denote $\vec{V} = V\Box$ and $\overleftarrow{V} = \Box V$, *i.e.* the superoperators corresponding to matrix multiplication from the left and from the right. Thus the matrix $\mathcal{H}_S^\times = \vec{\mathcal{H}}_S - \overleftarrow{\mathcal{H}}_S$ is the commutator super-operator, and we have

$$A_g = -\mathrm{i}\Big(\alpha+\alpha^*-\frac{\partial}{\partial\alpha}\Big)\vec{V} + \mathrm{i}\Big(\alpha+\alpha^*-\frac{\partial}{\partial\alpha^*}\Big)\overleftarrow{V}\ . \tag{2.15}$$

Explicitly, the matrices $\mathcal{H}_S^\times, A_g$ are given by

$$\langle ij|\,\mathcal{H}_S^\times(t)\,|rs\rangle = H_{ir}\delta_{sj} - \delta_{ir}H_{sj}\ , \tag{2.16}$$

$$\langle ij|\,A_g\,|rs\rangle = -\mathrm{i}\left(\alpha+\alpha^*-\frac{\partial}{\partial\alpha}\right)V_{ir}\delta_{sj} + \mathrm{i}\left(\alpha+\alpha^*-\frac{\partial}{\partial\alpha^*}\right)\delta_{ir}V_{sj}\ . \tag{2.17}$$

Here δ_{ij} is the Kronecker delta function, and Eqn. (2.15) is derived using the P-representation relations between operators and derivatives, given in Eqns. (1.47-1.50). It will be useful for later to define the anti-commutator as well, $V^\circ = \vec{V} + \overleftarrow{V}$ with elements

$$\langle ij|\,V^\circ\,|rs\rangle = V_{ir}\delta_{sj} + \delta_{ir}V_{sj}\ . \tag{2.18}$$

Note that $\mathcal{H}_S^\times$ is Hermitian, and the propagator $U(t)$ satisfies

$$\frac{\partial}{\partial t}U(t) = -\mathrm{i}\mathcal{H}_S^\times U(t)\ , \tag{2.19}$$

$$U(0) = \mathbb{1}\,. \tag{2.20}$$

The central strategy now is to solve Eqn. (2.13) perturbatively with g being the small parameter, based on the form (2.8) of the full solution in order to estimate the influence functional $\Theta(t)$.

2.3.1 Perturbation Series

For the perturbation treatment, we use the expansion

$$P = P^{(0)} + gP^{(1)} + g^2P^{(2)} + \cdots\ , \tag{2.21}$$

hence Eqn. (2.13) translates to:

$$\frac{\partial}{\partial t}P^{(0)} = -\mathrm{i}(\mathcal{H}_S^{\times} + L)P^{(0)} \ , \tag{2.22}$$

$$\frac{\partial}{\partial t}P^{(1)} = -\mathrm{i}(\mathcal{H}_S^{\times} + L)P^{(1)} + A_g P^{(0)} \ , \tag{2.23}$$

$$\frac{\partial}{\partial t}P^{(2)} = -\mathrm{i}(\mathcal{H}_S^{\times} + L)P^{(2)} + A_g P^{(1)} \ , \tag{2.24}$$

$$\cdots$$

$$\frac{\partial}{\partial t}P^{(n)} = -\mathrm{i}(\mathcal{H}_S^{\times} + L)P^{(n)} + A_g P^{(n-1)} \ . \tag{2.25}$$

The solution for the uncoupled system $P^{(0)}$ is simply given by

$$P^{(0)}(t) = U(t)\rho^S(0)\frac{1}{\pi N}e^{-|\alpha|^2/N} \ . \tag{2.26}$$

In principle it is possible to solve this series term by term. However, we are interested in the state of the system and not the oscillator, which makes things much easier: We use the boundary condition where $\alpha^k P^{(n)}(\alpha) \underset{\alpha\to\infty}{\longrightarrow} 0$ for all k, n. This is justified since the oscillator can be expected not to deviate by too much from a thermal, Gaussian state, and in any case should not occupy extreme high-energy states. Therefore, performing the integration $\int d^2\alpha \equiv \int_\alpha$ on Eqn. (2.23-2.25) yields

$$\frac{\partial}{\partial t}\int_\alpha P^{(1)} = -\mathrm{i}\mathcal{H}_S^{\times}\int_\alpha P^{(1)} - \mathrm{i}V^{\times}\underbrace{\int_\alpha (\alpha+\alpha^*)P^{(0)}}_{\to 0} \ , \tag{2.27}$$

$$\frac{\partial}{\partial t}\int_\alpha P^{(2)} = -\mathrm{i}\mathcal{H}_S^{\times}\int_\alpha P^{(2)} - \mathrm{i}V^{\times}\int_\alpha (\alpha+\alpha^*)P^{(1)} \ , \tag{2.28}$$

$$\cdots$$

$$\frac{\partial}{\partial t}\int_\alpha P^{(n)} = -\mathrm{i}\mathcal{H}_S^{\times}\int_\alpha P^{(n)} - \mathrm{i}V^{\times}\int_\alpha (\alpha+\alpha^*)P^{(n-1)} \ . \tag{2.29}$$

The initial condition is $\int_\alpha P^{(n>0)}(t=0) = 0$, *i.e.* at time $t = 0$ the system and the mode are factorized, and the mode is in the thermal state, which gives

$$\int_\alpha P^{(1)}(\alpha, t) = 0 \tag{2.30}$$

for all times. The first contribution in the expansion therefore comes from $\int_\alpha P^{(2)}(\alpha, t) \neq 0$, which is 2^{nd} order in the coupling constant g. This is in analogy to the usual

TCL treatment, where the influence of the environment also enters at the 2^{nd} order in the coupling constant. In order to solve Eqn. (2.28) we first need to evaluate $\int_\alpha(\alpha+\alpha^*)P^{(1)}$, which can be done by invoking the following mathematical procedure: (i) multiply Eqn. (2.23) by α or α^* from the left; (ii) perform the $\int_\alpha$ integral; (iii) integrate by parts all terms possessing a derivative. The sequence of these steps yields the following two equations:

$$\left[\frac{\partial}{\partial t}+\mathrm{i}\omega+\frac{1}{2}\gamma+\mathrm{i}\mathcal{H}_S^\times(t)\right]\int_\alpha \alpha P^{(1)}=\int_\alpha \alpha A_g(t)P^{(0)}\ , \tag{2.31}$$

$$\left[\frac{\partial}{\partial t}-\mathrm{i}\omega+\frac{1}{2}\gamma+\mathrm{i}\mathcal{H}_S^\times(t)\right]\int_\alpha \alpha^* P^{(1)}=\int_\alpha \alpha^* A_g(t)P^{(0)}\ , \tag{2.32}$$

which after a bit of algebra and ODE solving yield a solution for $\int_\alpha P^{(1)}$. Substituting this solution into Eqn. (2.28) then results in

$$\begin{aligned}\int_\alpha P^{(2)}=-U(t)\int_0^t dt'\int_0^{t'} dt'' e^{-\frac{1}{2}\gamma(t'-t'')}\tilde{V}^\times(t')\times\\ \Big[(2N+1)\cos[\omega(t'-t'')]\tilde{V}^\times(t'')\\ -\mathrm{i}\sin[\omega(t'-t'')]\tilde{V}^\circ(t'')\Big]\rho^S(0)\ .\end{aligned} \tag{2.33}$$

Here, the notation $\tilde{V}^\times,\tilde{V}^\circ$ denotes operators in the Heisenberg picture,

$$\tilde{V}(t)\equiv U^{-1}(t)V(t)U(t)\ , \tag{2.34}$$

and V° is given in Eqn. (2.18).

At this point we note that the influence functional $\Theta(t)$ up to second-order in g, is then given by Eqn. (2.33) and

$$U(t)\Theta(t)\rho^S(0)=g^2\int_\alpha P^{(2)}+O(g^4). \tag{2.35}$$

That is, if we write $\Theta=\Theta_2+\Theta_4+\cdots$ we get

$$\begin{aligned}\Theta_2=-g^2\int_0^t dt'\int_0^{t'} dt'' e^{-\frac{1}{2}\gamma(t'-t'')}\tilde{V}^\times(t')\times\\ \Big[(2N+1)\cos[\omega(t'-t'')]\tilde{V}^\times(t'')\\ -\mathrm{i}\sin[\omega(t'-t'')]\tilde{V}^\circ(t'')\Big]\ .\end{aligned} \tag{2.36}$$

We proceed by showing that this provides a highly accurate solution for the single mode case in the weak-coupling limit. We shall then generalise the technique to an environment consisting of a (quasi)continuous bath of oscillators. In Sec. 2.5 we sketch the derivation of higher-order terms in the perturbation series.

2.3.2 Example: the (damped) Rabi model

The Rabi model, consisting of a coupled 2LS to a harmonic oscillator, represents perhaps the most basic and ubiquitous compound quantum system. Focussing only on the dynamics of the 2LS and tracing over the oscillator then results in arguably the conceptually most simple and yet a highly non-trivial open systems problem. Let us consider the Rabi Hamiltonian

$$\mathcal{H} = \frac{\epsilon}{2}\sigma_z + \frac{\Delta}{2}\sigma_x + \omega a^\dagger a + g(a + a^\dagger)\sigma_z + \mathcal{H}_{EU} + \mathcal{H}_U \ , \tag{2.37}$$

where σ_i are the usual Pauli matrices referring to the 2LS, *i.e.* $\sigma_z = |1\rangle\langle 1| - |0\rangle\langle 0|$, $\sigma_x = |0\rangle\langle 1| + |1\rangle\langle 0|$. In this case, we immediately find that the matrices $\mathcal{H}_S^\times, V^\times, V^\circ$ are given by:

$$\mathcal{H}_S^\times \equiv \frac{1}{2}\begin{pmatrix} 0 & -\Delta & \Delta & 0 \\ -\Delta & -2\epsilon & 0 & \Delta \\ \Delta & 0 & 2\epsilon & -\Delta \\ 0 & \Delta & -\Delta & 0 \end{pmatrix} \ , \tag{2.38}$$

$$V^\times = \begin{pmatrix} 0 & 0 & 0 & 0 \\ 0 & -2 & 0 & 0 \\ 0 & 0 & 2 & 0 \\ 0 & 0 & 0 & 0 \end{pmatrix} \ , \tag{2.39}$$

$$V^\circ = \begin{pmatrix} -2 & 0 & 0 & 0 \\ 0 & 0 & 0 & 0 \\ 0 & 0 & 0 & 0 \\ 0 & 0 & 0 & 2 \end{pmatrix} \ , \tag{2.40}$$

when operating on the vector $\{|00\rangle, |01\rangle, |10\rangle, |11\rangle\}^\dagger$. Substituting these into Eqn. (2.36), we obtain an unwieldy analytical expression for $\Theta_2(t)$, which can give us insight if examined in the eigenbasis of the system (the $\mathcal{H}_S^\times$ eigenbasis). If the Hamiltonian $\mathcal{H}_S$ has eigenvectors $|\nu\rangle$ with corresponding eigenvalues λ_ν, then the eigenvectors of $\mathcal{H}_S^\times$ is $|\mu\nu\rangle$ with the corresponding eigenvalue $\lambda_\mu - \lambda_\nu$. In our case, the Hamiltonian

has two eigenstates $|\pm\rangle$, with corresponding eigenvalues $\pm\frac{1}{2}\sqrt{\epsilon^2+\Delta^2}$. Thus $\mathcal{H}_S^\times$ has two finite ($\pm\sqrt{\epsilon^2+\Delta^2}\}$) and two vanishing eigenvalues. In the subspace of the vanishing eigenvalue, one of the eigenvectors is the identity matrix (in vectorised form) $\sim |{+}{+}\rangle + |{-}{-}\rangle$. It is customary in the Rabi model to choose this as one of the eigenvectors, thus naturally defining the other eigenvector as $\sim |{+}{+}\rangle - |{-}{-}\rangle$ (*i.e.* $\tilde{\sigma}_z$ in the energy eigenbasis). In this basis, the real terms on the diagonal of $\Theta(t\to\infty)$ that are proportional to t and correspond to the finite eigenvectors ($|\pm\mp\rangle$), are both equal to the dephasing rate, *i.e.* the decay rate of the off-diagonal elements of the density matrix (in the energy eigenbasis). The one corresponding to the $\sim |{+}{+}\rangle - |{-}{-}\rangle$ eigenvector is the relaxation rate, *i.e.* the rate of which the diagonal elements of the density matrix decay from their initial values to their steady-state values. These rates are given by

$$\Gamma_{\text{relax}} = g^2 \coth\left(\frac{\beta\omega}{2}\right)\frac{\Delta^2}{\Omega^2}\left[\frac{\gamma}{(\frac{\gamma}{2})^2+(\Omega-\omega)^2}+\frac{\gamma}{(\frac{\gamma}{2})^2+(\Omega+\omega)^2}\right] , \tag{2.41}$$

$$\Gamma_{\text{dephase}} = \frac{1}{2}\Gamma_{\text{relax}} + 2g^2\coth\left(\frac{\beta\omega}{2}\right)\frac{\epsilon^2}{\Omega^2}\frac{\gamma}{(\frac{\gamma}{2})^2+\omega^2} , \tag{2.42}$$

where $\Omega = \sqrt{\epsilon^2+\Delta^2}$ is the Rabi frequency. Note that in the limit $\gamma \to 0$, *i.e.* no damping on the oscillator from the wider environment or universe, we recover the standard weak-coupling Lindblad master equation result for relaxation and dephasing, given in Eqns. (2.110-2.111) of Appendix B. The imaginary parts on the diagonal of $\Theta(t)$ correspond to the Lamb shift Hamiltonian, given by

$$\mathcal{H}_{LS} = \frac{1}{2}\tilde{\sigma}_z g^2 \coth\left(\frac{\beta\omega}{2}\right)\frac{\Delta^2}{\Omega^2}\times \left[\frac{\Omega-\omega}{(\frac{\gamma}{2})^2+(\Omega-\omega)^2}+\frac{\Omega+\omega}{(\frac{\gamma}{2})^2+(\Omega+\omega)^2}\right] , \tag{2.43}$$

where $\tilde{\sigma_z}$ is given by writing the system Hamiltonian, *i.e.* the first two terms in Eqn. (2.37) in its diagonal basis

$$\tilde{\mathcal{H}}_S = \frac{1}{2}\Omega\tilde{\sigma}_z . \tag{2.44}$$

Again, in the limit $\gamma \to 0$ we recover the "standard" Lamb shift given in Eqn. (2.106). Furthermore, we can extract the steady state of the system at long times: At times much larger than the relaxation time, the system tends to the state

$$\rho(t \gg \Gamma_{\text{relax}}^{-1}) \to \frac{1}{2} - \frac{1}{2}\tilde{\sigma}_z \frac{2\Omega\omega}{(\frac{\gamma}{2})^2 + \Omega^2 + \omega^2} \tanh\left(\frac{\beta\omega}{2}\right) . \tag{2.45}$$

This is indeed only the expected thermal system state when $\gamma \to 0$ and $\omega \to \Omega$, *i.e.* no damping and when oscillator and system are resonant. However, one should take this limit with caution, because for vanishing damping, $\gamma \to 0$ the relaxation time $\Gamma_{\text{relax}}^{-1}$ tends to infinity and the system will thus never actually reach this state. In Fig. 2.2 we plot the effective temperature, that is, the temperature T_{eff} given by equating $\exp[-\tilde{\mathcal{H}}_S/k_{\text{B}}T_{\text{eff}}]$ with Eqn. (2.45), as a function of the ratio of the two frequencies ω/Ω. On the same figure we plot the relaxation rate for the same parameters, showing a Lorentzian peak in efficiency near resonance.

We note that in general the effective temperature differs from the temperature of the universe. In order to explain this apparent discrepancy, we examine Eqn. (2.45): The universe is only directly coupled to the oscillator which has energy levels spacing of ω, this accounts for the term $\tanh(\frac{\beta\omega}{2})$ which is different from the expected $\tanh(\frac{\beta\Omega}{2})$. This term decreases (increases) the effective temperature T_{eff} when the mode is blue-shifted (red-shifted) with respect to the Rabi frequency Ω. The prefactor

$$\frac{2\Omega\omega}{(\frac{\gamma}{2})^2 + \Omega^2 + \omega^2} = 1 - \frac{(\Omega - \omega)^2 + (\frac{\gamma}{2})^2}{(\frac{\gamma}{2})^2 + \Omega^2 + \omega^2} \tag{2.46}$$

is maximized when on resonance ($\omega = \Omega$). In the detuned case, in order to extract energy from the TLS, the universe exchanges energy with the oscillator to match the detuning. This adds uncertainty to the system effectively increasing the temperature. The environment-universe coupling γ adds additional uncertainty.

We also note that in this scheme we do not keep track of the environment, instead we trace over it. The joint thermal state of system and environment is proportional

to $\exp[-\beta(\mathcal{H}_S + \mathcal{H}_E + \mathcal{H}_I)]$, *i.e.* the system and environment are entangled, and defining a temperature for just one subsystem is questionable.

The example we discuss in this section is formally equivalent to the reaction coordinate[87–89] or structured environment[90–93] model in the weak coupling and weak damping regime. Here, the reaction coordinate model maps the problem to one with an effective spectral density with a Lorentzian peak, instead of the 'universe'. This yields the same rates as Eqns. (2.41-2.43) except for the "counter rotating" terms $\sim (\Omega + \omega)^{-n}$ (which are typically small). Interestingly however, this nice agreement only extends to the real part of the response function, $D(t)$, which determines the damping rates. By contrast, the modified spectral density of the reaction coordinate method does not account for corrections to the imaginary part $D_1(t)$, which yields the long time asymptotic behaviour of the system.

To ensure that our approach does indeed deliver the correct steady state, we have made a comparison with an exact numerical simulation of the dynamics given by Hamiltonian (2.37) (with $\mathcal{H}_{EU} + \mathcal{H}_U$ replaced by a Lindblad dissipator). Technically this is done by cutting-off the oscillator's Hilbert space to a finite number, large enough to ensure we fully capture the state of the oscillator. We obtain near-perfect agreement between Eqn. (2.45) and a purely numerical simulation in the weak coupling regime.

Further, to check the dynamics, in Fig. 2.3 we plot a comparison between Eqn. (2.8) with $\Theta(t)$ approximated by $\Theta_2(t)$ given in Eqn. (2.36), and exact numerical simulation, again showing in the weak-coupling regime a very good agreement between the two.

2.4 Extending the analysis to a multimode environment

In the previous section the 'environment' consisted of only one single harmonic oscillator. However, the extension to multiple oscillators is straightforward. Up to second order in the system-environment coupling, each environmental mode contributes to

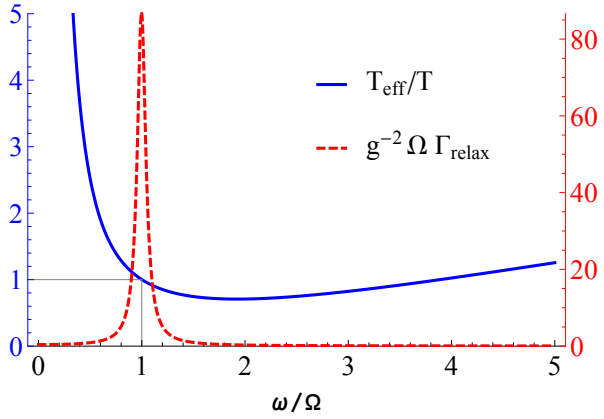

Figure 2.2: The apparent effective temperature of the system as defined by Eqn. (2.45) (blue), and the relaxation constant $\Omega\Gamma_{\text{relax}}/g^2$, as in Eqn. (2.41), (dashed red) as a function of ω/Ω. Other parameters are: $\beta\Omega = 1$, $\gamma/\omega = 0.1$ and $\epsilon = 0$ (no bias).

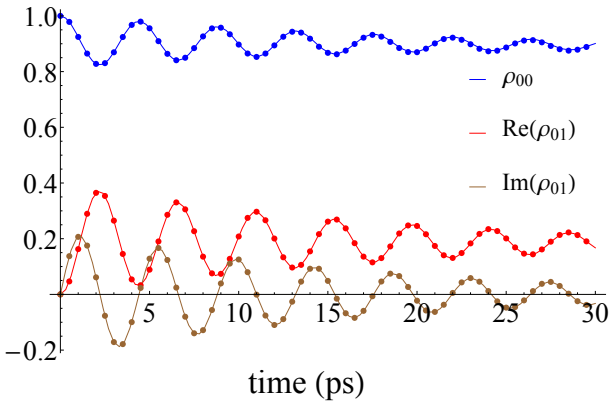

Figure 2.3: A comparison between the dynamics given by Eqn. (2.8) with $\Theta(t)$ approximated by Eqn. (2.36) (solid) and exact numerical simulation of Hamiltonian (2.37) dynamics (dotted). The Parameters used here are $\Delta = 0.6$ ps^{-1} , $\gamma = 0.8$ ps^{-1} , $\epsilon = 1.3$ ps^{-1} , $\omega = 0.2$ ps^{-1} , $T = 7.638$ K , $g = 0.03$ ps^{-1} . The approach to equilibrium is not prominent in this case because of the long relaxation time $\Gamma^{-1}_{\text{relax}} \approx$ 3000ps. The dephasing time is much shorter with $\Gamma^{-1}_{\text{dephase}} \approx 17$ ps.

the influence functional $\Theta_2(t)$ independently. The difference is that now the environment Hamiltonian $\mathcal{H}_E$ has a set of modes $a^\dagger_{\nu,k}$, each of them is independently damped with a rate $\gamma_{\nu,k}$, and we allow ourselves to have multiple independent environments in the system. The change in the Hamiltonian from the previous section is that now we have

$$\mathcal{H}_E = \sum_{\nu,k} \omega_{\nu,k} a^\dagger_{\nu,k} a_{\nu,k} \ , \tag{2.47}$$

$$\mathcal{H}_I(t) = \sum_{\nu} S_\nu(t) \sum_k g_{\nu,k}(a_{\nu,k} + a^\dagger_{\nu,k}) \ . \tag{2.48}$$

Here S_ν is a system operator, and the creation and annihilation operators satisfy the usual relations $[a_{\nu,k}, a^\dagger_{\nu',k'}] = \delta_{\nu,\nu'}\delta_{k,k'}$, and $[a_{\nu,k}, a_{\nu',k'}] = [a^\dagger_{\nu,k}, a^\dagger_{\nu',k'}] = 0$. The derivation for this case is very similar to the single mode case and is given in full detail in Appendix A. Once more, the influence of the bath on the system's dynamics is given by Eqn. (2.8), where now

$$\Theta_2(t) = -\sum_\nu \int_0^t dt' \int_0^{t'} dt'' \tilde{S}^\times_\nu(t') \tilde{R}_{\nu\nu}(t', t'') \ , \tag{2.49}$$

with

$$\tilde{R}_{\nu\nu}(t', t'') = \alpha^\nu_\gamma(t' - t'') \tilde{\vec{S}}_\nu(t'') - [\alpha^\nu_{\gamma 1}(t' - t'')]^* \tilde{\bar{S}}_\nu(t'') \tag{2.50}$$

$$= D^\nu_\gamma(t' - t'') \tilde{S}^\times_\nu(t'') + \mathrm{i} D^\nu_{\gamma 1}(t' - t'') \tilde{S}^\circ_\nu(t'') \ . \tag{2.51}$$

Here, the $\tilde{S}$ are given by Eqn. (2.34), and we adapt our notation to match that common in the literature on phonon baths, introducing the (damped) phonon response function defined as

$$\alpha^\nu_\gamma(\tau) = \sum_\nu \sum_k g^2_{\nu,k} e^{-\frac{1}{2}\gamma_{\nu,k}\tau} \frac{\cosh(\frac{\beta\omega_k}{2} - \mathrm{i}\omega_k\tau)}{\sinh(\frac{\beta\omega_k}{2})}$$

$$\equiv D^\nu_\gamma(\tau) + \mathrm{i} D^\nu_{1\gamma}(\tau) \ . \tag{2.52}$$

Here $D_\gamma(\tau)$ and $D_{1\gamma}(\tau)$ are the (damped) dissipation and response kernels, respectively. In terms of the spectral density function,

$$J_\nu(\omega) = \sum_k g^2_{\nu,k} \delta(\omega - \omega_{\nu,k}) \ , \tag{2.53}$$

we can express the response function as

$$\alpha_\gamma^\nu(\tau) = \int_0^\infty d\omega e^{-\frac{1}{2}\gamma_\nu(\omega)\tau} J_\nu(\omega) \frac{\cosh(\frac{\beta\omega}{2} - \mathrm{i}\omega\tau)}{\sinh\left(\frac{\beta\omega}{2}\right)} \ , \tag{2.54}$$

where $\gamma_\nu(\omega)$ is the damping rate of modes with angular frequency $\omega_{\nu,k}$. If the modes are not damped, *i.e.* for $\gamma_\nu(\omega) = 0$, we recover the standard response function from the literature[4] $\alpha(\tau) = D(\tau) + \mathrm{i}D_1(\tau)$.

Interestingly, for the case of $\gamma(\omega) = 0$, *i.e.* when there is no external universe, the result (2.49) directly relates to the well-studied time-convolutionless projection operator technique (TCL) to second order in the system-environment coupling[§] , *i.e.* the TCL2 generator (Eqn. 1.84), with (going to interaction picture)

$$\Theta_2(t) = \int_0^t d\tau \mathcal{K}_2(\tau) \ . \tag{2.55}$$

Notice that for the TCL map to become completely positive, one needs to employ the so called "secular approximation"[§§], to discard oscillating terms. For the P-mat method, any oscillating terms in $\mathcal{K}_2(t)$ are bounded at long time after integrating the RHS of (2.55), while the constant terms are proportional to t at long time, thus this naturally captures the secular approximation at long times, even when not adding it 'by hand'.

It is interesting to note that the thermalisation of the immediate environment by the wider universe is fully captured by switching to the above generalised form of the response kernel (2.52)[§§§]. At $T = 0$ our expression is in full agreement with the previously derived zero temperature response function of the damped spin-boson model given in Ref. [82]. We suggest that the same kernel redefinition might also be applicable to other methods of studying open quantum systems, giving a simple recipe to adding a wider universe on top of a standard open system.

[§]Note that this analysis here was only done for the case of *independent baths*, where we have $[a_{\nu,k} \ , \ a^\dagger_{\nu',k'}] = \delta_{\nu\nu'}\delta_{kk'}$

[§§]see Chapter 1.3.

[§§§]within a perturbative treatment to second order, higher orders give additional corrections, see Sec. 2.5 .

2.4.1 Example: The Spin-Boson Model

To apply our generalized multimode technique to a particular example, we look at the well studied case of the (biased) spin-boson model with the following Hamiltonian:

$$\mathcal{H}_{SE} = \frac{1}{2}\epsilon\sigma_z + \frac{1}{2}\Delta\sigma_x + \sum_k \omega_k a_k^\dagger a_k + \sigma_z \sum_k g_k(a_k + a_k^\dagger) \ . \tag{2.56}$$

In this case, just like for the Rabi model, the system is two-dimensional and its P vector has four components $(\sigma_x, \sigma_y, \sigma_z, \mathbb{1})$, and $\mathcal{H}_S^\times, V^\times, V^\circ$ are again given by Eqns. (2.38-2.40). Since we have already calculated the relaxation and dephasing rates for the single mode case, showing that the different modes contribute independently for $\Theta_2(t)$, we can immediately write down the following expressions for the relaxation rates: we only need to add a summation $\sum_k$ over the different modes to Eqns. (2.41-2.42),

$$\Gamma_{\text{relax}} = \sum_k g_k^2 \coth\left(\frac{\beta\omega_k}{2}\right)\frac{\Delta^2}{\Omega^2}\times \tag{2.57}$$
$$\left[\frac{\gamma_k}{(\frac{\gamma_k}{2})^2 + (\Omega-\omega_k)^2} + \frac{\gamma_k}{(\frac{\gamma_k}{2})^2 + (\Omega+\omega_k)^2}\right] ,$$
$$\Gamma_{\text{dephase}} = \frac{1}{2}\Gamma_{\text{relax}} + 2\sum_k g_k^2 \coth\left(\frac{\beta\omega_k}{2}\right)\frac{\epsilon^2}{\Omega^2}\frac{\gamma_k}{(\frac{\gamma_k}{2})^2 + \omega_k^2} \ . \tag{2.58}$$

We note that, as discussed at the end of Section 2.4, in the limit of $\gamma_k \to 0$, we recover the known weak-coupling rates, cf. Ref. [95] or Appendix B. The second part of Eqn. (2.58) is known as the pure dephasing constant.

Below we study the no-bias case, setting $\epsilon = 0$: the system Hamiltonian ($\mathcal{H}_S^\times$ in our language) is static, hence the propagator U is given by $U = \exp[-\mathrm{i}\mathcal{H}_S^\times t]$. To calculate $\Theta_2(t)$, we can make a change of variables in the double integral $\int_0^t dt' \int_0^{t'} dt'' = \int_0^t d\tau \int_\tau^t dt'$, with $\tau = t' - t''$, to get the expression in the eigenbasis of the system Hamiltonian $\mathcal{H}_S^\times$,

$$\Theta_2(t) = \Theta_{\text{relax}}(t) + \Theta_{\text{LS}}(t) + \Theta_{\text{th}}(t) + \Theta_{\text{RW}}(t) \tag{2.59}$$

with

$$\Theta_{\text{relax}} = -2\int_0^t d\tau D_\gamma(\tau)(t-\tau)\cos\Delta\tau \begin{pmatrix} 2 & 0 & 0 & 0 \\ 0 & 1 & 0 & 0 \\ 0 & 0 & 1 & 0 \\ 0 & 0 & 0 & 0 \end{pmatrix} , \tag{2.60}$$

$$\Theta_{\text{LS}} = -2\int_0^t d\tau D_\gamma(\tau)(t-\tau)\sin\Delta\tau \begin{pmatrix} 0 & 0 & 0 & 0 \\ 0 & 0 & 1 & 0 \\ 0 & -1 & 0 & 0 \\ 0 & 0 & 0 & 0 \end{pmatrix} , \tag{2.61}$$

$$\Theta_{\text{th}} = 4\int_0^t d\tau D_{1\gamma}(\tau)(t-\tau)\sin\Delta\tau \begin{pmatrix} 0 & 0 & 0 & 1 \\ 0 & 0 & 0 & 0 \\ 0 & 0 & 0 & 0 \\ 0 & 0 & 0 & 0 \end{pmatrix} , \tag{2.62}$$

$$\Theta_{\text{RW}} = -2\int_0^t d\tau D_\gamma(\tau)\frac{1}{\Delta}\sin\Delta(t-\tau)\times \begin{pmatrix} 0 & 0 & 0 & 0 \\ 0 & \cos\Delta t & -\sin\Delta t & 0 \\ 0 & -\sin\Delta t & -\cos\Delta t & 0 \\ 0 & 0 & 0 & 0 \end{pmatrix} . \tag{2.63}$$

In the above expression, Θ_{relax} induces the relaxation and decoherence, Θ_{LS} induces the Lamb-shift, and Θ_{th} steers the system towards the thermal state. Θ_{RW} is the rotating term that is ignored in the secular approximation. If one is interested in times $t \gg \tau_b$ much longer than the memory of the bath $D(t > \tau_b) \to 0$, it is justified to let the upper limit of the integrals go to infinity. For this case it is most insightful to examine this result in terms of the standard Lindblad master equation, given by taking the Markov and secular approximation on the TCL2 generator: In the standard approach, remarkably one gets exactly the same expressions as the above Eqn. (2.59) [without Eqn. (2.63)], but with an interesting substitution:

$$t - \tau \to t \ . \tag{2.64}$$

The terms which are *not* proportional to t capture non-Markovian contributions, giving information about the bath's *reorganization time*. Interestingly, each of the

environmental effects possesses its own timescale, and these are estimated by

$$t^R_{\rm relax} = \frac{\int_0^\infty \tau d\tau D_\gamma(\tau)\cos\Delta\tau}{\int_0^\infty d\tau D_\gamma(\tau)\cos\Delta\tau}\ , \tag{2.65}$$

$$t^R_{\rm LS} = \frac{\int_0^\infty \tau d\tau D_\gamma(\tau)\sin\Delta\tau}{\int_0^\infty d\tau D_\gamma(\tau)\sin\Delta\tau}\ , \tag{2.66}$$

$$t^R_{\rm th} = \frac{\int_0^\infty \tau d\tau D_{1\gamma}(\tau)\sin\Delta\tau}{\int_0^\infty d\tau D_{1\gamma}(\tau)\sin\Delta\tau}\ . \tag{2.67}$$

It is noteworthy that the reorganization times can be negative. This could happen when, for example, initially for $t \lesssim \tau_b$ the dephasing process, which includes a non-Markovian component, is more aggressive than at later times when it assumes a stable value. Then, as the aggressive decay stops, the population of the system has fallen by a greater amount than it would have done under the stable, long lived decay process. Thus the system appears as if it has been evolving under the stable dephasing rate for a longer time than it actually has, and hence the negative reorganization time. We note that the terms (2.65-2.67) in the limit $\gamma \to 0$ are known in the literature as those leading to the slippage of initial conditions, and are important for preserving the positivity of the reduced density matrix.[42,43]

The steady-state of the system is given by

$$\rho(t \gg \Gamma^{-1}_{\rm relax}) \to \frac{1}{2} + \frac{1}{2}\sigma_x \frac{\int_0^\infty d\tau D_{1\gamma}(\tau)\sin\Delta\tau}{\int_0^\infty d\tau D_\gamma(\tau)\cos\Delta\tau}\ . \tag{2.68}$$

A comparison between the standard Markovian Lindblad master equation, the current method and exact numerical simulation for the case of a super-Ohmic environment is shown in Fig. 2.4. The QUAPI technique[62–64] is used as an exact numerical benchmark curve: Our calculation uses nine kernel time steps, covering a total kernel memory time of 2 ps and is fully converged. The Lindblad weak-coupling approach is given in Appendix B. Clearly, our method's non–Markovian nature results in an impressive improvement over the standard Lindblad ME approach. For this particular comparison, there is no wider universe involved, $\gamma(\omega) = 0$. However, a key strength of the current formulation is that it is trivial to include a wider universe, which simply enters in the form of an exponential cut–off to the response function.

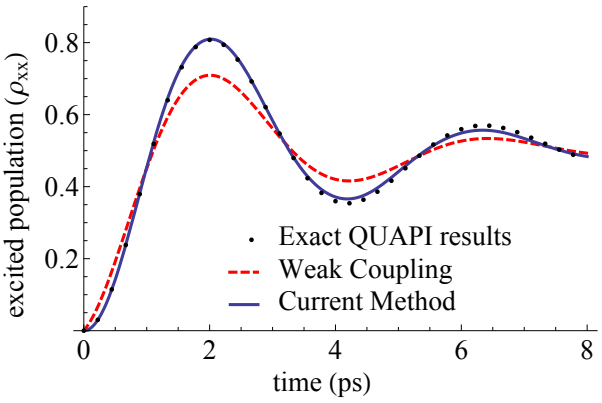

Figure 2.4: A comparison between the dynamics given by Eqn. 2.8 (solid), standard Born-Markov weak-coupling master equation approach (dashed) given in Appendix 2.6, and exact QUAPI simulation of the model (dotted). For details of the calculations, see main text. The parameters for this figure are taken from Ref. [96]: $\Delta = \pi/2$ ps^{-1} , $\gamma(\omega) = 0$, $\epsilon = 0$, $T = 50$ K , $J(\omega) = \alpha\omega^3 e^{-\omega^2/\omega_c^2}$, $\alpha = 0.00675$ ps^{-2} , $\omega_c = 2.2$ ps^{-1} .

We note that this method allows us to easily study the case where the spectral density has several discrete sharp peaks as well as a smooth background, which is believed to be the case in many (if not all) systems studied in quantum biology[66,97]. In this case the response function vanishes very slowly, which makes an exact numerical treatment extremely demanding, as a long history of the system needs to be tracked. In some papers, such as Ref. [97] this issue is resolved by approximating a delta-function peak in the spectral density as a Lorentzian with a finite width. We note that if one allows this single peak to be damped, then in light of Eqn. (2.45), this mode drives the system to an effective temperature different from the initial temperature of the environment T. Hence replacing discrete modes with Lorentzian distributions added to a continuous spectral density may in some parameter regimes become a questionable approximation. By contrast, the additive property of modes to the influence functional $\Theta_2(t)$ here allows us to combine a discrete set of modes with a smooth background by taking

$$\Theta(t) = \Theta_{\text{smooth}}(t) + \Theta_{\text{discrete}}(t) \ . \tag{2.69}$$

As an example for this, let us study the spin boson model with a smooth background of oscillators plus a more strongly coupled discrete peak of frequency ω_s in

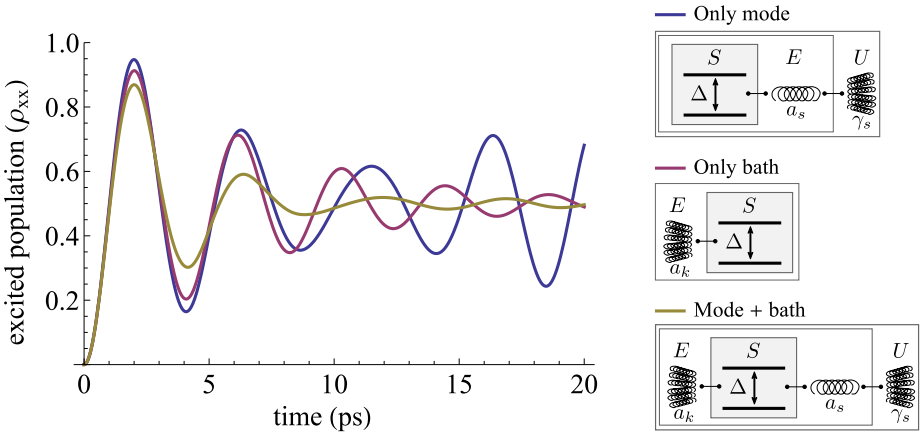

Figure 2.5: A comparison of quantum dynamics in a two level system that is coupled individually to a single mode, or to a continuous bath, or to a combination of the two. The parameters used here are the same as the ones of Fig. 2.4, but with a smaller coupling $\alpha = 0.0027$ ps^{-2}, and with an added detuned single peak according to Hamiltonian (2.70) with $g_s = 0.1$ ps^{-1}, $\omega_s = 1.02\Delta$. The mode is damped with rate $\gamma_s = 0.05$ ps^{-1}.

the environment. We single out this peak and label it henceforth with a subscript s, writing the system-environment Hamiltonian as

$$\begin{aligned}\mathcal{H}_{SE} =& \frac{1}{2}\epsilon\sigma_z + \frac{1}{2}\Delta\sigma_x + \sum_k \omega_k a_k^\dagger a_k + \omega_s a_s^\dagger a_s \\ &+ \sigma_z \left[\sum_k g_k(a_k + a_k^\dagger) + g_s(a_s^\dagger + a_s)\right].\end{aligned} \tag{2.70}$$

In Fig. 2.5 we start with the system in its ground state and plot the excited state population ρ_{xx} as a function of time, for the cases where the system is only coupled to a smooth environment ($g_s \to 0$), only coupled to a single mode ($\{g_k\} \to 0$), and for the combined case.

Due to the non-Markovian nature of this method, we are able to capture the revival effect[98] of the Rabi model. These revivals can be damped via a combination of two mechanisms: Either the mode itself is coupled to a wider environment damping it, or there might be an additional continuous bath directly damping the system. In Fig. 2.6 we plot the first case, where the environment consists of a single damped mode. The damping of the mode induces relaxation rate, Γ_{relax}, given by Eqn. (2.41). We also plot the decay envelope, $\frac{1}{2} + \frac{1}{2}\exp\Theta_{\text{relax}}(t)$, for this case, as well as the

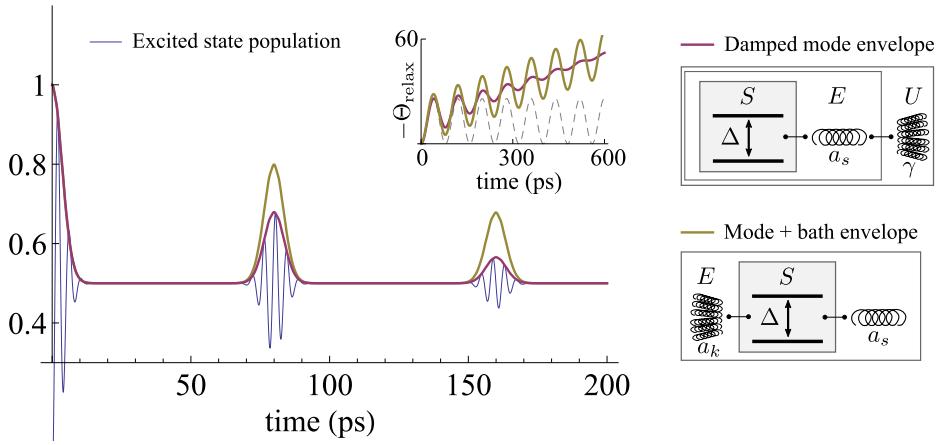

Figure 2.6: Long time population of a TLS (blue), illustrating the revivals which occur when a discrete system is coupled to a single (damped) oscillator mode. The corresponding relaxation envelope (purple) and that of an undamped mode but where the system is coupled to a bath (yellow) are also shown. Here, we have chosen a bath coupling strength to obtain the same average relaxation rate for both cases (c.f. inset), even though this does not become apparent during the first two revivals. The parameters in this figure are chosen to show revivals, so that the mode is almost resonant with the TLS and the damping is weak, $\Delta = \pi/2$ ps^{-1}, $\gamma = 0.001$ ps^{-1}, $\epsilon = 0$, $\omega_s = 1.05\Delta$, $T = 50$ K, and $g_s = 0.1$ ps^{-1}. The inset shows the relaxation exponent $-\theta_{\text{relax}}(t)$ with the same parameters as the main figure but increased $\gamma = 0.01$ ps^{-1}. Here it becomes apparent that the average gradient, *i.e.* average relaxation rate, is matched. The dashed curve of the inset is for reference, indicating the frequency of revivals by setting $\gamma = 0$.

decay envelope produced by coupling of the system to a continuous bath and no damping on the mode, choosing parameters such that the relaxation rate induced by the bath Eqn. (2.58) is equal to Γ_{relax}. This second decay envelope is then given by the expression $\frac{1}{2} + \frac{1}{2}\exp[\Theta^{\text{single mode}}_{\text{relax}}(t) + \Theta^{\text{smooth}}_{\text{relax}}(t)]$. We note that the second case yields an exponential envelope to the dynamics for times $t \gg t^R_{\text{relax}}$, while for a single damped mode with damping rate γ, the envelope only becomes exponential for times $t \gg 1/\gamma$, which could be much longer. We note that the Lamb-shift given by Eqn. (2.61) also differs between the two cases, albeit in the plotted parameter regime this difference is very subtle and not shown.

2.5 Higher Order Calculation

In this section, we show how to calculate higher orders of the influence functional $\Theta(t)$ defined in Eqn. 2.8, in contrast to the 2nd order expression given so far. We also show that, in analogy to the known result of the non-hierarchical case[4], all of the odd orders vanish when the initial state factorises $\rho(0) = \rho_S(0) \otimes \rho_E^{th}$.

We start by giving a formal expression of the quantity

$$\int_\alpha \prod_{\nu,k} (\alpha_{\nu,k})^{a_{\nu,k}} (\alpha^*_{\nu,k})^{b_{\nu,k}} P^{(n)}(t) \equiv U(t) \chi_n\big(\{a_{\nu,k}\}, \{b_{\nu,k}\}; t\big) \rho^S(0) \ , \tag{2.71}$$

where $\{a_{\nu,k}\}$ and $\{b_{\nu,k}\}$ are non-negative integers. These are the different moments of $P^{(n)}$, from which we obtain our solution.

We begin by multiplying Eqn. (2.92) by $\prod_{\nu,k} (\alpha_{\nu,k})^{a_{\nu,k}} (\alpha^*_{\nu,k})^{b_{\nu,k}}$ and integrate over α. Using the relation

$$\alpha^n \frac{\partial}{\partial \alpha} = -n\alpha^{n-1} + \frac{\partial}{\partial \alpha} \alpha^n \ , \tag{2.72}$$

and the boundary condition that P vanishes at infinity faster than any power of α, we obtain for $n > 0$,

$$\begin{aligned} \left\{ \frac{\partial}{\partial t} + \mathrm{i}\mathcal{H}_S^\times + \sum_{\nu,k} \Big[\mathrm{i}\omega_{\nu,k}(a_{\nu,k} - b_{\nu,k}) + \frac{1}{2}\gamma_{\nu,k}(a_{\nu,k} + b_{\nu,k}) \Big] \right\} \times \int_\alpha \prod_{\nu,k} (\alpha_{\nu,k})^{a_{\nu,k}} (\alpha^*_{\nu,k})^{b_{\nu,k}} P^{(n)} \\ = \sum_{\nu,k} \gamma_{\nu,k} N_{\nu,k} a_{\nu,k} b_{\nu,k} \int_\alpha \prod_{\nu,k} (\alpha_{\nu,k})^{a_{\nu,k}-1} (\alpha^*_{\nu,k})^{b_{\nu,k}-1} P^{(n)} \\ + \sum_{\nu,k} \tilde{g}_{\nu,k} \int_\alpha \prod_{\nu,k} (\alpha_{\nu,k})^{a_{\nu,k}} (\alpha^*_{\nu,k})^{b_{\nu,k}} A_g^\nu(k) P^{(n-1)} \ , \end{aligned} \tag{2.73}$$

which gives

$$\begin{aligned} &\chi_n\big(\{a_{\nu,k}\}, \{b_{\nu,k}\}; t\big) = \\ &\qquad \int_0^t d\tau e^{-\sum_{\nu,k} [\mathrm{i}\omega_{\nu,k}(a_{\nu,k} - b_{\nu,k}) + \frac{1}{2}\gamma_{\nu,k}(a_{\nu,k} + b_{\nu,k})](t-\tau)} S_n(\{a_{\nu,k}\}, \{b_{\nu,k}\}; \tau) \ , \end{aligned} \tag{2.74}$$

where $U(\tau) S_n(\{a_{\nu,k}\}, \{b_{\nu,k}\}; \tau) \rho^S(0)$ is the RHS of Eqn. (2.73). Using the definition

of A_g [Eqn. (2.86)] we get the following expressions (for $n > 0$):

$$\begin{aligned} S_n(\{a_{\nu,k}\},\{b_{\nu,k}\};t) = &\sum_{\nu,k} \gamma_{\nu,k} N_{\nu,k} a_{\nu,k} b_{\nu,k} \chi_n(a_{\nu,k}-1, b_{\nu,k}-1;t) \\ &- \mathrm{i} \sum_{\nu,k} \tilde{S}^{\times}_{\nu}(t)_{\nu} \tilde{g}_{\nu,k} \Big[\chi_{n-1}(a_{\nu,k}+1;t) + \chi_{n-1}(b_{\nu,k}+1;t) \\ &\qquad + \frac{a_{\nu,k}}{2}\chi_{n-1}(a_{\nu,k}-1;t) + \frac{b_{\nu,k}}{2}\chi_{n-1}(b_{\nu,k}-1;t) \Big] \\ &- \frac{\mathrm{i}}{2} \sum_{\nu,k} \tilde{S}^{\circ}_{\nu}(t) \tilde{g}_{\nu,k} \left[a_{\nu,k}\chi_{n-1}(a_{\nu,k}-1;t) - b_{\nu,k}\chi_{n-1}(b_{\nu,k}-1;t) \right] . \end{aligned} \tag{2.75}$$

In the above expression we used $\tilde{V}(t)$ which is defined by Eqn. (2.34), and the abbreviated notation $\chi_n(a_{\nu,k}-1;t) = \chi_n(a_{1,1},\cdots,a_{\nu,k}-1,\cdots,b_{1,1},b_{1,2},\cdots;t)$.

Complemented by the initial condition

$$\chi_0\big(\{a_{\nu,k}\},\{b_{\nu,k}\}\big) = \begin{cases} \prod_{\nu,k}(a_{\nu,k}!)(N_{\nu,k})^{a_{\nu,k}} & \forall(\nu,k), a_{\nu,k} = b_{\nu,k} \\ 0 & \text{otherwise} \end{cases} \tag{2.76}$$

we can in principle get the expression for Eqn. (2.71). From examination of Eqns. (2.74-2.76) it is evident that if $n + \sum_{\nu,k}(a_{\nu,k}+b_{\nu,k})$ is odd, then

$$\int_{\alpha} \prod_{\nu,k} (\alpha_{\nu,k})^{a_{\nu,k}} (\alpha^{*}_{\nu,k})^{b_{\nu,k}} P^{(n)} = 0. \tag{2.77}$$

This is because $\chi_n(\{a_{\nu,k}\},\{b_{\nu,k}\};t)$ is a linear function of $\chi_n(a_{\nu,k}-1,b_{\nu,k}-1;t)$, $\chi_{n-1}(a_{\nu,k}\pm 1;t)$ and $\chi_{n-1}(b_{\nu,k}\pm 1;t)$. This means that in the series $\Theta(t) = \sum_i \Theta_i(t)$, all terms with odd i vanish. As an example, in order to evaluate $\chi_2(0) = \chi_2(\{a_{\nu,k}=0\},\{b_{\nu,k}=0\};t)$ we have four "routes" that lead to a non-vanishing χ_0, *i.e.* $\chi_2(0)$ is a sum of four terms, which are calculated via:

- $\chi_2(0) \to \chi_1(a_{\nu,k}=1) \to \chi_0(0)$,
- $\chi_2(0) \to \chi_1(a_{\nu,k}=1) \to \chi_0(a_{\nu,k}=1, b_{\nu,k}=1)$,
- $\chi_2(0) \to \chi_1(b_{\nu,k}=1) \to \chi_0(0)$,
- $\chi_2(0) \to \chi_1(b_{\nu,k}=1) \to \chi_0(a_{\nu,k}=1, b_{\nu,k}=1)$.

Higher order terms scale quickly, where for $\chi_4(0)$ we have $(32+8)$ terms, where 32 of them map to quad integrals $\int_0^t dt_1 \int_0^{t_1} dt_2 \int_0^{t_2} dt_3 \int_0^{t_3} dt_4$, and 8 of them only appear when a universe is present, and correspond to 5-fold integrals.[§]

Finally, we can express the influence functional $\Theta(t)$ as

$$\Theta(t) = g^2\Theta_2 + g^4\Theta_4 + g^6\Theta_6 + \cdots \tag{2.78}$$

with

$$\Theta_2 = \chi_2(0;t) \ , \tag{2.79}$$

$$\Theta_4 = \chi_4(0;t) - \frac{\Theta_2^2}{2!} \ , \tag{2.80}$$

$$\Theta_6 = \chi_6(0;t) - \frac{\Theta_2\Theta_4 + \Theta_4\Theta_2}{2!} - \frac{\Theta_2^3}{3!} \ , \tag{2.81}$$

$$\Theta_8 = \chi_8(0;t) - \frac{\Theta_4\Theta_4 + \Theta_6\Theta_2 + \Theta_2\Theta_6}{2!} - \frac{\Theta_2\Theta_4\Theta_4 + \Theta_4\Theta_2\Theta_4 + \Theta_4\Theta_4\Theta_2}{3!} - \frac{\Theta_2^4}{4!} \ , \tag{2.82}$$

etc. Here we used $\chi(0;t) = \chi(\{a_i = 0\}, \{b_i = 0\}; t)$.

2.6 Discussion and Conclusion

We have introduced a novel method for studying a ubiquitous open quantum systems problem. Our approach differentiates between the immediate environment of the system of interest and a wider universe which effectively serves as a heat bath for this environment; this hierarchy of environments corresponds to many practical situations and is – remarkably – accomplished by a simple redefinition of the response kernel, at least in the weak-coupling case. The expressions resulting from our method are easy to evaluate numerically, and scale favourably with increasing system size. Moreover, the method still leads to soluble equations when the system of interest possesses a general time dependent Hamiltonian.

Whilst our method is limited to the weak coupling regime, it performs favourably when compared with traditional weak coupling Lindblad master equations. Its approximate analytical expressions scale well with increasing system size and permit

[§]When no universe is present, the number of terms for the first few $\chi_n(0)$ are $4, 32, 320, 3584, 43008, 540672, 7028736$.

valuable physical insight, in contrast to some numerically exact approaches. Like many recent developments in the field of open systems, see e.g. Refs. [30,80,99,100] (and with the notable exception of Ref. [101]), we do not presently have stringent criteria demarcating its precise regime of validity, which must thus be established by comparison with exact numerics. When no wider universe is present, however, we show in Chapter 3 that our technique is expected to perform well whenever other weak coupling approaches such as the time-convolutionless or the Nakajima-Zwanzig projection operator expansions[4] are valid, and we also present a criterion for validity. As an additional criterion, our treatment of the wider universe (if present) assumes that $\gamma_k \ll \omega_k$, *i.e.* each mode is weakly coupled to its heat bath.

We have benchmarked our technique against the well-studied spin boson model and the Rabi model, finding it leads to expressions that are indeed highly accurate when compared with numerically converged solutions. This remains true even for coupling strengths where a conventional standard second order Lindblad master equation begins to performs poorly. In Chapter 3 we show that it compares similarly to the time-convolutionless solution when no wider universe is present. For cases when the system-environment coupling is not sufficiently weak for the second order expansion of the interaction, we provide an explicit recipe to calculate higher orders in the perturbation series. Perhaps a unique advantage of this approach is that these two models, *i.e.* the Rabi and the spin-boson models can easily be combined even for long-time dynamics. This makes our method eminently suitable for studying the exciton energy transfer in photosynthetic or artificial molecular systems, since the coupling of the excitonic degree of freedom to both the vibrational quasi-continuum of the wider protein scaffolding as well as to specific localised vibronic modes is believed to be of crucial functional importance.

Appendix A: Multiple Modes

We start from Hamiltonian (2.1) and Eqns. (2.47-2.48). For multiple modes the density matrix is represented by Eqn. (2.6), and the operator correspondence between

ρ and $\vec{P}$ is:

$$\frac{\partial}{\partial t}\rho = -\,\mathrm{i}[H,\rho] + D(\rho) \leftrightarrow \tag{2.83}$$

$$\frac{\partial}{\partial t}\vec{P} = -\,\mathrm{i}(\mathcal{H}_S^{\times} + L)\vec{P} + \sum_{\nu}\sum_{k} g_{\nu,k} A_g^{\nu}(k)\vec{P}\ , \tag{2.84}$$

where now, similar to Eqn. (2.14), L is given by

$$L = \sum_{\nu}\sum_{k}\Bigg[\left(-\omega_{\nu,k} + \frac{\mathrm{i}}{2}\gamma_{\nu,k}\right)\frac{\partial}{\partial\alpha_{\nu,k}}\alpha_{\nu,k} + \left(\omega_{\nu,k} + \frac{\mathrm{i}}{2}\gamma_{\nu,k}\right)\frac{\partial}{\partial\alpha^*_{\nu,k}}\alpha^*_{\nu,k} + \mathrm{i}\gamma_{\nu,k}N_{\nu,k}\frac{\partial^2}{\partial\alpha_{\nu,k}\partial\alpha^*_{\nu,k}}\Bigg]\ , \tag{2.85}$$

$N_{\nu,k} = (e^{\beta\omega_{\nu,k}} - 1)^{-1}$ and $\gamma_{\nu,k} = \gamma(\omega_{\nu,k})$ is the damping rate of mode $a^{\dagger}_{\nu,k}$. The matrices $A_g^{\nu}(k)$ are given, equivalently to Eqn. (2.15), by

$$A_g^{\nu}(k) = -\mathrm{i}\left(\alpha_{\nu,k} + \alpha^*_{\nu,k} - \frac{\partial}{\partial\alpha_{\nu,k}}\right)\vec{S}_{\nu} + \mathrm{i}\left(\alpha_{\nu,k} + \alpha^*_{\nu,k} - \frac{\partial}{\partial\alpha^*_{\nu,k}}\right)\overleftarrow{S}_{\nu}\ . \tag{2.86}$$

Assuming all of the couplings $g_{\nu,k}$ are sufficiently small, at the order of $\sum_{\nu,k} g_{\nu,k} \sim g$, we can rewrite Eqn. (2.84) to become

$$\frac{\partial}{\partial t}\vec{P} = -\mathrm{i}(\mathcal{H}_S^{\times} + L)\vec{P} + g\left(\sum_{\nu,k}\tilde{g}_{\nu,k}A_g^{\nu}(k)\right)\vec{P} \tag{2.87}$$

with $g_k = g\tilde{g}_k$. Now consider the perturbative expansion

$$P = P^{(0)} + gP^{(1)} + g^2P^{(2)} + \cdots\ , \tag{2.88}$$

so that Eqn. (2.87) translates to:

$$\frac{\partial}{\partial t}P^{(0)} = -\mathrm{i}(\mathcal{H}_S^{\times} + L)P^{(0)}\ , \tag{2.89}$$

$$\frac{\partial}{\partial t}P^{(1)} = -\mathrm{i}(\mathcal{H}_S^{\times} + L)P^{(1)} + \sum_{\nu,k}\tilde{g}_{\nu,k}A_g^{\nu}(k)P^{(0)}\ , \tag{2.90}$$

$$\frac{\partial}{\partial t}P^{(2)} = -\mathrm{i}(\mathcal{H}_S^{\times} + L)P^{(2)} + \sum_{\nu,k}\tilde{g}_{\nu,k}A_g^{\nu}(k)P^{(1)}\ , \tag{2.91}$$

$$\cdots$$

$$\frac{\partial}{\partial t}P^{(n)} = -\mathrm{i}(\mathcal{H}_S^{\times} + L)P^{(n)} + \sum_{\nu,k}\tilde{g}_{\nu,k}A_g^{\nu}(k)P^{(n-1)}\ . \tag{2.92}$$

The solution for the uncoupled system $P^{(0)}$ is then equivalent to the single mode case, and is given by (assuming a factorized initial state):

$$P^{(0)}(t) = U(t)\rho^S(0)\prod_{\nu,k}\frac{1}{\pi N_{\nu,k}}e^{-|\alpha_{\nu,k}|^2/N_{\nu,k}} \ . \tag{2.93}$$

We assume that $(\alpha_{\nu,k})^l P^{(n)}(\alpha) \underset{\alpha\to\infty}{\longrightarrow} 0$ for all ν, k, n, l for the same reasons given in the main text. Performing the integration $\int_\alpha$ on Eqns. (2.90-2.92) yields

$$\frac{\partial}{\partial t}\int_\alpha P^{(1)} = -\mathrm{i}\mathcal{H}_S^\times \int_\alpha P^{(1)} - \mathrm{i}\sum_{\nu,k}\tilde{g}_{\nu,k}S_\nu^\times \underbrace{\int_\alpha (\alpha_{\nu,k}+\alpha_{\nu,k}^*)P^{(0)}}_{\to 0} \ , \tag{2.94}$$

$$\frac{\partial}{\partial t}\int_\alpha P^{(2)} = -\mathrm{i}\mathcal{H}_S^\times \int_\alpha P^{(2)} - \mathrm{i}\sum_{\nu,k}\tilde{g}_{\nu,k}S_\nu^\times \int_\alpha (\alpha_{\nu,k}+\alpha_{\nu,k}^*)P^{(1)} \ , \tag{2.95}$$

$$\cdots \ ,$$

$$\frac{\partial}{\partial t}\int_\alpha P^{(n)} = -\mathrm{i}\mathcal{H}_S^\times \int_\alpha P^{(n)} - \mathrm{i}\sum_{\nu,k}\tilde{g}_{\nu,k}S_\nu^\times \int_\alpha (\alpha_{\nu,k}+\alpha_{\nu,k}^*)P^{(n-1)} \ , \tag{2.96}$$

where the integral $\int_\alpha$ is an integral over all of the environments parameters $\int_\alpha = \prod_{\nu,k}\int d^2\alpha_{\nu,k}$, and the initial condition is $\int_\alpha P^{(n>0)}(t=0) = 0$, *i.e.* at time $t=0$ the system and the environment were factorized. The first contribution in the expansion comes from $\int_\alpha P^{(2)} \neq 0$, which is 2^{nd} order in the coupling constant g. In order to solve Eqn. (2.95) we first need to evaluate the expression $\int_\alpha(\alpha_{\nu,k}+\alpha_{\nu,k}^*)P^{(1)}$ for each (ν,k), which is accomplished by multiplying Eqn. (2.90) by $\alpha_{\nu',k'}$ or $\alpha^*_{\nu',k'}$ from the left, and then performing the $\int_\alpha$ integral. As a consequence, all of the terms in the sum with index $\nu \neq \nu', k \neq k'$ vanish, and we are left with

$$\frac{\partial}{\partial t}\int_\alpha \alpha_{\nu,k}P^{(1)} = -\mathrm{i}\int_\alpha \alpha_{\nu,k}(\mathcal{H}_S^\times + L)P^{(1)} + \tilde{g}_{\nu,k}\int_\alpha \alpha_{\nu,k}A_g^\nu(t,k)P^{(0)} \ , \tag{2.97}$$

and a corresponding equation for $\alpha^*_{\nu,k}$. Crucially, there is no sum over k here, which means each k gives rise to exactly two equations of the type of Eqns. (2.31, 2.32), which we have already solved. The first non-vanishing term is hence given by

$$\begin{aligned}\int_\alpha P^{(2)} = &-U(t)\sum_\nu \int_0^t dt' \int_0^{t'} dt'' \tilde{S}_\nu^\times(t')\times \\ &\sum_k \tilde{g}_{\nu,k}^2 e^{-\frac{1}{2}\gamma_{\nu,k}(t'-t'')}\Big[(2N_{\nu,k}+1)\cos[\omega_{\nu,k}(t'-t'')]\tilde{S}_\nu^\times(t'') \\ &-\mathrm{i}\sin[\omega_{\nu,k}(t'-t'')]\tilde{S}_\nu^\circ(t'')\Big]\rho^S(0) \ ,\end{aligned} \tag{2.98}$$

which is just Eqn. (2.33) with an added sum over all the indices. Thus we conclude that

$$\begin{aligned}\Theta_2 = &-\sum_{\nu}\int_0^t dt'\int_0^{t'} dt''\tilde{S}_\nu^{\times}(t')\times \\ &\sum_k g_{\nu,k}^2 e^{-\frac{1}{2}\gamma_{\nu,k}(t'-t'')}\Big[(2N_{\nu,k}+1)\cos[\omega_{\nu,k}(t'-t'')]\tilde{S}_\nu^{\times}(t'') \\ &-\mathrm{i}\sin[\omega_{\nu,k}(t'-t'')]\tilde{S}_\nu^{\circ}(t'')\Big] \ . \end{aligned} \tag{2.99}$$

From here we continue to Eqn. (2.49).

Appendix B: Standard Markovian Weak-Coupling Master Equation

In this Appendix, we follow the recipe given in Chapter 1.3.2 in order to derive the standard Lindblad master equation that is one of our benchmarks throughout the chapter. We start from the Rabi Hamiltonian given by Eqn. (2.37), ignoring $\mathcal{H}_{EU}=0$ for now. With the suitable change of basis we can write this Hamiltonian as

$$\tilde{\mathcal{H}}_R = \frac{\Omega}{2}\tilde{\sigma}_x + \omega a^\dagger a + \frac{g}{\Omega}[\epsilon\tilde{\sigma}_x + \Delta(\tilde{\sigma}_+ + \tilde{\sigma}_-)](a^\dagger + a) \ , \tag{2.100}$$

where the tilde denotes the new basis, $\tilde{\sigma}_\pm$ are the lowering and raising operators, and $\Omega = \sqrt{\epsilon^2+\Delta^2}$ is the Rabi frequency. Adopting the notation from Ref. [4] and Chapter 1.3.2, we have

$$A(\pm\Omega) = g\frac{\Delta}{\Omega}\tilde{\sigma}_\pm \ , \tag{2.101}$$

$$A(0) = g\frac{\epsilon}{\Omega}\tilde{\sigma}_x \ , \tag{2.102}$$

$$S(\alpha) = \frac{N(\omega)}{\alpha+\omega} + \frac{N(\omega)+1}{\alpha-\omega} \ , \tag{2.103}$$

$$\gamma(\alpha) = \frac{\pi}{2}\delta(\alpha+\omega)N(\omega) + \frac{\pi}{2}\delta(\alpha-\omega)[N(\omega)+1] \ . \tag{2.104}$$

This defines the Lamb-Shift Hamiltonian as

$$\tilde{\mathcal{H}}_{\mathrm{LS}} = \sum_{\alpha=0,\pm\Omega} S(\alpha)A(\alpha)A^\dagger(\alpha) \tag{2.105}$$

$$= g^2\frac{\Delta^2}{\Omega^2}\frac{\Omega}{\Omega^2-\omega^2}\coth(\frac{\beta\omega}{2})\tilde{\sigma}_x \ , \tag{2.106}$$

up to a constant that does not affect the dynamics. The dissipator is given by

$$D(\rho_s) = \sum_{\alpha=0,\pm\Omega} \gamma(\alpha)\left[A(\alpha)\rho_s A^\dagger(\alpha) - \frac{1}{2}\{A^\dagger(\alpha)A(\alpha),\rho_s\}\right] \tag{2.107}$$

$$\begin{aligned} &= g^2\frac{\Delta^2}{\Omega^2}\frac{\pi}{2}\delta(\Omega-\omega)\times \\ &\quad\Big[(N(\omega)+1)(\tilde{\sigma}_+\rho_s\tilde{\sigma}_- - \frac{1}{2}\{\tilde{\sigma}_-\tilde{\sigma}_+,\rho_s\}) \\ &\quad + N(\omega))(\tilde{\sigma}_-\rho_s\tilde{\sigma}_+ - \frac{1}{2}\{\tilde{\sigma}_+\tilde{\sigma}_-,\rho_s\})\Big] \\ &\quad + g^2\frac{\epsilon^2}{\Omega^2}\frac{\pi}{2}\delta(\omega)\coth\left(\frac{\beta\omega}{2}\right)(\tilde{\sigma}_x\rho_s\tilde{\sigma}_x - \rho_s)\ , \end{aligned} \tag{2.108}$$

and the dynamics of the system is then governed by

$$\frac{\partial}{\partial t}\rho_s = -\mathrm{i}[\tilde{\mathcal{H}}_R + \tilde{\mathcal{H}}_{\mathrm{LS}},\rho_s] + D(\rho_s)\ . \tag{2.109}$$

From the above expression we can extract the relaxation and dephasing rates, obtaining

$$\Gamma_{\mathrm{relax}} = 2\pi g^2\coth\left(\frac{\beta\Omega}{2}\right)\frac{\Delta^2}{\Omega^2}\delta(\Omega-\omega)\ , \tag{2.110}$$

$$\Gamma_{\mathrm{dephase}} = \frac{1}{2}\Gamma_{\mathrm{relax}} + 4\pi g^2\coth\left(\frac{\beta\omega}{2}\right)\frac{\epsilon^2}{\Omega^2}\delta(\omega)\ . \tag{2.111}$$

At this point we can easily calculate the relaxation and dephasing rates, as well as the Lamb-shift Hamiltonian for the spin-boson Hamiltonian from Eqn. (2.56), simply by summing over the contributions from each mode of the bath. In terms of the spectral density Eqn. (2.53), the rates are then given by

$$\tilde{\mathcal{H}}_{\mathrm{LS}} = \tilde{\sigma}_x\frac{\Delta^2}{\Omega^2}\int_0^\infty d\omega J(\omega)\coth\left(\frac{\beta\omega}{2}\right)\frac{\Omega}{\Omega^2-\omega^2}\ , \tag{2.112}$$

$$\Gamma_{\mathrm{relax}} = 2\pi\frac{\Delta^2}{\Omega^2}J(\Omega)\coth\left(\frac{\beta\Omega}{2}\right)\ , \tag{2.113}$$

$$\Gamma_{\mathrm{dephase}} = \frac{1}{2}\Gamma_{\mathrm{relax}} + 4\pi\frac{\epsilon^2}{\Omega^2}k_{\mathrm{B}}T\lim_{\omega\to0}\frac{J(\omega)}{\omega}\ . \tag{2.114}$$

Chapter 3

When do perturbative approaches accurately capture the dynamics of complex quantum systems?

3.1 Introduction

In this Thesis we have discussed two techniques that are perturbative in the system-environment coupling, for approximating the evolution of a generic open quantum system that is linearly coupled to an environment of harmonic oscillators. These are the Time-Convolutionless (TCL) expansion, described in Chapter 1.3, and the P-mat method introduced in Chapter 2.

An important question to address is: when is an approach that is perturbative to second order in the coupling strength 'good enough' for capturing the essentials of the dynamics on a qualitative, or even quantitative, level? Here, we develop a criterion for predicting when such an approach is expected to perform well. Our criterion is based on a reasonably straightforward analytical expression that is, crucially, easy to evaluate, whilst also lending itself to an intuitive physical interpretation.

We wish to stress that we are focussing on the question when a second-order perturbative treatment can be used reliably, as opposed to when environmental effects only perturb the system slightly. In the latter case the perturbative treatment should be automatically valid, however, a second-order treatment may remain valid even when it changes the dynamics dramatically from those of an isolated system.

Hereafter, we shall use the term 'weak-coupling' synonymously with 'perturbative to second-order'.

We consider both the TCL expansion and P-mat[§] methods. Interestingly, we find that both approaches give rise to exactly the same criterion, despite their rather different nature. This suggests that our criterion has applicability beyond just one particular perturbative approach.

We apply both approaches to the canonical spin boson model[40] as well as the much studied FMO complex[29,32,66,77,102,103]. The latter has received a significant amount of attention and is a prime example of the complicated interplay between coherent dynamics interwoven with significant environmental influences. The advantage of this system is that a large body of literature and numerically converging methods exist. Interestingly, our criterion indicates that despite the relatively strong coupling, a second-order treatment is appropriate at lower but not necessarily at higher temperatures. We note that the FMO problem has previously been tackled with weak-coupling techniques[102,104–108], but here we not only use a novel method but also introduce a rigorous criterion for when such approaches are indeed permissible.

In the 'grey area' where a second-order expansion is no longer strictly justified, we find that the quality of the different approaches differs. In Chapter 2 we found that the P-mat method outperformed the commonly used secular, second-order Markovian master equation. For the examples studied here, we find that a TCL ME gives slightly better short time dynamics than P-mat, whilst the latter frequently performs better at longer times as the system approaches thermalisation. As expected, fourth-order TCL typically (but not always) beats second-order approaches, but may also lead to unphysical results in the strong-coupling regime. To arrive at robust conclusions, we supplement comparisons of the population dynamics (as in Refs. [30,106]) by the trace distance, which is also sensitive to the agreement between the coherences of the approximate and exact methods.

[§]We consider here the case of a 'standard' open quantum system for the P-mat method, *i.e.* without the wider universe introduced in Chapter 2.

As a starting point we use the 'standard' open-systems Hamiltonian, as described in Chapter 1.1.5, which is given by

$$\mathcal{H} = \mathcal{H}_S + \mathcal{H}_E + \mathcal{H}_I \ , \tag{3.1}$$

where $\mathcal{H}_S$ is a finite-dimensional Hamiltonian for the system of interest, and $\mathcal{H}_E$, $\mathcal{H}_I$ are the environment and interaction Hamiltonians, respectively. The baths are modelled by a collection of harmonic oscillators that are linearly coupled to the system according to:

$$\mathcal{H}_E = \sum_{\nu,k} \omega_{\nu,k} a^\dagger_{\nu,k} a_{\nu,k} \ , \tag{3.2}$$

$$\mathcal{H}_I = \eta \sum_\nu S_\nu E_\nu = \eta \sum_\nu S_\nu \sum_k g_{\nu,k}(a^\dagger_{\nu,k} + a_{\nu,k}) \ . \tag{3.3}$$

Here, S_ν are system and E_ν the environment operators with environment index ν. The $g_{\nu,k}$ are the coupling constants (in units of energy), and $a^\dagger_{\nu,k}$ the bosonic creation operators satisfying $[a_{\nu,k}, a_{\nu',k'}] = [a^\dagger_{\nu,k}, a^\dagger_{\nu',k'}] = 0$, $[a_{\nu,k}, a^\dagger_{\nu',k'}] = \delta_{k,k'}\delta_{\nu,\nu'}$.

Note that for the case of phonons, the justification for the linear form of (3.3) usually hinges on a weak-coupling argument: We assume that the equilibrium position of the atoms hosting the vibrational modes only vary slightly when an electron or an exciton is present. Expanding the potential energy between these atoms to first order leads to the linear coupling term of Eqn. (3.3)[40,109]. Conversely, for very strong coupling, one would not be able to justify the linear approximation.

3.2 Previous estimations of validity

The canonical definition of the coupling strength of an open system to its environment is the reorganisation energy, introduced in Section 1.2. This is the potential energy associated with shifting the oscillator modes into their new equilibrium position in the presence of an excitation of the system. The reorganisation energy is given by[§]

$$\lambda_\nu = \int_0^\infty d\omega \frac{J_\nu(\omega)}{\omega} \ , \tag{3.4}$$

[§]This is Eqn. (1.66), written here again for clarity.

where $J_\nu(\omega) = \eta^2 \sum_k g_{k,\nu}^2 \delta(\omega - \omega_{\nu,k})$ is the spectral density of bath ν.

Weak-coupling is sometimes defined by the condition $\lambda_\nu \ll V_{ij}$ where V_{ij} represent off-diagonal coupling elements of the Hamiltonian between distinct basis states (typically chosen as the site basis)[32,33]. Whilst straightforward for a two level system, in higher-dimensional systems, one may wonder exactly which V_{ij} ought to be considered. Arguably, some off-diagonal terms in the Hamiltonian may be small or even vanish without automatically implying a strong coupling scenario. The authors of Ref. [30] write that in many cases the " ...reorganization energy is not a reasonable measure for the coupling strength ..." because the system's dynamic frequencies are not taken into consideration. They suggest, without any mathematical rigour, circumventing this shortcoming by defining an effective reorganisation energy $\lambda_{\text{eff}} = \int_{E_{\min}}^{E_{\max}} d\omega J(\omega)/\omega$, which only spans the relevant energy interval containing the system frequencies. On the other hand, in Ref. [110] the authors present a heuristic approach for estimating when a weak-coupling approach is valid by introducing a measure that depends on the temperature of the bath, but in that case not on the frequencies of the system.

A more rigorous discussion about the validity of the perturbation can be found in Ref. [4], where the error of the TCL perturbation is defined as

$$e_r^{(2)} = \frac{\|\mathcal{K}(t) - \mathcal{K}_2(t)\|}{\|\mathcal{K}(t)\|} \ . \tag{3.5}$$

Here $\mathcal{K}$ is the full (exact) TCL kernel and $\mathcal{K}_2$ is its second order approximation, whilst $\|\square\|$ denotes "any appropriate norm for the super-operator". Of course the full $\mathcal{K}$ is often intractable, which is the very reason for why we approximate it. In any case, to leading order (in the coupling strength) we can approximate the error of a second-order approximation by

$$e_r^2 \approx \frac{\|\mathcal{K}_4(t)\|}{\|\mathcal{K}_2(t)\|} \ . \tag{3.6}$$

In Ref. [4] this is where the discussion stops. In this chapter we start from a similar idea and derive an explicit error estimation.

3.3 Proposed Criterion

Here we propose a criterion for the validity of a perturbative solution, which takes into account both the system frequencies and the temperature of the environment. Essentially, we let ourselves be guided by wishing to apply the term "weak-coupling" to situations when higher order expansion terms beyond the second order are not required for reliably capturing the open systems dynamics. To this end, similarly to Eqn. (3.6), we explicitly compare terms from a 4^{th} order expansion to 2^{nd} order terms, obtaining the following weak-coupling criterion:

$$\left| \frac{\langle ii| \mathcal{K}_4 |ii\rangle}{\langle ii| \mathcal{K}_2 |ii\rangle} \right| \ll 1 \ , \tag{3.7}$$

which must hold separately for each eigenstate i of the system Hamiltonian $\mathcal{H}_S$, and where $\langle ii| \mathcal{K}_2 |ii\rangle$ and $\langle ii| \mathcal{K}_4 |ii\rangle$ will be explicitly given in Eqns. (3.14) and (3.16) further on, and are approximated rates derived from the TCL2 and TCL4 perturbation expansions. This "full" criterion, whilst evaluated straightforwardly enough, does not easily lend itself to providing much analytical insight. Therefore, we also consider a "simplified" version that is more amenable to physical interpretation. This simplified criterion reads

$$\sum_{j \neq i} \Upsilon_{ij} \ll 1 \ , \tag{3.8}$$

where

$$\Upsilon_{ij} = 2|S_{ij}|^2 \int_0^t \tau d\tau D(\tau) \cos \Delta_{ij} \tau \ . \tag{3.9}$$

Here, $|S_{ij}|^2 = \sum_\nu \left|\langle i|S_\nu|j\rangle\right|^2$ with $|j\rangle$ being the eigenstates of the system Hamiltonian $\mathcal{H}_S$, $\Delta_{ij} = \epsilon_i - \epsilon_j$ is the energy difference between two eigenenergies i, j, and we have assumed that all spectral densities take the same form $J_\nu(\omega) = J(\omega)$[§]. For a thermal environment we have $D(t) = \int_0^\infty d\omega J(\omega) \coth(\beta\omega/2) \cos(\omega t)$. Further, t is the time-scale of interest (*i.e.* the duration over which we want the calculations to remain accurate). When $D(\tau > t) \approx 0$, it is justified to take the upper limit of the integral

[§]Generalising for different spectral densities is straightforward.

to infinity. We provide the explicit derivation of Eqn. (3.8) in the next Section (3.4), and note that TCL and P-mat both lead to exactly the same final expression.[§]

Note that in the case of a delta-function response function $\alpha(t) \sim \delta(t)$, the fourth-order term vanishes exactly[§§], and indeed we get $\Upsilon_{ij} = 0$, which means that the criterion suggests that a second order treatment is exact in this case.

For the examples studied in the following Sections of this chapter, the simplified criterion of Eqn. (3.8) turns out to be as stringent as the full criterion. However, not having been able to mathematically prove that it will always be sufficiently rigorous, we suggest using it carefully and supplementing it by Eqn. (3.7) if in doubt.

Interestingly, the quantities written in the RHS of Eqn. (3.9) are exactly the terms leading to the "slippage of initial conditions" [42,43], explained in Appendix B, indicating that if the initial slippage for each eigenstate is small, then the perturbative treatment is a good approximation, otherwise one should look for alternative methods. Note that appreciable slippage of initial conditions marks the onset of non-Markovian effects, rendering a perturbative second-order expansion (and thus our definition of weak coupling) invalid.

3.4 Derivation of the Criterion

In this Section we derive the criterion (3.8). For that we first estimate the rates $\langle ii| \mathcal{K}_2 |ii\rangle$ and $\langle ii| \mathcal{K}_4 |ii\rangle$, given by the TCL expansion, as described in Chapter 1.3.1, and explain why we chose to focus on these elements.

For this analysis we look at the case where all of the different baths are independent, and they are all coupled to the system in the same manner, *i.e.* $J_\nu(\omega) = J(\omega)$ for all ν. This simplifies Eqns. (1.84-1.85) with $R_{n_a,n_b}(t_a,t_b) = \delta_{n_a,n_b} R_{n_a,n_a}(t_a,t_b)$, and $D^{n_a,n_b}(\tau) = \delta_{n_a,n_b} D(\tau), D_1^{n_a,n_b}(\tau) = \delta_{n_a,n_b} D_1(\tau), \alpha^{n_a,n_b}(\tau) = \delta_{n_a,n_b}\alpha(\tau)$.

Working in the Liouville Space $\mathcal{H}_S \otimes \mathcal{H}_S$, with $|i\rangle\langle j| \to |ij\rangle$, where $|i\rangle$ are the system's energy eigenstates, it is straightforward to write down an explicit expression

[§]For P-mat the definition of the criterion is not the same, as discussed in Section 3.4.

[§§]Physically, in the high-temperature limit, only the *real* part of the response function becomes a delta function[41].

for $\mathcal{K}_2$:[§]

$$\begin{aligned}\langle ij|\mathcal{K}_2\,|rs\rangle = -e^{-\mathrm{i}(\Delta_{rs}-\Delta_{ij})t}\sum_\nu\int_0^t d\tau\Big\{ \\ \sum_k\Big[\delta_{js}e^{-\mathrm{i}\Delta_{kr}\tau}S^\nu_{ik}S^\nu_{kr}\alpha(\tau)+\delta_{ir}e^{+\mathrm{i}\Delta_{ks}\tau}S^\nu_{sk}S^\nu_{kj}\alpha^*(\tau)\Big] \\ -S^\nu_{ir}S^\nu_{sj}\Big[e^{-\mathrm{i}\Delta_{ir}\tau}\alpha(\tau)+e^{+\mathrm{i}\Delta_{js}\tau}\alpha^*(\tau)\Big]\Big\}\,,\end{aligned} \tag{3.10}$$

where $\Delta_{ij}=\epsilon_i-\epsilon_j$, and $S^\nu_{ij}=\langle i|\,S_\nu\,|j\rangle$.

The dephasing, decoherence, and Lamb-shift rates are given by matrix elements in the superoperator $\mathcal{K}(t)$ that do not oscillate with t as $t\to\infty$, meaning that in $\mathcal{K}_2$ only elements with $\Delta_{rs}-\Delta_{ij}=0$ contribute to the rates. In the same manner one can show that the t-dependence of the fourth order is $\langle ij|\,\mathcal{K}_4\,|rs\rangle\sim e^{-\mathrm{i}(\Delta_{rs}-\Delta_{ij})t}$, for times much longer than the bath's memory time. Assuming that the energies are non-degenerate in the broad sense, meaning $\sum_i(\epsilon_{n_i}-\epsilon_{m_i})=0\leftrightarrow\{n_i\}=\{m_i\}$, then the only matrix elements with these rates are either diagonal terms

$$\begin{aligned}\langle ij|\,\mathcal{K}_2\,|ij\rangle = -\sum_\nu\int_0^t d\tau\Big\{(S^\nu_{ii}-S^\nu_{jj})[S^\nu_{ii}\alpha(\tau)-S^\nu_{jj}\alpha^*(\tau)] \\ +\sum_{k\neq i}|S^\nu_{ki}|^2e^{-\mathrm{i}\Delta_{ki}\tau}\alpha(\tau)+\sum_{k\neq j}|S^\nu_{jk}|^2e^{-\mathrm{i}\Delta_{jk}\tau}\alpha^*(\tau)\Big\}\,,\end{aligned} \tag{3.11}$$

or elements between two different eigenstate projectors,

$$\langle ii|\,\mathcal{K}_2\,|jj\rangle_{i\neq j}=\sum_\nu\int_0^t d\tau|S^\nu_{ij}|^2\left[e^{-\mathrm{i}\Delta_{ij}\tau}\alpha(\tau)+e^{+\mathrm{i}\Delta_{ij}\tau}\alpha^*(\tau)\right]\,. \tag{3.12}$$

The part proportional to the diagonal of the coupling operator S is known in the literature as "pure dephasing". Incidentally because our model only considers linear coupling between the system and environment, if there were only diagonal terms in the interaction, then the exact contributions of these terms are equal to their second order expansion[111].

Moreover, we are only interested in the real parts of the rates, as the imaginary parts are responsible for the Lamb shift. Finally, in Eqn. (3.11), the rates for $i\neq j$ are the ones for which the off-diagonal elements of the density matrix decay. For the

[§]This formula is Eqn. 1.91 for multiple baths, written here again for clarity.

sake of this discussion we focus on the dephasing rates, *i.e.* the rates in which the diagonal elements of the density matrix decay,

$$\langle ii|\,\mathcal{K}_2\,|ii\rangle = -2\sum_{\nu}\int_0^t d\tau \sum_{k\neq i}|S_{ik}^{\nu}|^2\left[D(\tau)\cos(\Delta_{ik}\tau) - D_1(\tau)\sin(\Delta_{ik}\tau)\right]\ . \tag{3.13}$$

The part proportional to $D_1 = \mathrm{Im}(\alpha)$ in the above equation is normally much smaller and will be ignored for the purpose of our discussion, hence we approximate the second order rates as

$$\langle ii|\,\mathcal{K}_2\,|ii\rangle \approx -2\sum_{\nu}\int_0^t d\tau \sum_{k\neq i}|S_{ik}^{\nu}|^2 D(\tau)\cos(\Delta_{ik}\tau)\ . \tag{3.14}$$

In the Markovian limit, where the time of the experiment is much longer than the memory-kernel decay time $t \gg t_c$, we may take the integral in Eqn. (3.14) to infinity and obtain the usual rates

$$\langle ii|\,\mathcal{K}_2\,|ii\rangle_{\infty} \approx -\pi\sum_{\nu}\sum_{k\neq i}|S_{ik}^{\nu}|^2 J(|\Delta_{ik}|)\coth(\beta|\Delta_{ik}|/2)\ . \tag{3.15}$$

By contrast, for times comparable to or shorter than the decay time of the response kernel $D(t)$, or if the spectral density is not smooth and has sharp peaks, it is not justified to take the Markovian limit and one should evaluate the rates (3.14) over the time of the experiment.

Using a similar analysis for the fourth-order terms, we find that corrections to the rates introduced by a fourth order treatment are given by

$$\begin{aligned}
&\langle ii|\,\mathcal{K}_4\,|ii\rangle \approx \\
&-2\sum_{\nu_1,\nu_2}\int_0^t d\tau_1\left[\int_0^{t-\tau_1}\tau_2 d\tau_2 + \int_{t-\tau_1}^{t}(t-\tau_2)d\tau_2\right]D(\tau_1)D(\tau_2) \\
&\qquad\qquad \times \sum_{k\neq i,p\neq i}|S_{ik}^{\nu_1}|^2|S_{ip}^{\nu_2}|^2\cos(\Delta_{ik}\tau_1+\Delta_{ip}\tau_2)(1+\delta_{kp}) \\
&+2\sum_{\nu_1,\nu_2}\int_0^t d\tau_1\int_0^{\tau_1}d\tau_2(\tau_1-\tau_2)D(\tau_1)D(\tau_2)\times\Big[\sum_{i\neq k}|S_{ik}^{\nu_1}|^2 S_{ii}^{\nu_2}(S_{ii}^{\nu_2}-S_{kk}^{\nu_2})\cos(\Delta_{ik}\tau_1) \\
&\qquad\qquad + \sum_{k\neq i}\sum_{p\neq\{i,k\}}|S_{ik}^{\nu_1}|^2|S_{kp}^{\nu_2}|^2\cos(\Delta_{ik}\tau_1+\Delta_{kp}\tau_2)\Big]\ .
\end{aligned} \tag{3.16}$$

In the above equation we only kept terms that have τ_1 or τ_2 in their integrand. We note that there are other terms, namely terms with integrands similar to $(e^{-\mathrm{i}\Delta\tau}-1)/\Delta$ where Δ is an eigenfrequency of the system, which are generally, but not always, smaller than their τ equivalents derived by taking the limit $\Delta \to 0$. Further, we ignore contributions from D_1 as in Eqn. (3.14). Also, we assume that the system's energies and frequencies are not degenerate in the sense that $\sum_i E_i = \sum_j E_j \Rightarrow \{E_i\} = \{E_j\}$.

The ratio between Eqns. (3.16) and (3.14) defines our 'full' criterion [Eqn. (3.7)]. To arrive at the 'simplified' criterion, we shall make some further approximations and assumptions in the following. We note that Eqn. (3.16) consists of two terms and we conjecture that these are both of the same order (noting that this is a good approximation for for the spin-boson model and the FMO complex examples studied here), so we continue with the first one for the sake of this analysis. Now, because we are looking for a criterion for when the fourth order contribution is small, we are being conservative by artificially enlarging it via the substitution $1+\delta_{kp} \to 2$, and taking the upper limit of the τ_2 integral to t. Further, we expand the cosine and ignore any terms proportional to $\tau_2 \sin(\Delta_{ik}\tau_1)\sin(\Delta_{ip}\tau_2)$, which are smaller than their cosine equivalents. Thus we arrive at

$$\langle ii|\,\mathcal{K}_4\,|ii\rangle \sim -4\sum_{\nu_1,\nu_2}\int_0^t d\tau_1\int_0^t d\tau_2\tau_2 D(\tau_1)D(\tau_2) \times \sum_{k\neq i,p\neq i}|S_{ik}^{\nu_1}|^2|S_{ip}^{\nu_2}|^2\cos(\Delta_{ik}\tau_1)\cos(\Delta_{ip}\tau_2)\ . \tag{3.17}$$

Now considering the ratio $\langle ii|\,\mathcal{K}_4\,|ii\rangle \,/\, \langle ii|\,\mathcal{K}_2\,|ii\rangle$ leaves us with the following 'simplified' criterion [Eqn. (3.8)] for when weak-coupling is a good approximation:

$$2\sum_{\nu}\sum_{k\neq i}|V_{ik}^{\nu}|^2\int_0^t d\tau\tau D(\tau)\cos(\Delta_{ik}\tau) \ll 1\ . \tag{3.18}$$

The above inequalities must hold for all of the system's energy levels i.

We note that we can define the equivalent weak-coupling criterion for the P-mat expansion, using the following criterion:

$$\left|\frac{\langle ii|\,\Theta_4(t)\,|ii\rangle}{\langle ii|\,\Theta_2(t)\,|ii\rangle}\right| \ll 1\ , \tag{3.19}$$

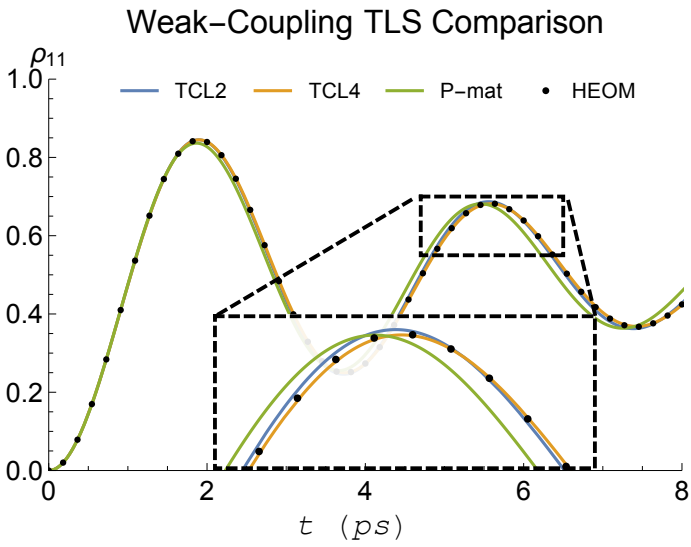

Figure 3.1: Comparison of the spin boson dynamics calculated using HEOM (points) to our perturbative techniques (solid). Here we consider the weak-coupling case with $\eta = 1$ (see main text for other parameters). HEOM data taken from Ref. [2].

where Θ is the P-mat influence functional as described in Chapter 2. Following a very similar derivation as the one above, we find that P-mat predicts the exact same simplified criterion for the case of large t.

3.5 Examples

3.5.1 Spin-Boson Model Example

As a first case study, we apply our criteria to the canonical example of the spin-boson model[40] with Hamiltonian given by:

$$\mathcal{H} = \frac{1}{2}\Delta\sigma_x + \sum_k \omega_k a_k^\dagger a_k + \sigma_z \sum_k g_k(a_k^\dagger + a_k) \ , \tag{3.20}$$

where σ_x, σ_z are the usual Pauli matrices and Δ represents the Rabi frequency of the spin. Further, a ($a^\dagger$) denotes the annihilation (creation) operator of a bosonic mode k with frequency ω_k, and g_k are the spin-boson coupling elements. We consider an Ohmic spectral density with exponential cutoff as follows

$$J(\omega) = \sum_k g_k^2 \delta(\omega - \omega_k) = \eta\lambda(\omega/\omega_c)e^{-\omega^2/\omega_c^2} \ , \tag{3.21}$$

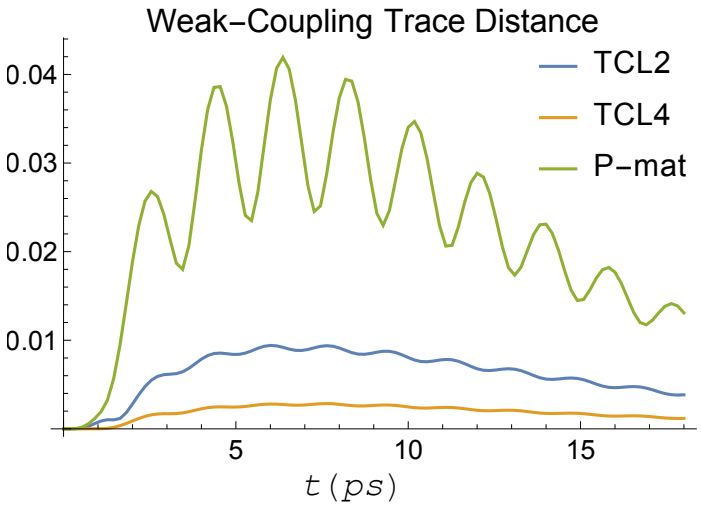

Figure 3.2: Trace distance between the spin boson dynamics calculated using HEOM and the different perturbative techniques. Again, we consider a clearly cut weak coupling scenario with parameters as in Fig. 3.1. HEOM data taken from Ref. [2].

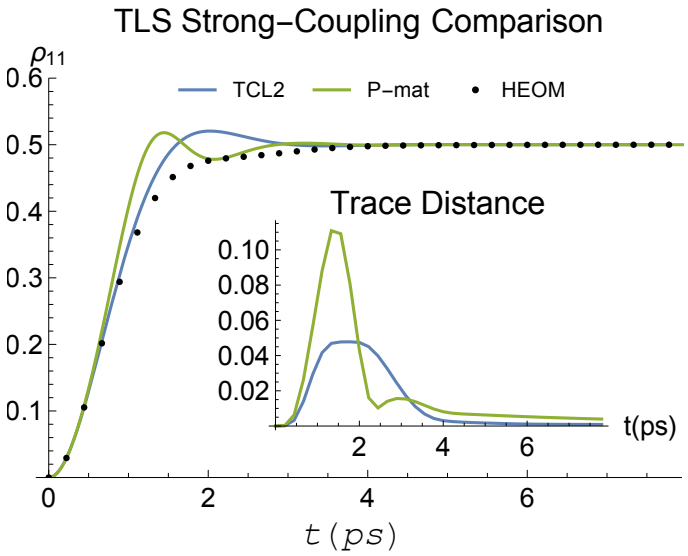

Figure 3.3: Comparison between the spin boson dynamics calculated using HEOM and weak-coupling techniques, for a strong-coupling case, $\eta = 10$. Other parameters as in Fig. 3.1. HEOM data taken from Ref. [2].

where η is a dimensionless parameter allowing us to easily interpolate between weak and strong coupling. We choose $\Delta = \pi/2$ ps^{-1}, $T = 50$ K, $\lambda = 0.01485$ ps^{-1}, and $\omega_c = 2.2$ ps^{-1}.

Evaluating our weak-coupling criteria, the LHS of Eqns. (3.8, 3.7) for these parameters gives 0.04 η (0.06 η) for the simplified (full) version of the criterion, meaning the system is well into the weak-coupling regime when we set $\eta = 1$. This can be seen in Figs. 3.1 and 3.2 which show a comparison of TCL2, TCL4, and P-mat techniques with the numerically exact HEOM dynamics. As expected the perturbative techniques capture the dynamics very accurately in this case. P-mat performs worst in this case (despite having previously been shown to outperform a standard secular Markovian master equation in a comparable scenario[1]), although the gap narrows towards longer times when the system approaches thermal equilibrium. The trace distance of all three perturbative approaches features oscillations at twice the Rabi frequency of the natural precession time of the spin, clearly visible in Fig. 3.2. For completeness, the trace distance between two density matrices is defined by

$$\mathcal{T}(\rho_1, \rho_2) = \frac{1}{2} Tr\{\sqrt{(\rho_1 - \rho_2)^2}\} = \frac{1}{2} \sum_i |\lambda_i| \,, \tag{3.22}$$

where λ_i is the i'th eigenvalue of $(\rho_1 - \rho_2)$. Its physical meaning is related to the probability of correctly distinguishing between the two states if a measurement was performed. For a two-level system, the trace distance is equal to half the Euclidean distance between two points in the Bloch sphere[112]. Generally, its interpretation depends on the dimensionality of the system, making it difficult to say what "small" means in absolute terms. However, this does not affect its usefulness as a relative metric for benchmarking several approximate methods against an exact solution.

When we increase the system and environment coupling by setting $\eta = 10$, our criteria indicate that we can no longer expect to be in the weak-coupling regime. In Fig. 3.3 we show a comparison between TCL2 and P-mat techniques with exact HEOM calculations, and it is apparent that both fail not only quantitatively but also qualitatively at intermediate times around $t \approx 1.5$ ps. We do not show TCL4 in this

case because the TCL4 generator features an unphysical positive eigenvalue in the long time limit.

3.5.2 FMO Complex Dynamics Example

We now turn to the dynamics of the Fenna-Matthews-Olsen (FMO) complex – a prime example of complex quantum dynamics in the difficult regime between weak and strong environmental coupling in a higher-dimensional Hilbert space. We follow the 7-site FMO model considered by Ishizaki and Fleming[32], where all chlorophylls have the same environment given by a Drude-Lorentz spectral density $J_\nu(\omega) = \frac{2}{\pi}\lambda\frac{\gamma\omega}{\omega^2+\gamma^2}$ with $\lambda = 6.59$ ps^{-1}. We consider the three cases for the environmental parameters discussed in Ref. [32], namely $T = 77$ K, $\gamma^{-1} = 50$ ps; $T = 300$ K, $\gamma^{-1} = 50$ ps; and $T = 300$ K, $\gamma^{-1} = 166$ fs. Once again comparing HEOM results to two perturbative methods, we will find that our criteria predict the validity of the methods not only for the spin boson model considered above but also for this much more involved case.

Table 3.1 lists the values of the criteria for the different sets of parameters mentioned above, plus the case of $T = 77$ K, $\gamma^{-1} = 166$ fs, added for completeness. Here we observe a factor of roughly $\sim 2-3$ between the simplified, Eqn. (3.8) and full criterion, Eqn. (3.7), with the simplified version being the more stringent one. However, we note that both agree in their classifications of whether the perturbative solution should be valid or not. Further, the reorganisation energy is constant across all cases as it does not depend on the temperature or the cut-off frequency (for this choice of spectral density), and is thus clearly not a good measure for the coupling strength in the sense discussed in this chapter.

We visualise the Υ_{ij} of Eqn. (3.8) for all three FMO cases in Fig. (3.4). Notably, two of the system eigenstates are almost resonant, being split by only ~ 2.8 ps^{-1}. This pair experiences strong environmental interactions for the $\gamma^{-1} = 166$ fs cutoff ($\Upsilon_{ij} \sim 2.8$), clearly placing the system into the strong-coupling domain, according to our definition. By contrast, for $\gamma^{-1} = 50$ fs this pair sits in an intermediate regime (at $T = 300$ K), whereas all other occurring frequencies satisfy our weak-coupling criterion. Consequently, we would expect a very good agreement between

Temperature	γ^{-1}	Max Full Criterion	Max Simplified Criterion	λ_n/ max $\lvert V_{12}\rvert$
77 K	50 fs	0.04	0.09	0.4
77 K	166 fs	0.22	0.66	0.4
300 K	50 fs	0.19	0.38	0.4
300 K	166 fs	1.09	2.6	0.4

Table 3.1: Full and simplifed criteria applied to different FMO configurations. In each case we choose the largest value of LHS of Eqns. (3.7) and (3.8) over all i. The reorganisation energy, $\lambda_n = 6.59$ ps^{-1}, does not depend on the cut-off frequency γ or the temperature, and we show the value of the reorganisation energy divided by the largest dipole-dipole coupling in the system, $|V_{12}| = 16.5$ ps^{-1} (note that here 1 and 2 refer to the site basis, whereas throughout the rest of this chapter we use the energy eigenbasis).

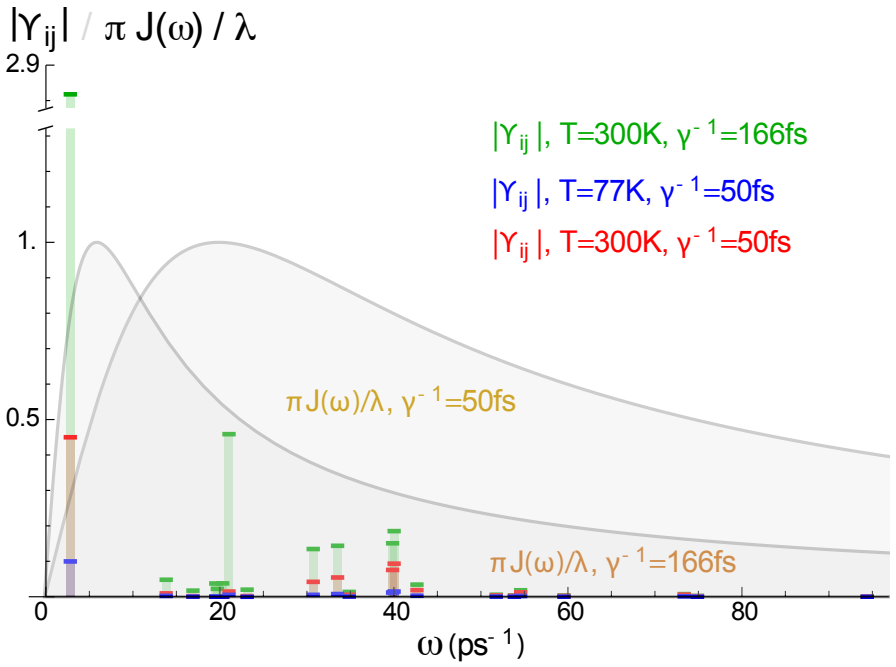

Figure 3.4: Visualisation of the simplified criterion: the different $|\Upsilon_{ij}|$ are shown at their corresponding frequencies Δ_{ij}. The rescaled and dimensionless respective spectral densities, $\pi J(\omega)/\omega$, are also shown as the coloured background areas, to illustrate at which frequencies environmental effects are expected to be dominant.

exact numerics and weak-coupling techniques in the low-temperature cases at $T = 77$ K, but at $T = 300$ K we expect the weak-coupling techniques to work only for $\gamma^{-1} = 50$ fs and not for $\gamma^{-1} = 166$ fs. We shall see that these expectations are met by our dynamical simulations discussed in the following.

To perform our simulations, the real part of the response function $D(t)$ is approximated by a single exponent and a delta function

$$D(t) \to 2\lambda k_{\mathrm{B}} T \left(1 - \frac{2\gamma^2}{(2\pi k_{\mathrm{B}} T)^2 - \gamma^2}\right) e^{-\gamma t} + \frac{8\lambda k_{\mathrm{B}} T \gamma}{(2\pi k_{\mathrm{B}} T)^2 - \gamma^2} \delta(t) \ , \tag{3.23}$$

while the exact imaginary part of the response function has a single exponent. This approximation is made to overcome memory restrictions of the HEOM implementation. For a fair comparison, we use the same response function for the TCL and P-mat methods, though these methods are not restricted to a certain structure of the response function. We note that HEOM calculations for the same FMO model, but with a more accurate approximation for the response function, using 3 (2) exponents for approximating the $77K$ $(300K)$ response function, have been reported in Ref. [113].

To capture the full density matrix dynamics as opposed to just the evolution of the site-basis populations ρ_{ij}, we shall also plot and discuss the trace-distance between the perturbative solutions and the HEOM benchmark.

Figs. 3.5 and 3.6 show the trace distances and populations from the weak-coupling techniques against the numerically exact HEOM calculations, all using $\gamma^{-1} = 50$ fs and for $T = 77, 300$ K as indicated. We find that TCL2 compares favourably to P-mat at short times, while for longer times, with the notable exception of Fig. 3.6 I, P-mat becomes more accurate. We suspect that this is because in the P-mat formalism, the secular approximation is inherently included. By contrast, in TCL a full or partial secular approximation[108] still needs to be performed explicitly to guarantee that the system will go to the thermal state with respect to the temperature of the bath (provided there is no decoherence-free subspace[114] and all the baths have a single temperature). Note, however, that in a stronger-coupling regime the system is no longer expected to fully evolve into its canonical thermal state at all[80].

We conclude that in all these three cases, our weak-coupling techniques capture the relevant oscillations in the dynamics well, as expected. Rather surprisingly, in Fig. 3.6 panel I ($\gamma^{-1} = 50$ fs and $T = 300$ K) when using site 1 as the initial state, TCL2 outperforms not only P-mat but also TCL4. We note that this is not the case in the same configuration but with site 6 as the location of the initial excitation, as shown in panel II of the same figure.

We now consider the lower cutoff frequency $\gamma^{-1} = 166$ fs at $T = 300$ K, having already identified this case as one which violates our weak-coupling criterion. As shown in Fig. 3.7, exact numerics suggest that the difference in the dynamics is deceptively small between $\gamma^{-1} = 50$ fs and 166 fs, borne out both by the populations [subplot (a)] and the trace distance [subplot (d)]. Nonetheless, according to Table 3.1, the two cases are vastly different from the point of view of the perturbation series, and indeed we find that TCL2 overestimates the damping and does not capture the oscillations, whilst P-mat underestimates the damping and shows more oscillations than HEOM. Yet the main difference in this case is actually what is not shown in the figure: We do not present TCL4 results in this plot because in this regime, the TCL4 generator once more possesses an unphysical eigenvalue in the long-time limit. This means that, even though according to the trace-distance measure, TCL2 is not vastly different from Fig. 3.6 ($\gamma^{-1} = 50$ fs and $T = 300$ K), the 4th order of the perturbation is larger than the 2nd order in this case. This means that the 2nd order is neither justifiable nor trustworthy, and this is what our criterion captures.

3.6 Discussion

We have introduced and discussed a straightforward criterion for the often difficult problem of deciding when when weak coupling approaches perform adequately for capturing higher-dimensional quantum dynamics in complex environments. We have discussed a rigorous as well as a simplified version of the criterion, with the latter constituting essentially a measure of the degree of 'slippage of initial conditions'[42,43].

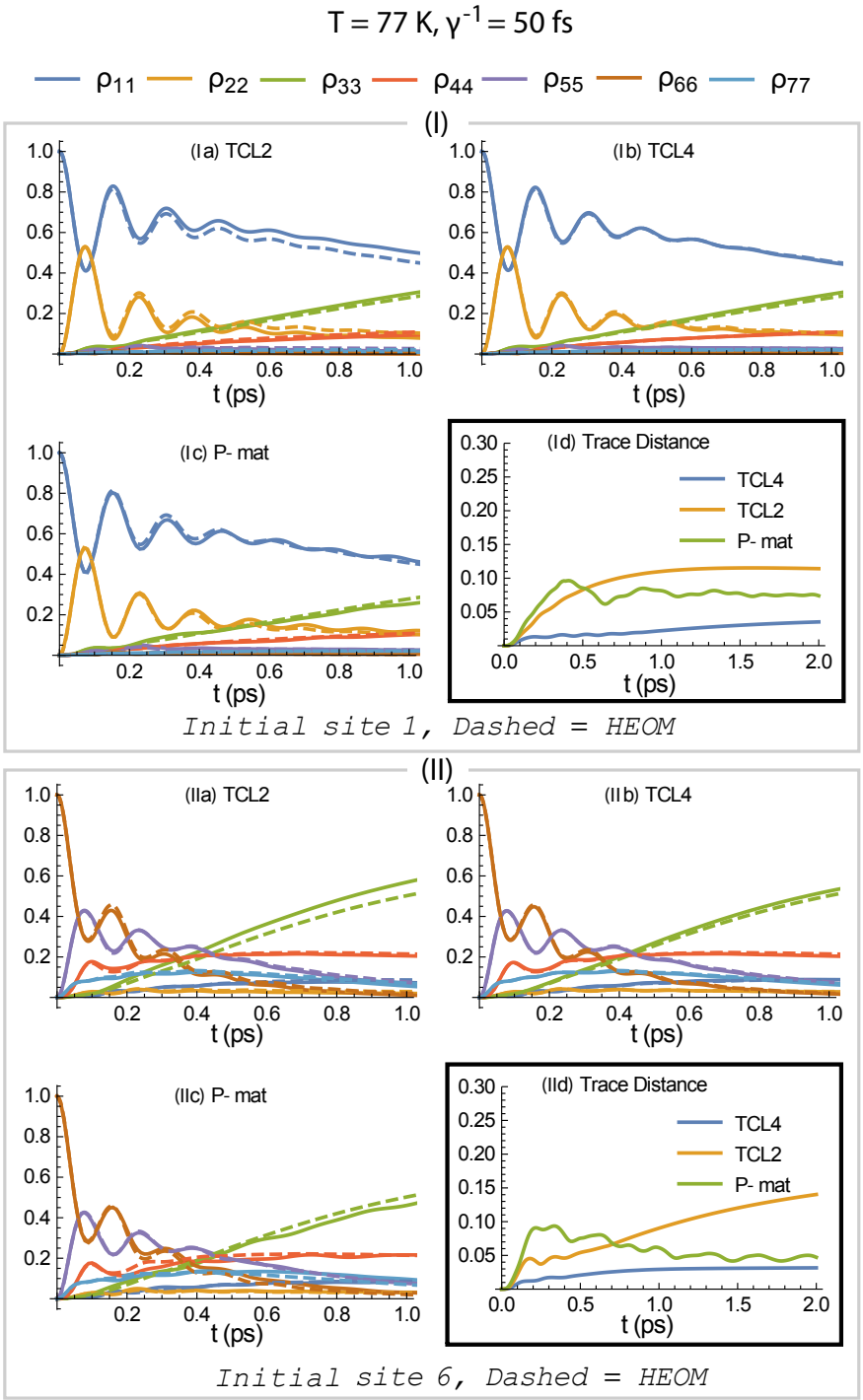

Figure 3.5: Benchmarking of FMO dynamics obtained from perturbative techniques (solid) against numerically converged HEOM (dashed), for temperature $T = 77\ K$ and cutoff frequency $\gamma^{-1} = 50$ fs. Initial excitation is localised at site indicated at the bottom of each panel. Subplots (a)-(c) show comparisons of TCL2, TCL4, and P-mat, respectively, vs HEOM. Subplots (d) give the trace distance between HEOM and the aforementioned perturbative approaches (extending out to longer times). All other parameters are as in Ref. [32]. HEOM data taken from Ref. [2].

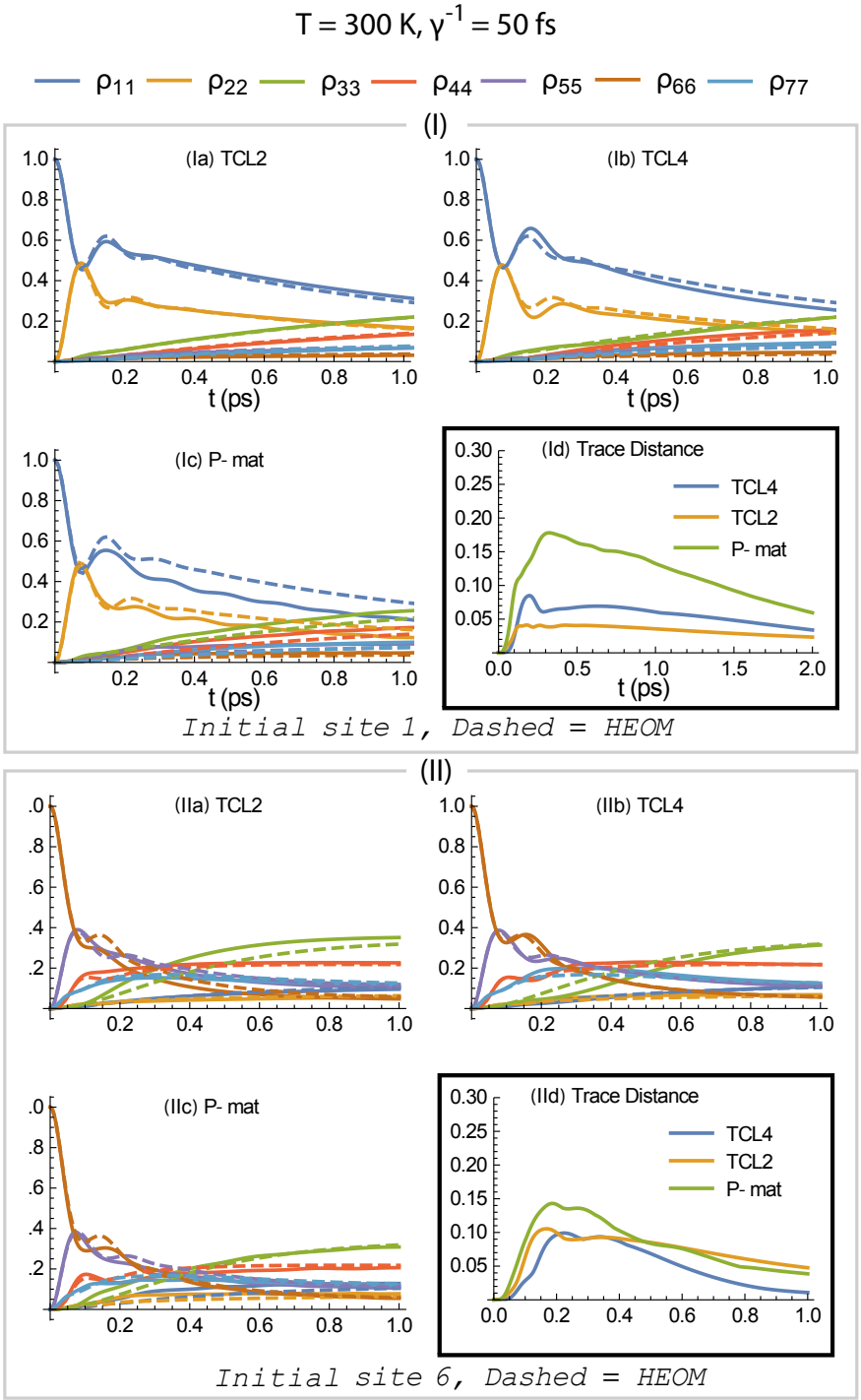

Figure 3.6: Benchmarking of FMO dynamics obtained from perturbative techniques (solid) against numerically converged HEOM (dashed), for temperature $T = 300\ K$ and cutoff frequency $\gamma^{-1} = 50$ fs. Initial excitation is localised at site indicated at the bottom of each panel. Subplots (a)-(c) show comparisons of TCL2, TCL4, and P-mat, respectively, vs HEOM. Subplots (d) give the trace distance between HEOM and the aforementioned perturbative approaches. All other parameters are as in Ref. [32]. HEOM data taken from Ref. [2].

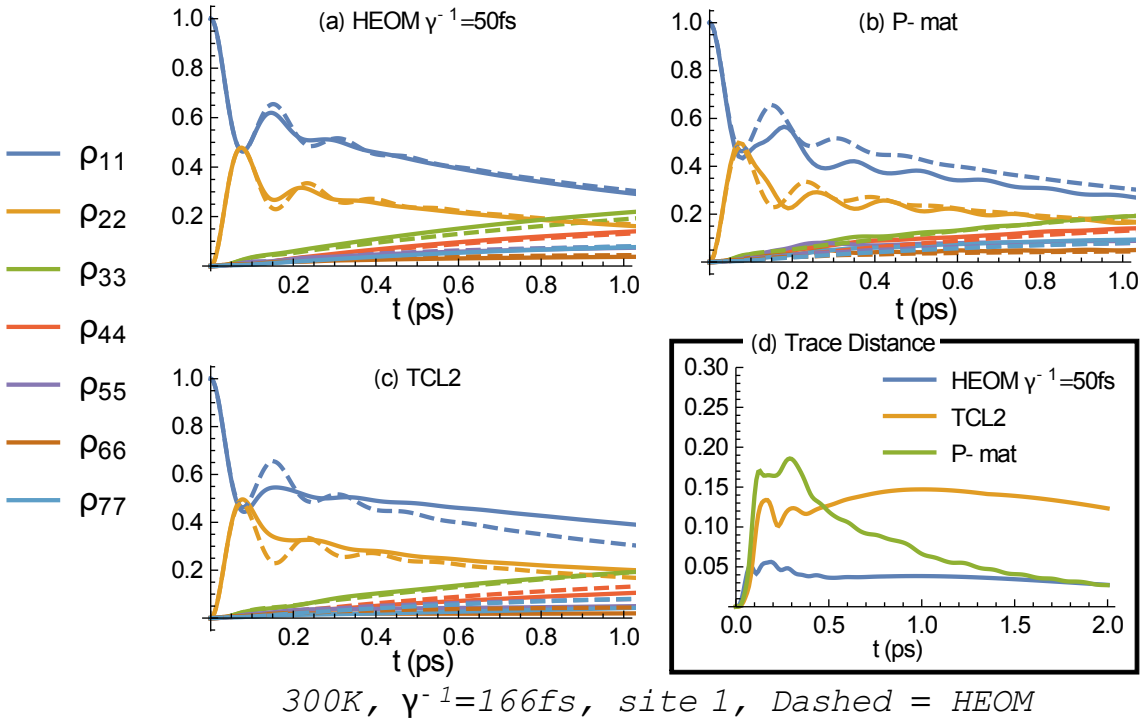

Figure 3.7: FMO dynamics comparison with a stronger coupling: Subplot (a) contrasts HEOM for cutoff frequency $\gamma^{-1} = 166$ fs against HEOM for $\gamma^{-1} = 50$ fs. Subplots (b) and (c) show P-mat and TCL2 (solid) against HEOM, all using cutoff frequency $\gamma^{-1} = 166$ fs and initial excitation localised at site 1. Notably, P-mat performs worse than TCL2 at short times but then improves. TCL4 provides unphysical solutions and has therefore not been included. HEOM data taken from Ref. [2].

By presenting a comparative numerical study of two different classes of weak-coupling methods, contrasted against numerically converged HEOM results, we have verified the validity and predictive power of both variants of the criterion. We have used the canonical spin boson model and the much-studied energy excitation dynamics in the FMO complex as two representative examples to make this case.

Interestingly, we have identified two room temperature FMO configurations with almost identical HEOM results, whilst our perturbative solutions diverge significantly, to the point that it yields un-physical results in the 4th order. This discrepancy is captured by our criterion which confirms that despite the apparent similarity of numerically converged results, one configuration sits well in the weak-coupling regime, whilst the other is sufficiently strongly coupled such that a perturbative approach is no longer justifiable. We note that, surprisingly, although not justified, it still gives fairly adequate results.

Finally, we have seen that P-mat stands its ground reasonably well compared to TCL2, particularly in the long-time limit.

Appendix A: Response Function Estimation Using Exponents

In our simulation, the response function

$$\alpha(t) = D(t) + \mathrm{i}D_1(t) = \int_0^\infty d\omega J(\omega)[\coth(\beta\omega/2)\cos(\omega t) - \mathrm{i}\sin(\omega t)] \tag{3.24}$$

is approximated by a series of exponents[§],

$$D(t) = \sum_{k=1}^{N_R} c_k^R e^{-\mu_k^R t}, \qquad D_1(t) = \sum_{k=1}^{N_I} c_k^I e^{-\mu_k^I t} \ . \tag{3.25}$$

The reason for this is because we are comparing the approximated solutions to exact ones using HEOM, and HEOM only accepts response functions of the form (3.25).

As discussed in Chapter 1.4.2, there are examples of spectral densities where this is analytically the case, such as the Drude-Lorentz spectral density[47], a Lorentzian

[§]This is Eqn 1.114, written here again for clarity.

spectral density[51] and an underdamped Brownian oscillator[52–55]. In the FMO example above we use a Drude-Lorentz spectral density. However, in general one can also numerically fit the response function of an arbitrary bath to a sum of exponential terms, similar in spirit to Ref. [115]. We find that this approach works well for both a Ohmic and super-Ohmic spectral densities.

Technically this was done by evaluating the exact response function at 0.1 ps intervals up to 8 ps, and using Mathematica's "FindFit" function for non-linear least-squares fitting a function to a set of datapoints. This is done separately for the real and the imaginary parts of the response function, where the actual functions we fit are $\sum_{i=1}^{N} a_i e^{-\gamma_i t} \cos b_i t + c_i$ where γ_i, a_i, b_i, c_i are (real) fitting parameters, and N is the hyper-parameter defining the number of exponents we end up with ($2N$ exponents). In our examples we choose $N = 2$ for all cases.

Using this procedure we can fit a large class of response functions using a small number of exponents. As an example, we examine spectral densities with an exponential cut-off with the following form

$$J(\omega) = \eta\lambda(\omega/\omega_c)^s e^{-\omega^2/\omega_c^2} \ , \tag{3.26}$$

where η is a dimensionless parameter used in the main text to interpolate between weak and strong coupling regimes, λ is an energy scale related to the reorganisation energy[§] , ω_c is the cut-off frequency, and s is a parameter. When $s = 1$ we call the spectral density 'Ohmic', and when $s > 1$ or $s < 1$ we call it 'super-Ohmic' or 'sub-Ohmic', respectively. In Fig. (3.8) we show how well the fitting procedure works for the case of $s = 1, 2, 3$. Specifically for the Ohmic case we use in the Spin-Boson example (Section 3.5.1), we get the parameters given in Table. 3.2, with the accuracy

$$\int_0^\infty dt \left(D_{\text{exact}}(t) - D_{\text{approx}}(t)\right)^2 = 1.68 \times 10^{-9} \eta^2 ps^{-4} \ , \tag{3.27}$$

$$\int_0^\infty dt \left(D_{1\ \text{exact}}(t) - D_{1\ \text{approx}}(t)\right)^2 = 4.02 \times 10^{-10} \eta^2 ps^{-4} \ . \tag{3.28}$$

We find that for this case HEOM converges at $N_c = 3$ for $\eta = 1$ and $N_c = 9$ for $\eta = 10$.

[§]The reorganisation energy in this case is given by $\frac{1}{2}\eta\lambda\Gamma(s/2)$, where $\Gamma(s/2)$ is the gamma function.

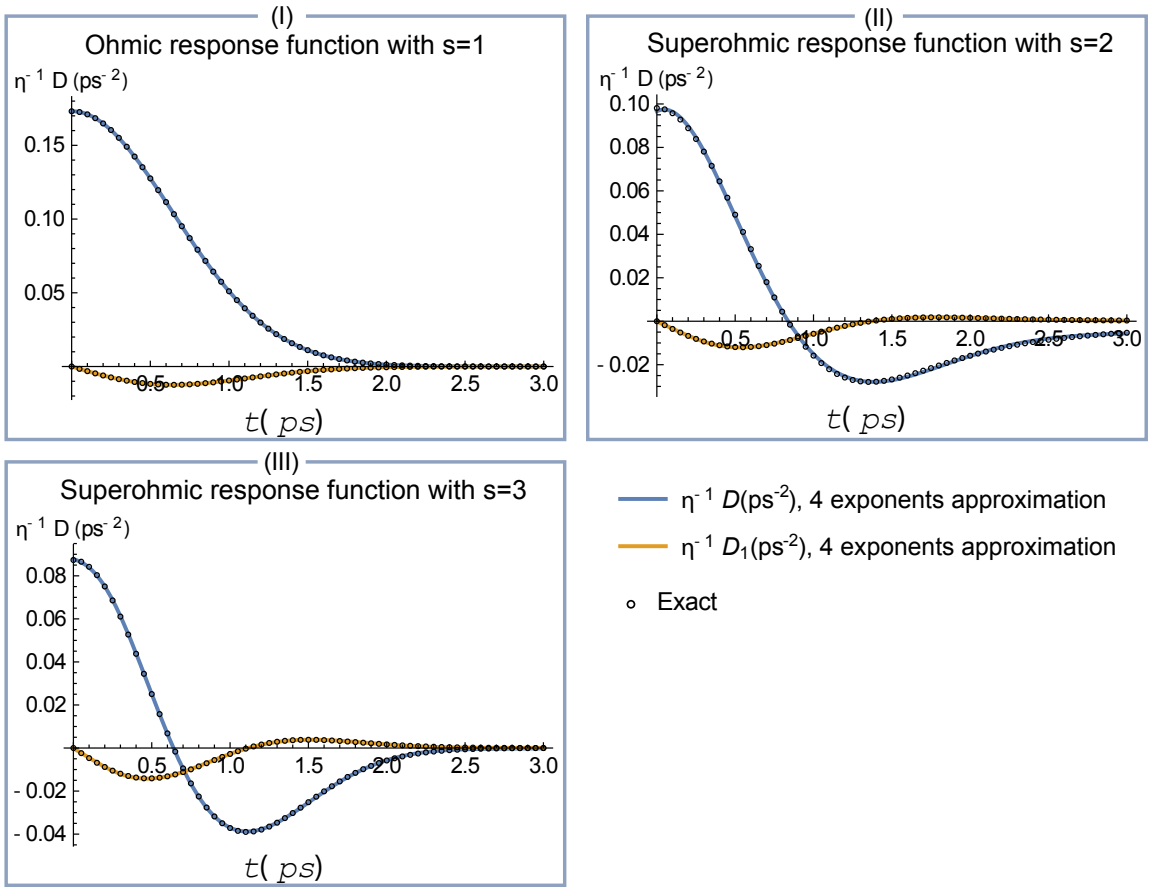

Figure 3.8: Exact and approximated response functions, for Ohmic and super-Ohmic baths characterised by a spectral density given by Eqn. (3.26), with $s = 1, 2, 3$ in panels I, II, III. Other parameters are $T = 50\ K$, $\lambda = 0.01485\ \text{ps}^{-1}$, and $\omega_c = 2.2\ \text{ps}^{-1}$. The dot are exact values, and solid lines are approximations with $N = 2$, *i.e.* 4 exponents. The fitting parameters for Panel I (Ohmic spectral density) are given in Table 3.2.

Parameter	Value $(ps^{-}2)$	Parameter	Value $(ps^{-}1)$
c_1^R/η	$0.145 + 0.316i$	μ_1^R	$2.77 + 0.986i$
c_2^R/η	$0.145 - 0.316i$	μ_2^R	$2.77 - 0.986i$
c_3^R/η	$-0.0588 - 0.0207i$	μ_3^R	$2.68 + 3.12i$
c_4^R/η	$-0.0588 + 0.0207i$	μ_4^R	$2.68 - 3.12i$
c_1^I/η	$-0.00683 + 0.0449i$	μ_1^I	$2.35 - 1.04i$
c_2^I/η	$0.00683 + 0.00938i$	μ_2^I	$2.34 + 3.22i$
c_3^I/η	$0.00683 - 0.00938i$	μ_3^I	$2.34 - 3.22i$
c_4^I/η	$-0.00683 - 0.0449i$	μ_4^I	$2.35 + 1.04i$

Table 3.2: Fitting parameters for a series of exponents form [Eqn. (3.25)] of the response function of an Ohmic bath characterised by a spectral density given by Eqn. (3.21), with $T = 50\ K$, $\lambda = 0.01485\ \text{ps}^{-1}$, and $\omega_c = 2.2\ \text{ps}^{-1}$.

Appendix B: The Slippage of Initial Conditions

Let us explain what the slippage of initial conditions is: This is a second-order argument, and is related to the relationship between the Redfield master equation and the TCL2 master equation: In the Schrödinger picture, the TCL2 kernel $\tilde{\mathcal{K}}_2(t)$ becomes constant for times larger than the memory time of the environment τ_b. This means that after $t \gg \tau_b$ the dynamics become Markovian. In fact, making the substitution $\tilde{\mathcal{K}}_2(t) \to \tilde{\mathcal{K}}_2(\infty)$ yields exactly the (Markovian) Redfield equations for the dynamics of the system. The slippage of initial conditions is a mathematical trick that enables one to recover the long-time TCL2 dynamics of the system using Redfield equations, by introducing a modified initial density matrix $\rho(0) \to \rho_{\text{effective}}(0)$, that captures the difference in the initial dynamics between time-dependent TCL2 and Redfield. That is, after an initial transient and non-Markovian period, the density matrix calculated using TCL2 will be similar to one calculated using Redfield starting from a modified initial state. This "initial slippage" also guarantees the positivity of the density matrix, which is not true in general for the Redfield equations[43].

To put it mathematically, going back to the interaction picture, the claim is that if according to the TCL2 expansion the dynamics are governed by $\frac{\partial}{\partial t}\rho(t) = \mathcal{K}_2(t)\rho(t)$, we can perform a formal integration to get

$$\rho(t) = \rho(0) + \int_0^t d\tau \mathcal{K}_2(\tau)\rho(\tau) \approx \rho(0) + \int_0^t d\tau \mathcal{K}_2(\tau)\rho(0) \ , \tag{3.29}$$

where the approximation is keeping terms up to second order in the expansion. In a similar manner, if the Redfield equation is $\frac{\partial}{\partial t}\rho(t) = \mathcal{R}_2(t)\rho(t)$, with $\mathcal{R}_2$ the Redfield kernel (which is simply the TCL kernel after the Markovian approximation), then we have

$$\begin{aligned}\rho(t) = \rho_{\text{effective}}(0) + \int_0^t d\tau \mathcal{R}_2(\tau)\rho(\tau) &\approx \rho_{\text{effective}}(0) + \int_0^t d\tau \mathcal{R}_2(\tau)\rho_{\text{effective}}(0) \\ &\approx \rho_{\text{effective}}(0) + \int_0^t d\tau \mathcal{R}_2(\tau)\rho(0) \ . \end{aligned} \tag{3.30}$$

The 'slippage operator' $\mathcal{S}$ is defined as

$$\rho_{\text{effective}}(0) = \rho(0) + \mathcal{S}\rho(0) \ , \tag{3.31}$$

and to get to the second line of Eqn. (3.30) we assumed $\mathcal{S} = \mathcal{S}_2$ is second order in the coupling. Now we demand that after time t larger than the memory time of the bath ($t \gg \tau_b$), the two density matrices become the same. Equating the RHS of Eqns. (3.29) and (3.30), we find that

$$\mathcal{S}_2 = \int_0^t d\tau \left[\mathcal{K}_2(\tau) - \mathcal{R}_2(\tau)\right] \ . \tag{3.32}$$

In the above equation we may take the upper limit of the integral to infinity $t \to \infty$ because we assume that the integrand vanishes for times longer than the memory.

The explicit entries of the slippage operator $\mathcal{S}_2$ are given by (cf. Eqn. 3.10):

$$\begin{aligned}\langle ij|\mathcal{S}_2\,|rs\rangle = \\ \sum_\nu \int_0^\infty d\tau \Bigg\{ \sum_k \Big[\delta_{js} e^{-\mathrm{i}\Delta_{kr}\tau} S^\nu_{ik} S^\nu_{kr} \alpha(\tau) + \delta_{ir} e^{+\mathrm{i}\Delta_{ks}\tau} S^\nu_{sk} S^\nu_{kj} \alpha^*(\tau)\Big] \\ - S^\nu_{ir} S^\nu_{sj} \Big[e^{-\mathrm{i}\Delta_{ir}\tau}\alpha(\tau) + e^{+\mathrm{i}\Delta_{js}\tau}\alpha^*(\tau)\Big]\Bigg\} \int_0^\tau dt' e^{-\mathrm{i}(\Delta_{rs}-\Delta_{ij})t'} \ .\end{aligned} \tag{3.33}$$

Notice that if we ignore $D_1(\tau)$, then we have

$$\langle ii|\,\mathcal{S}_2\,|ii\rangle \approx \sum_{k\neq i} \Upsilon_{ik} \ , \tag{3.34}$$

where Υ_{ik} are exactly the terms that appear in the simplified weak-coupling criterion, and are given in Eqn. (3.9).

In the same manner one can obtain higher-order corrections to the slippage operator. For example, the fourth-order term is given by

$$\begin{aligned}\mathcal{S}_4 = \int_0^t d\tau \left[\mathcal{K}_4(\tau) - \mathcal{R}_4(\tau)\right] + \int_0^t d\tau \int_0^\tau dt' \left[\mathcal{K}_2(\tau)\mathcal{K}_2(t') - \mathcal{R}_2(\tau)\mathcal{R}_2(t')\right] \\ - \int_0^t d\tau \mathcal{R}_2(\tau)\mathcal{S}_2 \ ,\end{aligned} \tag{3.35}$$

where $\mathcal{R}_4$ is simply $\mathcal{K}_4$ after the Markovian approximation, and up to fourth order, the slippage operator is $\mathcal{S} = \mathcal{S}_2 + \mathcal{S}_4$.

Chapter 4

Photocell optimisation using dark state protection

4.1 Introduction

In this chapter we study the (quantum) efficiency of an abstract photocell – an apparatus that converts photon energy into chemical energy. We explore the limits of this efficiency, and ways to optimise the photocell to maximise it.

The general framework (explained below) was introduced in a paper by Dorfman *et al*[116], who showed that the operation of a solar energy harvesting device can be enhanced by clever design of a nanoscopic, quantum mechanical system. Though thermodynamical considerations lead to the famous Shockley-Queisser efficiency limit for classical photocell devices[117], the 'detailed balance' underlying this limit can be broken by careful use of quantum interference. In particular, by tailoring the interactions between two[118,119] or more[120,121] idealised and identical two-level energy absorbers, it is possible to prevent the re-emission of absorbed light by arranging that excitations end up in 'dark', *i.e.* optically inaccessible, states. This allows for a larger fraction of an absorbed photon's energy to be dissipated across a target load, rather than dissipated via spontaneous emission.

It is conjectured that Nature already exploits quantum-mechanical properties in order to increase the light-harvesting efficiency of photosynthesis[122]. The most well studied system in this context is the FMO complex[123], which connects the antenna

to the reaction centre in the light harvesting apparatus of green sulfur bacteria. It consists of eight[124] bacteriochlorophyll (BChl a) molecules that are held in place by a messy protein scaffold, and surrounded by water at room temperature, resulting in non-identical BChl excitation energies. True quantum effects may seem unlikely in the 'hot and wet' conditions of such systems. However, the observation of quantum coherent beats in experimentally measured two-dimensional electronic spectroscopy suggests otherwise[29,31–33,77,97,103].

A good definition of the term efficiency is key to quantifying a quantum advantage. One such measure is the energy transfer efficiency, *i.e.* the probability of an excitation reaching the target electron acceptor after starting from a spatially localised state[106,125,126], but this does not capture all aspects of the process, such as the excitation of the system or the work-load. An alternative approach is placing a system between two electrodes, and measuring the current through them as a function of the voltage[127–130]. This way one could calculate power output, but again this way does not model the 'reaction centre' found in biological systems, where the work is taking place. Dorfman *et al.* proposed a different canonical measure[116]: They consider the entire cycle, from absorbing a photon to extracting work, as a quantum heat engine (QHE). Procedurally, they abstract the electron acceptor to become a two-level 'trap', in which transferred electrons 'fill' the excited state before the action of driving a load resistor is mimicked by decay to the lower level of the trap. This gives a straightforward way of defining the power and the efficiency of the heat engine. In this picture, they find that Fano interference may boost the photocurrent by 27% over that of a classical cell. Subsequently, Creatore *et al.*[118] reported an efficiency gain of 35% by introducing the different effect of *dark-state protection* using two identical dipole-coupled emitters. Further gains become possible for more than two chromophores[120,121].

In this chapter, we use the QHE framework to determine whether a quantum advantage is achievable in non-idealised situations typical of real devices and conditions more closely resembling the photosynthetic apparatus. In particular, we consider a light harvesting device where the two constituent chromophores are not identical. In

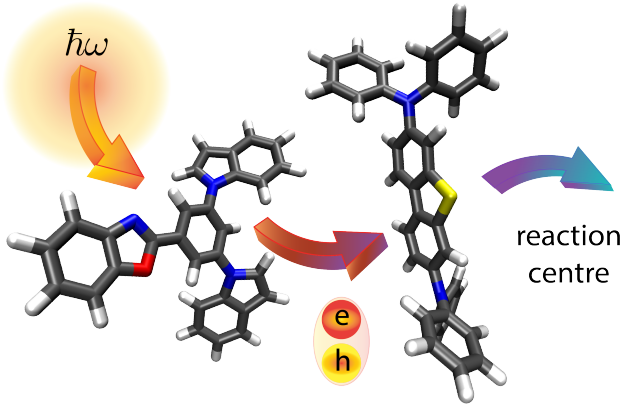

Figure 4.1: Energy flow through the asymmetric model: the dibenzothiophenediamine derivative (BTA) with strong optical oscillator strength absorbs a photon and transfers it to the darker partner diindolylphenylbenzooxazole (IPBO) chromophore via Förster transfer. Delocalisation across the dimer of the relevant quantum eigenstates is not depicted.

Fig. 4.1 we present a cartoon image of our system, featuring a molecule pair that has been numerically modelled and found to exhibit a good dark state. Surprisingly, we find that under realistic constraints an 'asymmetric' dimer may even significantly outperform previously studied systems.

The theory presented here was tailored for and developed in tandem with chemistry calculations, in order to make it apply to real systems. In Ref. [3] our theoretical model and insight has been used by a theoretical chemistry collaborator to identify several example molecules that would be highly efficient light harvesters according to our model. We thus argue that the number of conceivable molecular dimers with a quantum advantage is vast.

4.2 Model

We now introduce a general framework that will allow us to define three specific models shortly. We consider two, generally different, light-absorbing molecules with dipolar coupling. There is a further coupling to an abstracted reaction centre 'trap', modelled as a two level system $|\alpha\rangle$, $|\beta\rangle$ with corresponding energies $\epsilon_\alpha, \epsilon_\beta$, following

Ref. [116]. An excitation absorbed by the molecules can be incoherently transferred into the reaction centre via a phonon-assisted process. In what follows we restrict the dynamics to the subspace with one or zero excitations across the entire system: this approximation is valid since in realistic configurations inspired by natural photosynthetic systems, the average excitation number is very small ($N \approx 0.02$ for an energy gap of 2 eV and sunlight temperature of 6000 K). Since photoexcitation is very rare, once captured it is paramount to prevent spontaneous emission back into the environment. Hence, access to a dark state, *i.e.* a state that is decoupled from the photon field and thus not susceptible to spontaneous emission decay, can enhance the engine's efficiency. By Kasha's rule[131] re-emission of absorbed photons will be dominated by the lowest excited state, motivating our approach of only considering a single excited level per chromophore.

We denote the excited states in the molecules as $|1\rangle, |2\rangle$ with energies ϵ_1, ϵ_2, respectively, and the ground state as $|g\rangle$ with energy ϵ_g. We assume a dipolar coupling between the molecules, which translates to coherent coupling J_{12}. The Hamiltonian of the system is thus of dimension five and given by (see Fig. 4.2)

$$\begin{aligned}\mathcal{H}_s =& \epsilon_1 |1\rangle\langle 1| + \epsilon_2 |2\rangle\langle 2| + \epsilon_g |g\rangle\langle g| \\ &+ \frac{J_{12}}{2}\big(|1\rangle\langle 2| + |2\rangle\langle 1|\big) + \epsilon_\alpha |\alpha\rangle\langle\alpha| + \epsilon_\beta |\beta\rangle\langle\beta| \qquad (4.1)\\ =& \epsilon_+ |+\rangle\langle +| + \epsilon_- |-\rangle\langle -| + \epsilon_g |g\rangle\langle g| \\ &+ \epsilon_\alpha |\alpha\rangle\langle\alpha| + \epsilon_\beta |\beta\rangle\langle\beta| \ . \qquad (4.2)\end{aligned}$$

In the second equation, $|\pm\rangle$ are the usual eigenstates diagonalising the subspace spanned by $|1\rangle, |2\rangle$.

In addition to the bare system we also have the solar photonic bath at $T_h = 6000$ K, which can induce spontaneous and stimulated transitions $|1\rangle \leftrightarrow |g\rangle$ and $|2\rangle \leftrightarrow |g\rangle$. Further, each molecule is embedded in its own local environment of vibrational modes, treated as phonon baths at room temperature $T_c = 300$ K. We assume that the dynamics of the system is Markovian, and follow the second order treatment as explained in Chapter 1.3.2, including making the secular approximation,

which decouples the populations from the coherences, yielding transitions between the energy eigenstates $|+\rangle \leftrightarrow |-\rangle, |+\rangle \leftrightarrow |\alpha\rangle, |-\rangle \leftrightarrow |\alpha\rangle, |\beta\rangle \leftrightarrow |g\rangle$. In Appendix A we verify that the secular approximation is indeed valid for our system by comparing to the full Redfield equations.

Further, we include the reaction centre decay $|\alpha\rangle \leftrightarrow |\beta\rangle$ with rate $\gamma_{\alpha\beta}$, and some leakage between $|\alpha\rangle$ and $|g\rangle$ with rate $\chi\gamma_{\alpha\beta}$. This loss channel brings the system back to the ground state but does not produce work current, and it is often a significant source of inefficiency in organic solar cells[132,133].

The interaction Hamiltonian is thus

$$\mathcal{H}_I = \hat{I}_{1g} + \hat{I}_{2g} + \hat{I}_{11} + \hat{I}_{22} + \hat{I}_{1\alpha} + \hat{I}_{2\alpha} + I_{\beta g} \ , \tag{4.3}$$

where $\hat{I}_{ab} = \frac{1}{2}(|a\rangle\langle b| + |b\rangle\langle a|)\hat{\mu}_{ab}$, and $\hat{\mu}$ are operators of the coupling to the different environments: $\hat{\mu}_{1g}, \hat{\mu}_{2g}$ are dipole operators, and the rest are phonon operators.

The resulting set of Pauli master equations is thus given by:

$$\frac{\partial}{\partial t}\vec{P} = \mathcal{Q}\vec{P} \ . \tag{4.4}$$

Here $\vec{P} = \{P_+, P_-, P_\alpha, P_\beta, P_g\}^\dagger$ is a vector of the populations in the diagonal basis of the system, and $\mathcal{Q}$ is a matrix of the different rates, respecting detailed balance for photon and phonon baths independently. Note that this is not related to the P-mat

method introduced in Chapter 2. Explicitly, the rate equations are given by

$$\begin{aligned}\frac{\partial}{\partial t}P_+ =& -\gamma_{+-}[(N_{\omega_{+-}}+1)P_+ - N_{\omega_{+-}}P_-] \\ &-\gamma_{+g}[(N^{T_h}_{\omega_{+g}}+1)P_+ - N^{T_h}_{\omega_{+g}}P_g] \\ &-\gamma_{+\alpha}[(N_{\omega_{+\alpha}}+1)P_+ - N_{\omega_{+\alpha}}P_g]\ ,\end{aligned} \tag{4.5}$$

$$\begin{aligned}\frac{\partial}{\partial t}P_- =& +\gamma_{+-}[(N_{\omega_{+-}}+1)P_+ - N_{\omega_{+-}}P_-] \\ &-\gamma_{-g}[(N^{T_h}_{\omega_{-g}}+1)P_- - N^{T_h}_{\omega_{-g}}P_g] \\ &-\gamma_{-\alpha}[(N_{\omega_{-\alpha}}+1)P_- - N_{\omega_{-\alpha}}P_g]\ ,\end{aligned} \tag{4.6}$$

$$\begin{aligned}\frac{\partial}{\partial t}P_\alpha =& +\gamma_{+\alpha}[(N_{\omega_{+\alpha}}+1)P_+ - N_{\omega_{+\alpha}}P_\alpha] \\ &+\gamma_{-\alpha}[(N_{\omega_{-\alpha}}+1)P_- - N_{\omega_{-\alpha}}P_\alpha] \\ &-\gamma_{\alpha\beta}[(N_{\omega_{\alpha\beta}}+1)P_\alpha - N_{\omega_{\alpha\beta}}P_\alpha] \\ &-\chi\gamma_{\alpha\beta}[(N_{\omega_{\alpha g}}+1)P_\alpha - N_{\omega_{\alpha g}}P_g],\end{aligned} \tag{4.7}$$

$$\begin{aligned}\frac{\partial}{\partial t}P_\beta =& +\gamma_{\alpha\beta}[(N_{\omega_{\alpha\beta}}+1)P_\alpha - N_{\omega_{\alpha\beta}}P_\alpha] \\ &-\gamma_{\beta g}[(N_{\omega_{\beta g}}+1)P_\beta - N_{\omega_{\beta g}}P_g]\ ,\end{aligned} \tag{4.8}$$

combined with the population normalisation condition $\sum_i P_i = 1$. Here $\omega_{ab} = \epsilon_a - \epsilon_b$ and N_ω ($N^{T_h}_\omega$) is the thermal occupation number for a given frequency ω and temperature T_c (T_h). Resulting transition rates are depicted in Fig. 4.2.

Following Refs. [116,118,134] we define the reaction center current and voltage as

$$I = e\gamma_{\alpha\beta}P_\alpha\ , \tag{4.9}$$

$$V = \epsilon_\alpha - \epsilon_\beta + k_{\mathrm{B}}T_c\ln(P_\alpha/P_\beta)\ , \tag{4.10}$$

and the power generated by the reaction centre as

$$P = IV\ . \tag{4.11}$$

Here T_c is the (cold) phonon temperature, k_{B} the Boltzmann constant, and e the electron charge. We are interested in the steady-state power output, which is found by setting the LHS of Eqn. (4.4) to zero and solving the resulting simultaneous algebraic equations. In the absence of sunlight, the system thermalises to the phonon bath

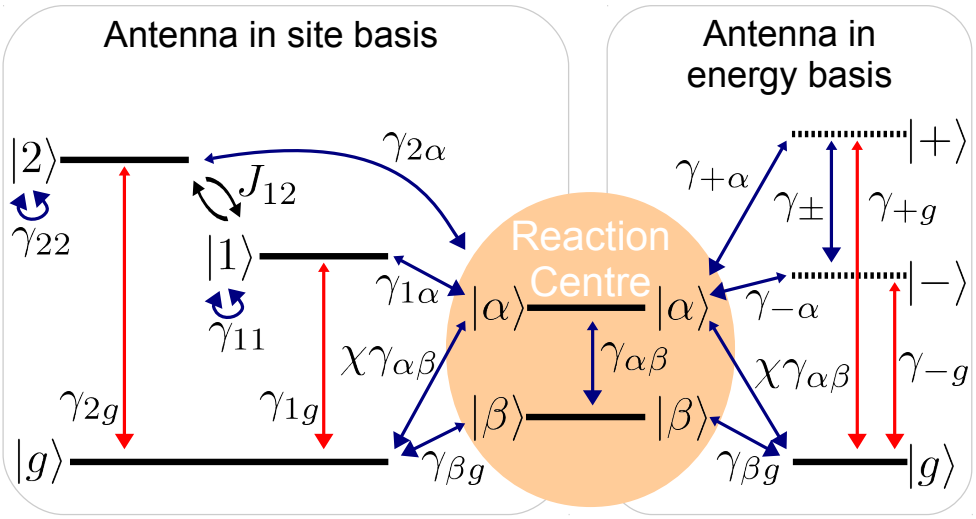

Figure 4.2: Level structure schematic of the three models. On the left we show the system in the site basis and on the right in the energy basis. The reaction centre is the same in both. We denote radiative transitions by red arrows, and non-radiative phonon-induced transitions by blue arrows.

temperature, and the voltage vanishes. Thus V is a measure of the deviation from the thermal state with temperature T_c.[§]

Note that our Hamiltonian is static, and there is thus no cycle as there would be for conventional quantum heat engines[135–137]. Formally our system is therefore rather a heat flow device[138–140], where the heat flowing through the reaction centre is then used to produce work. Henceforth, we adopt the maximal achievable steady state power as our measure of efficiency: we treat the reaction centre as a black box optimizing its $\gamma_{\alpha\beta}$ to generate maximal power (keeping all other parameters fixed). A representative example of the behaviour of P and I as a function of V is given in Fig. 4.3, which was produced by varying only the transfer rate inside the reaction centre $\gamma_{\alpha\beta}$, while fixing all other parameters. The power output of the cell is then given by the maximal power of this plot.

Throughout this chapter we follow Ref. [118] and use a value of $\chi = 0.2$ for the loss channel. Since the reaction centre is abstracted, the exact value of χ is difficult to estimate. We do note that an ideal photovoltaic device with a single band gap

[§]This is in contrast to Refs. [116,118,134], where the transfer $|\alpha\rangle \to |\beta\rangle$ was one-directional, which is equivalent to setting the temperature of the reaction centre to zero, and negative voltage occurs if no sunlight is present.

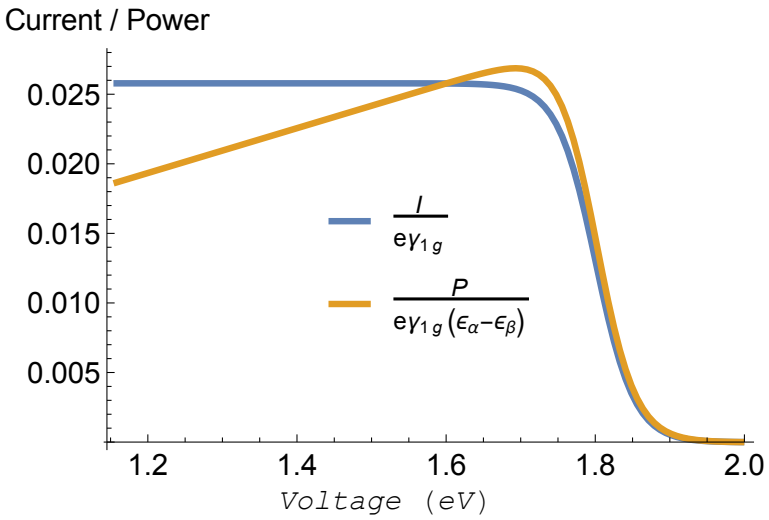

Figure 4.3: An example of a current/power plot as a function of voltage for the asymmetric model. The parameters are: $\gamma_{1g} + \gamma_{2g} = 1.24 \times 10^{-6}$ eV, $\gamma_{11} = \gamma_{22} = 0.005$ eV, $\gamma_{\beta g} = 0.0248$ eV, $T_h = 6000$ K, $T_c = 300$ K, $\epsilon_- = 2$ eV, $\epsilon_2 - \epsilon_1 = 0.1$ eV $J_{12} = 10$ meV $\epsilon_\alpha = 1.8$ eV, $\epsilon_\beta = 0.2$ eV, $\chi = 0.2$.

loses $\sim 50\%$ of its absorbed energy into heat[141], assuming every photon above the energy gap is captured. In organic photovoltaic, the loss in the electronic transport phase amounts for a drop of an empirical $\sim 0.3eV$ in the voltage of the device[133]. The recombination rate strongly depends on the solvent and the molecules of the structure, and can be in the order of a few picoseconds or even less[142,143]. It is thus possible that our value of $\chi = 0.2$ underestimates the losses in the reaction centre (predicting higher overall efficiency of the device). Detailed modelling of the reaction centre is required for an accurate estimation of this parameter.

We now define the three specific models which we shall compare. Namely, these are the *independent model*, the *symmetric model*, and the *asymmetric model*. These have contrasting molecular geometries and are depicted in Fig. 4.4. Below, the rates γ_{1g} and γ_{2g} are the excitation rates of each molecule when the other molecule is not present, and in the same manner $\gamma_{1\alpha}$, $\gamma_{2\alpha}$ denote the independent rates into the reaction centre. The rates γ_{11} and γ_{22} denote the dephasing rates induced by the local phonon bath of each molecule.

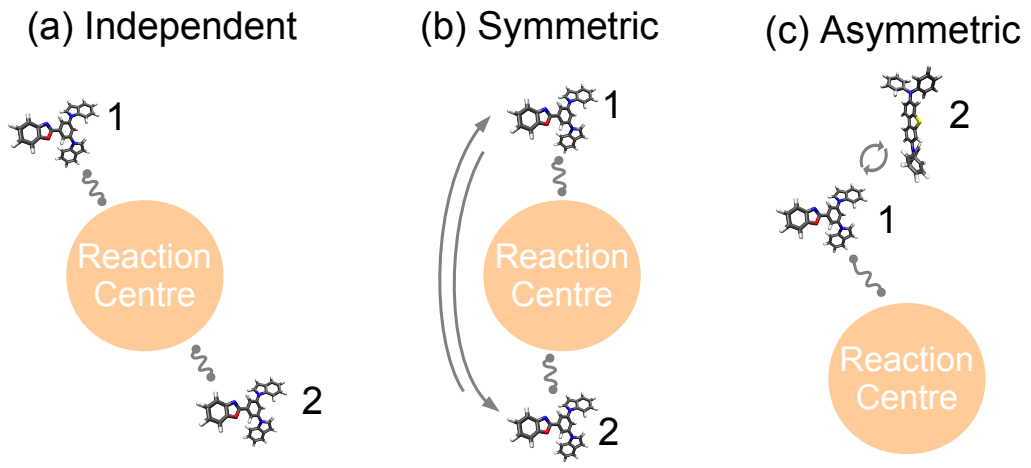

Figure 4.4: Schematic of the different models: (a) independent, (b) symmetric, and (c) asymmetric . (In)coherent coupling is denoted by (wiggly) rounded arrows and the circle denotes the reaction center.

4.2.1 The Independent Model

The independent model has two identical light harvesting molecules that are not directly coupled to one another whilst each is independently coupled to the reaction centre. Specifically $\hat{\mu}_{1g} = \hat{\mu}_{2g}$; $\hat{\mu}_{1\alpha}, \hat{\mu}_{2\alpha}$ represent the coupling to different phonon baths, and $J_{12} = \gamma_{+-} = 0$, *i.e.* the molecules are not coupled to each other. Further, we let $\epsilon_1 = \epsilon_2$ and $\gamma_{+g} = \gamma_{-g}$, which means that both molecules have the same excitation energy and excitation rate, and $\gamma_{+\alpha} = \gamma_{-\alpha}$ which means both molecules are coupled to the reaction centre in the same manner. This model does not exhibit dark state protection and serves as a benchmark for the other models.

4.2.2 The symmetric model

The symmetric model mirrors the model described in Ref. [118] and consists of two identical, directly coupled molecules: $\epsilon_1 = \epsilon_2$, $\hat{\mu}_{1g} = \hat{\mu}_{2g}$, and $J_{12} > 0$. This arrangement leads to a dark and bright state, $|+\rangle$ and $|-\rangle$ respectively, with $\gamma_{-g} = 0$ and $\gamma_{+g} = \gamma_{1g} + \gamma_{2g}$. The phonon environments induce the transition $\gamma_{+-} = \frac{1}{4}(\gamma_{11} + \gamma_{22})$. The molecules couple to the reaction centre in anti-phase $\hat{\mu}_{1\alpha} = -\hat{\mu}_{2\alpha}$ [118], rendering $\gamma_{+\alpha} = 0$. The π phase-shift between the transition operators would for example result

from the wave function of the state $|\alpha\rangle$ having p symmetry, and the two molecules coupling to it from opposite sides. We discuss deviations from this idealised scenario in Section 4.4.

4.2.3 The asymmetric model

The asymmetric model is the main focus of this chapter. It comprises two non-identical molecules $\epsilon_1 < \epsilon_2$ with different dipole moments $\hat{\mu}_{1g} = z\hat{\mu}_{2g}$ where $z < 1$ represents the asymmetry. The dark(er) $|-\rangle$ state has a larger overlap with molecule 1, which we imagine closer to the reaction center, and we assume molecule 2 only has negligibly small reaction center coupling ($\hat{\mu}_{2\alpha} = 0$). We believe that this configuration should be easier to realise than the symmetric model, while allowing engineering of the energy gap $\epsilon_+ - \epsilon_-$. For flat spectral densities of the environments around the transition frequencies, we find that the different rates are given by

$$\gamma_{+g} = |z\langle +|1\rangle + \langle +|2\rangle|^2 \gamma_{2g} \ , \tag{4.12}$$

$$\gamma_{-g} = |z\langle -|1\rangle + \langle -|2\rangle|^2 \gamma_{2g} \ , \tag{4.13}$$

$$\gamma_{+-} = |\langle +|1\rangle|^2 |\langle -|1\rangle|^2 (\gamma_{11} + \gamma_{22}) \ , \tag{4.14}$$

$$\gamma_{+\alpha} = |\langle +|1\rangle|^2 \gamma_{1\alpha} \ , \tag{4.15}$$

$$\gamma_{-\alpha} = |\langle -|1\rangle|^2 \gamma_{1\alpha} \ . \tag{4.16}$$

This means that the asymmetric model exhibits a fully dark state, provided that J_{12}, z, and $\epsilon_2 - \epsilon_1$ satisfy the relation:

$$J_{12} = \frac{2z}{1 - z^2}(\epsilon_2 - \epsilon_1) \ . \tag{4.17}$$

When Eqn. (4.17) is satisfied (*i.e.* we have a completely dark state), these reduce to

$$\gamma_{+g} = \gamma_{1g} + \gamma_{2g} \ , \tag{4.18}$$

$$\gamma_{-g} = 0 \ , \tag{4.19}$$

$$\gamma_{+-} = \frac{z^2}{(1+z^2)^2}(\gamma_{11} + \gamma_{22}) \ , \tag{4.20}$$

$$\gamma_{+\alpha} = \frac{z^2}{1+z^2}\gamma_{1\alpha} \ , \tag{4.21}$$

$$\gamma_{-\alpha} = \frac{1}{1+z^2}\gamma_{1\alpha} \ . \tag{4.22}$$

We note that in the case where both molecules are coupled *independently* to the reaction centre, *i.e.* $[\mu_{1\alpha}, \mu_{2\alpha}] = 0$, but with the same strength $\gamma_{1\alpha} = \gamma_{2\alpha}$, we get $\gamma_{-\alpha} = \gamma_{+\alpha} = \gamma_{1\alpha}$, regardless of the asymmetry.

Whether or not $|-\rangle$ is indeed fully dark, we can express the resulting total excitation rate through an angle Φ:

$$\gamma_{+g} = (\gamma_{1g} + \gamma_{2g}) \cos^2 \Phi \ , \tag{4.23}$$

$$\gamma_{-g} = (\gamma_{1g} + \gamma_{2g}) \sin^2 \Phi \ . \tag{4.24}$$

Thus $\tan^2 \Phi = \gamma_{-g}/\gamma_{+g}$, and $\tan^2 \Phi = 0$ in the presence of a completely dark state.

4.2.4 Deviation from the dark state

Several mechanisms may cause deviation from a fully dark state in both the symmetric and asymmetric models: First, different local environments would generally entail differing reorganisation energy shifts and thus excitation energies. For example, the FMO complex consists of identical BChl units, embedded in a protein scaffolding, resulting in on-site energies spanning a range of 25 meV[29]. Second, the two dipoles may be at an angle φ to each other instead of parallel[118], breaking the interference needed for a completely dark state. Third, the coherent coupling J_{12} depends on both the distance between the two molecules, and the angle φ: $J_{12} = J_{12}^0 \cos\varphi$, where J_{12}^0 is the coupling with parallel dipoles. Taking all this into account we get in the general case, *i.e.* for both models,

$$\tan^2\Phi = \frac{\Omega_R(1+z^2) - (\epsilon_2 - \epsilon_1)(1-z^2) - 2zJ_{12}\cos\varphi}{\Omega_R(1+z^2) + (\epsilon_2 - \epsilon_1)(1-z^2) + 2zJ_{12}\cos\varphi} \ , \tag{4.25}$$

with $\Omega_R = \sqrt{(\epsilon_2 - \epsilon_1)^2 + J_{12}^2}$ being the Rabi frequency of the bare system between sites 1 and 2. Further discussion about deviation from the fully dark state, and details on the coupling to the reaction centre are given in Section 4.4.

4.2.5 Coupling to the Reaction Centre

In our model we use nonlocal electron-phonon coupling[144–147] to capture the transfer into the reaction centre. We use this form because of its mathematical simplicity plus its ability to capture the suppression of the transfer $|+\rangle \rightarrow |\alpha\rangle$ as introduced in Ref. [118].

As this form is not as commonly used in the study of exciton transfer, we note that we could alternatively have implemented the reaction centre transfer with only local phonons. In that case, we would include the following additional coherent coupling term to the system Hamiltonian [Eqn. (4.1)]

$$\begin{aligned} \mathcal{H}_s \rightarrow & \mathcal{H}_s \\ & + \left(v_{1\alpha} |1\rangle \langle\alpha| + v_{2\alpha} |2\rangle \langle\alpha| + v_{\beta g} |\beta\rangle \langle g| + H.c.\right) \ , \end{aligned} \tag{4.26}$$

whilst substituting all of $\hat{I}_{1\alpha}, \hat{I}_{2\alpha}, \hat{I}_{\beta g}$ in Eqn. (4.3) for another local phonon bath $\hat{I}_{\beta\beta}$. This results in almost exactly the same final set of rate equations. The main difference is that there is no longer a complete cancellation of the $|+\rangle \rightarrow |\alpha\rangle$ transition in the symmetric model. The asymmetric model, which is the main focus of our paper, remains largely unaffected (there is an additional small rate $|+\rangle \rightarrow |\alpha\rangle$ which becomes negligible when the molecule is properly asymmetric). These slight differences in the rate equation model depend on the specifics of the reaction center (which we only model in an abstracted way anyway), and in particular they do not change any of our central conclusions. For this reason, we have adopted the nonlocal phonon model, which maps directly onto the approach used by Ref. [118], for ease of comparison.

4.3 Numerical results

In our numerical simulations we look for power enhancement of the (a)symmetric relative to the independent model, as measured by the ratio of the respective maximum

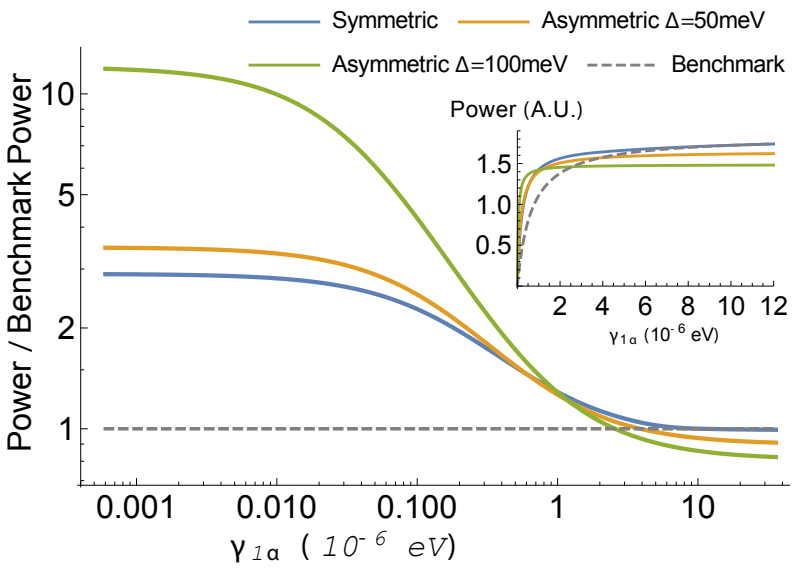

Figure 4.5: Power enhancement over the benchmark achievable through a dark state, as a function of the trapping rate on a log-log scale. The parameters were chosen to enable comparison with Ref. [118]: $\gamma_{1g} + \gamma_{2g} = 1.24 \times 10^{-6}$ eV, $\gamma_{11} = \gamma_{22} = 0.005$ eV, $\gamma_{\beta g} = 0.0248$ eV, $T_h = 6000$ K, $T_c = 300$ K, $\epsilon_- = 2$ eV, $\epsilon_\alpha = 1.8$ eV, $\epsilon_\beta = 0.2$ eV, $\chi = 0.2$. Inset: the total power output of the systems in arbitrary units.

powers. As previously discussed, $\gamma_{\alpha\beta}$ is varied to maximise the power output of the circuit $P = IV$ [see Eqn. (4.11)]. For a fair comparison, we keep $\gamma_{+g} + \gamma_{-g}$, ϵ_-, and $\gamma_{1\alpha}$ equal across all three models.

Fig. 4.5 presents the enhancement achievable by dark-state protection. Here we have optimized J_{12} and $\gamma_{\alpha\beta}$ with all other parameters fixed. We also constrain J_{12} to below 30 meV as an upper limit of realistic coupling strength. For the asymmetric model the dark state criterion (4.17) imposes an appropriate dipole asymmetry z for a given value of J_{12}. Quantum enhancement is only possible when the transfer into the reaction center is relatively slow and constitutes a bottleneck in the cycle. In the limit of $\gamma_{1\alpha} \to 0$ an upper bound to the enhancement emerges. Within a reasonable parameter range this limit grows with increasing J_{12} for the symmetric and with $\epsilon_2 - \epsilon_1$ for the asymmetric case. As strong coupling is harder to realise than site energy mismatch, asymmetric dimers might more easily achieve high performance. We note that deeper into the slow transfer limit the potential enhancement factors can significantly exceed the values of up to 50% reported by Refs. [116,118,120]. By

contrast, for fast transfer rates dark-state protection offers no advantage: absorbing photons at an energy higher than the extraction energy (*i.e.* at reduced thermal photon occupancy), combined with $\gamma_{2\alpha} = 0$, is now detrimental.

Fig. 4.6 shows the relative power enhancements of the asymmetric model as a function of the energy difference $\epsilon_1 - \epsilon_2$ and of the coupling J_{12}. We also plot the equivalent enhancement given by the symmetric model, and show there is a parameter regime, with boundaries marked by a black line, for which the asymmetric model outperforms the symmetric one. The asymmetric model displays a peak power enhancement at finite coupling and energy difference. This happens for two reasons: First, in the regime $\epsilon_+ - \epsilon_- \lesssim k_B T$, the rate $|-\rangle \to |+\rangle$ is non-negligible, and so the dark state is not protected. Second, if $\epsilon_+ - \epsilon_- \gg J_{12}$, the rate $|+\rangle \to |-\rangle$ becomes negligible, and the dark state is rarely populated. Note that in the limit $J_{12} \to 0$, the asymmetric model gives a smaller power than the independent benchmark. This is because we set $\gamma_{2\alpha} = 0$ for the asymmetric model, effectively making it a single antenna setup benchmarked against two antennae. We examine further realistic imperfections, including the presence of additional dephasing mechanisms, in the next Section.

4.4 Realistic imperfections

In this Section we discuss some imperfections that can induce deviations from the case discussed in the previous Section.

In Fig. 4.7 we plot the relative enhancement of the symmetric and asymmetric models when deviating from the dark state. We examine several different $\epsilon_2 - \epsilon_1$ values, for each we set a z value that satisfies Eqn. (4.17). Now adding a deviation from the dark state condition $\epsilon_2 - \epsilon_1 \to \epsilon_2 - \epsilon_1 + \Delta$, we plot the relative enhancement and the deviation from the dark state $\tan^2 \Phi$. We find that the performance of the symmetric model is relatively robust over deviations of tens of meV in the site energies, even-though its $|-\rangle$ state is then far from fully dark. We attribute this to the fact that for $J_{12} = 10$ meV there is a non-negligible rate $|-\rangle \to |+\rangle$, meaning population

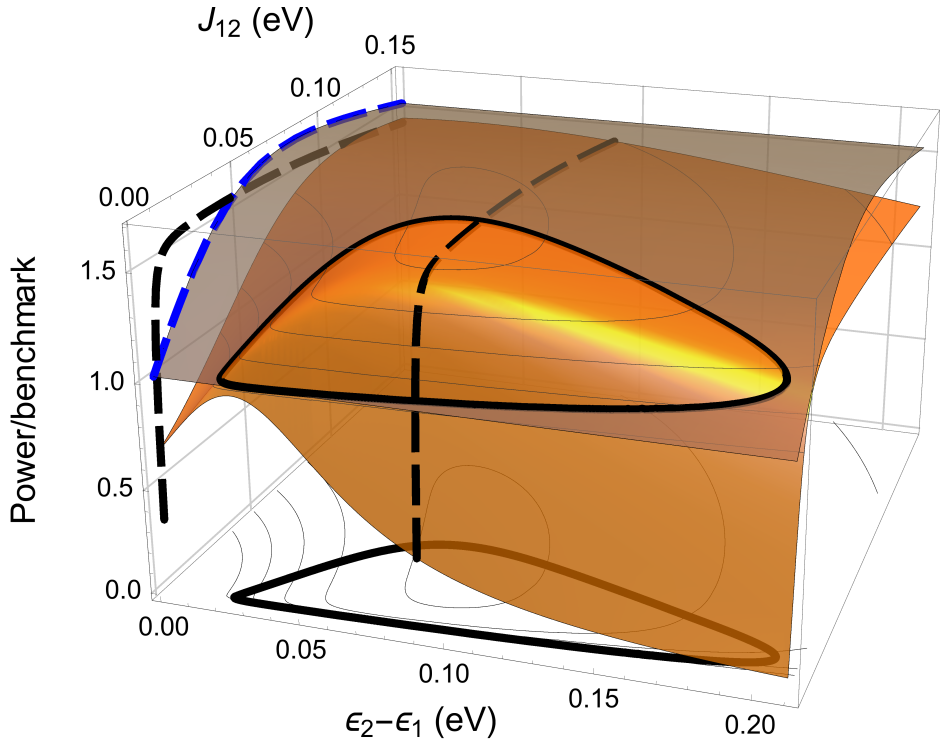

Figure 4.6: Orange surface: relative power enhancement of the asymmetric model, as a function of the energy difference $\epsilon_2 - \epsilon_1$ and coupling J_{12}. Gray surface: relative power enhancement of the symmetric model (independent of $\epsilon_2 - \epsilon_1$). Black dashed line: asymmetric model enhancement for a fixed $\epsilon_2 - \epsilon_1 = 90$ meV. The dashed line is projected onto $\epsilon_2 - \epsilon_1 = 0$ plane, for comparison with the symmetric equivalent (dashed blue). The black thick line is the contour where the symmetric and asymmetric power ratios are equal. Parameters are as in Fig. 4.5 and with $\gamma_{1\alpha} = 6 \times 10^{-7}$ eV.

in the dark state is not fully protected even at $\Delta = 0$. Deviating from an ideal dark state thus only results in minor corrections to the enhancement. We also find that for the asymmetric model, a deviation in the site energies only slightly shifts the system from the dark state ($\tan^2 \Phi < 0.05$). Interestingly, the performance generally increases either to the left or to the right of the $\Delta = 0$ case, *i.e.* when Eqn. (4.17) is not strictly satisfied. Not only does this imply robustness against fluctuations in the site energies, it could also be exploited to design optimised asymmetric dimers away from the dark-state criterion. The reason for this surprising power enhancement at $\Delta \neq 0$ is due to several competing processes that happen when increasing (decreasing) Δ: the transfer rate into the dark state γ_{+-} decreases (increases), as well as the opposite transfer from the dark to the bright state, while the transfer from the dark state into the reaction centre $\gamma_{-\alpha}$, which is an important bottleneck, increases (decreases). Reducing any bottleneck at the expense of sacrificing some degree of dark-state protection leads to higher overall performance.

Another factor affecting the power output is the coupling to the reaction centre. For the symmetric model, following Ref. [118], we assume that the two molecules are engineered in such a way that the two antenna chromophores couple to the reaction centre with a relative phase difference of π (this could, for example, arise from the form of the relevant wave-function orbitals at site $|\alpha\rangle$). This particular choice renders the $|+\rangle$ state completely decoupled from the reaction centre, whereas the rate from the dark-state $|-\rangle$ to the reaction centre is maximal. Deviations from this idealised situation are to be expected when the molecules do not occupy exactly diametrically opposed sides of the reaction centre. In this case we can define an angle θ_{RC} that capture the phase difference between the coupling of the two molecules to the reaction centre via

$$\hat{\mu}_{2\alpha} = e^{\mathrm{i}\theta_{RC}} \hat{\mu}_{1\alpha} \ . \tag{4.27}$$

When $\theta_{RC} \neq \pi$, due to a different geometrical arrangement, static disorder or

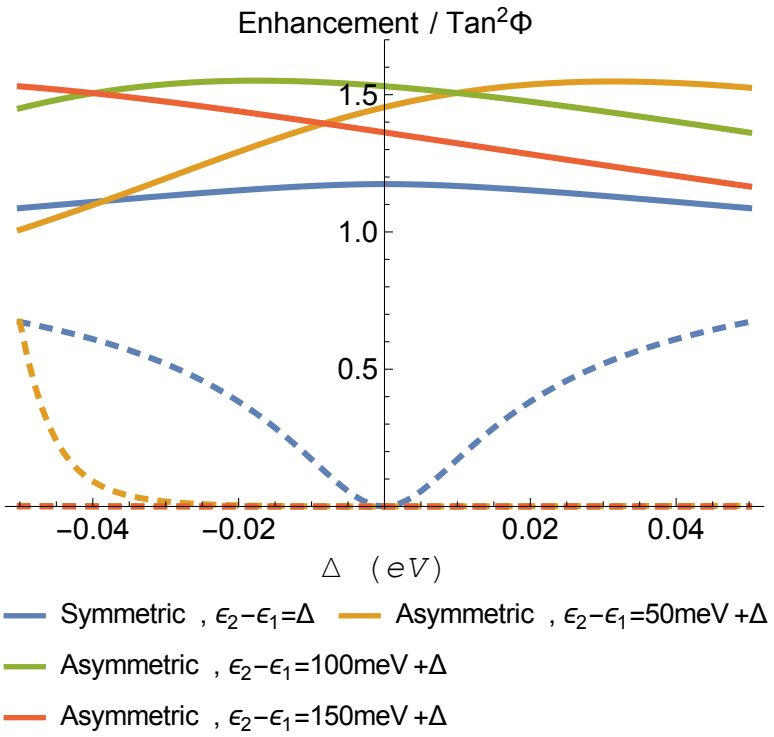

Figure 4.7: A comparison of the relative power enhancement achievable with a deviation from the dark state, as a function of the deviation Δ of the energy difference $\epsilon_2 - \epsilon_1$ from the ideal case where a dark state is present. The symmetric model and three different asymmetric model cases are shown. In solid is the relative enhancement of the symmetric and asymmetric models, and in dashed is $\tan^2\Phi$ for each model. Other parameters are inspired by Ref. [118]: $\gamma_{1g} + \gamma_{2g} = 1.2 \times 10^{-6}$ eV, $\gamma_{11} = \gamma_{22} = 0.005$ eV, $\gamma_{1\alpha} = 6 \times 10^{-7}$ eV, $\gamma_{\beta g} = 0.0248$ eV, $T_h = 6000$ K, $T_c = 300$ K $\epsilon_m = 2$ eV, $J_{12} = 10$ meV, $\epsilon_\alpha = 1.8$ eV, $\epsilon_\beta = 0.2$ eV, $\chi = 0.2$.

dynamical fluctuations, the transfer rates to the reaction centre are then given by:

$$\gamma_{+\alpha} = [1 + (J_{12}/\Omega_R)\cos\theta_{RC}]\gamma_{1\alpha} \ , \tag{4.28}$$

$$\gamma_{-\alpha} = [1 - (J_{12}/\Omega_R)\cos\theta_{RC}]\gamma_{1\alpha} \ . \tag{4.29}$$

Only for the case of no dipole mismatch ($\varphi = 0$) and perfect antisymmetric coupling to the reaction centre ($\theta_{RC} = \pi$) do we obtain $\gamma_{+\alpha}/\gamma_{-\alpha} = \gamma_{-g}/\gamma_{+g} = \tan^2\Phi$ as assumed so far. Figure 4.8 shows the relative enhancement of the symmetric model when the coupling to the reaction centre deviates from $\theta_{RC} = \pi$. We note that for small deviations (less than $\sim \pi/4$) the decrease in enhancement is only about 5%.

Turning to the asymmetric system, only molecule 1 is coupled to the reaction centre, so the concept of a relative phase difference does not arise. In this case, the transfer rates to the reaction centre are:

$$\gamma_{+\alpha} = \frac{1}{2}[1 - (\epsilon_2 - \epsilon_1)/\Omega_R]\gamma_{1\alpha} \ , \tag{4.30}$$

$$\gamma_{-\alpha} = \frac{1}{2}[1 + (\epsilon_2 - \epsilon_1)/\Omega_R]\gamma_{1\alpha} \ . \tag{4.31}$$

An interesting observation here is that in the case of deviation from the dark state, the rate $\gamma_{-\alpha}$ can actually increase. As described above, this is one reason why the optimal set of parameters of the asymmetric dimer can be away from the fully dark state, as shown in Fig. 4.7.

In Appendix B we discuss the case of some additional pure-dephasing noise in the site basis, and show how this type of noise can reduce the quality of the dark state and thus degrade the total efficiency.

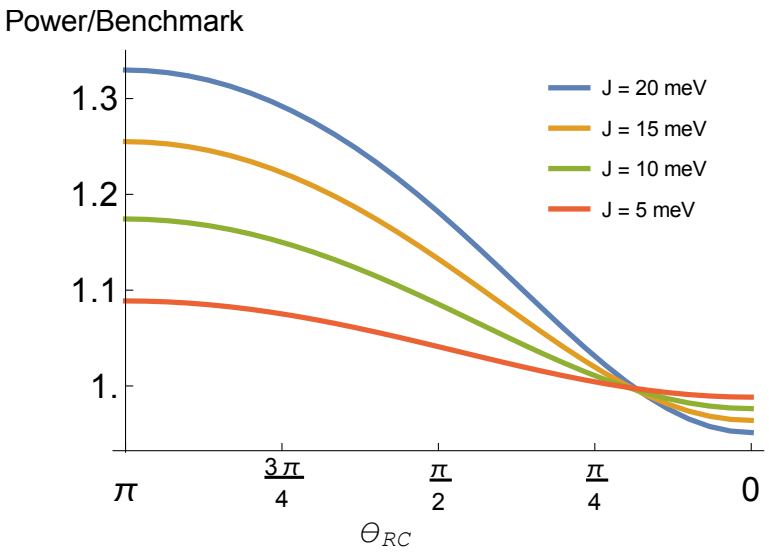

Figure 4.8: A plot of the power enhancement of the symmetric model when the coupling to the reaction centre is not perfectly antisymmetric. The parameters are inspired by Ref. [118]: $\gamma_{1g}+\gamma_{2g} = 1.2\times10^{-6}$ eV, $\gamma_{11} = \gamma_{22} = 0.005$ eV, $\gamma_{1\alpha} = 6\times10^{-7}$ eV, $\gamma_{\beta g} = 0.0248$ eV, $T_h = 6000$ K, $T_c = 300$ K $\epsilon_m = 1.8eV$, $\epsilon_\alpha = 1.8eV$, $\epsilon_\beta = 0.2eV$,$\chi = 0.2$.

4.5 Summary and Conclusions

In conclusion, we have presented a general model of light absorption by an asymmetric pair of coupled chromophores, finding that it can outperform both the symmetric dimer and a pair of independent molecules in realistic parameter regimes of operation for a solar cell device. Not relying on identically matched coupled chromophores, this approach is more robust to deviations from the delicate conditions required by its symmetric counterpart. Moreover, in Ref. [3] we continue the analysis using chemistry calculations performed by a theoretical chemistry collaborator, and describe a roadmap for identifying suitable molecular dimers for demonstrating this effect by screening a very large set of possible candidate molecules. We present several specific molecule pairs that have been numerically resolved to exhibit a good dark state ($\tan^2\Phi \lesssim 0.05$) while molecule 2 having a strongly allowed optical transitions (μ of 3.5 atomic units). We also show that an abundance of real pairs of molecules have the required asymmetric properties.

The reason our asymmetric model works so well is that it enables arbitrarily large

energy gaps between the bright and dark states, thus preventing phonon-assisted promotion from the dark to the bright state. In the regime where excitations are rare and the transfer into the reaction center is very slow, this translates into better protection of the excitations, thus increasing the overall efficiency of the device.

Appendix A: Bloch-Redfield equation model

The results shown in the main text are based on a rate equation model. We here discuss the validity of this treatment, by comparing its results to those obtained from full Bloch-Redfield equations. As we demonstrate below, the rate equation model is more than adequate in the parameter regimes of interest.

To compare the full Bloch-Redfield treatment to our simplified rate equation model, we need to make additional assumptions about the imaginary parts of the TCL2 generator, which correspond to unitary renormalisation terms that do not feature in the rate equations. Expecting them to be small, we neglect (optical) Lamb shift terms whilst keeping (phonon) reorganisation energies, which we assume to be 10% of the rates given by each bath, *i.e.* $\lambda_k = 0.1\gamma_k$ (the precise choice is not important). In Fig. 4.9 we plot the difference in enhancement given by the asymmetric and symmetric models, for the same parameters as in Fig. 4.5. We find that in all cases the secular approximation is fully justified. In Figs. 4.10 and 4.11 we plot the difference in enhancement given by the asymmetric model and symmetric models, respectively, for the same parameters as in Fig. 4.6. We find that for the asymmetric case, the secular approximation is fully justified whenever the difference between the $|+\rangle$ and the $|-\rangle$ states is sufficiently large, which is the relevant regime for this work. For the symmetric case the two treatments essentially coincide up to numerical inaccuracies.

Appendix B: Pure Dephasing

We expect phonons to be the dominant source of decoherence and dephasing of our exciton states. Since their effect has already been accounted for based on a microscopic treatment, we here only need to consider small additional contributions, either

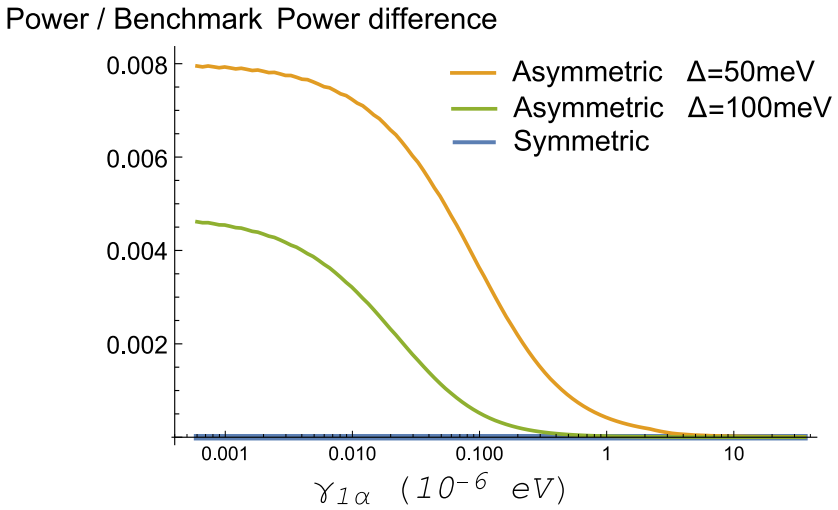

Figure 4.9: Difference between the enhancement given by the asymmetric and symmetric models with rate equations, and with the full Redfield theory. All parameters are the same as in Fig. 4.5.

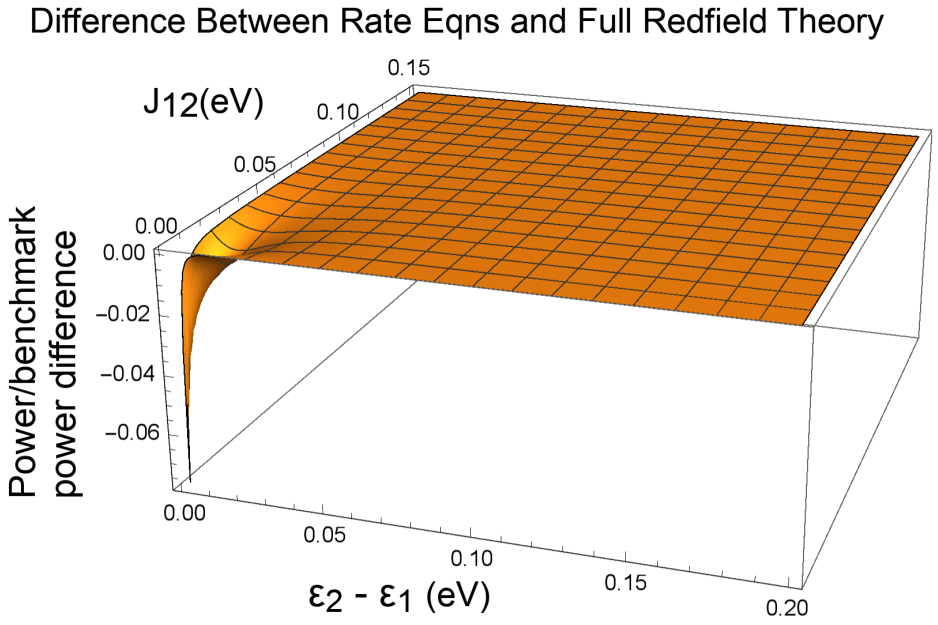

Figure 4.10: Difference between the enhancement given by the asymmetric model with rate equations, and with the full Redfield theory. All parameters are the same as in Fig. 4.6.

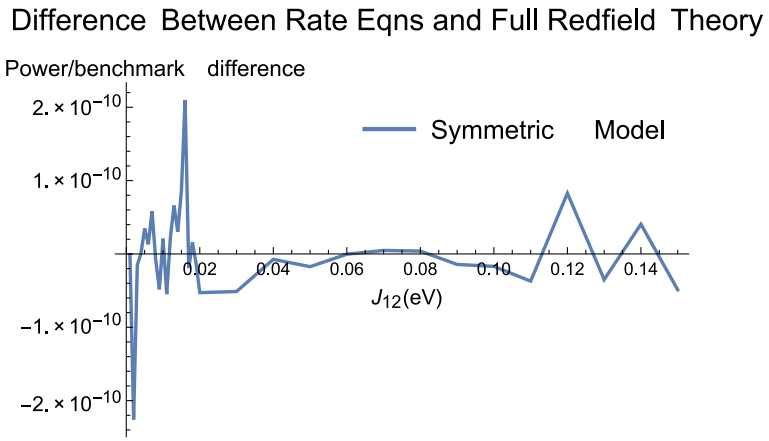

Figure 4.11: Difference between the enhancement given by the symmetric model with rate equations, and with the full Redfield theory. All parameters are the same as in Fig. 4.6.

due to other, unknown physical processes or inadequacies of our microscopic small, which does after all involve some approximations. Therefore, not being able to fall back on microscopically informed dephasing rates, we implement a phenomenological model to investigate how our results differ when pure dephasing terms defined in the site basis are included. Explicitly, we simply add a Lindblad operator to the Bloch-Redfield treatment, which is given by

$$A_{\mathrm{d}} = \sqrt{\gamma_{\mathrm{dephase}}}\left(|1\rangle\langle 1| - |2\rangle\langle 2|\right)/\sqrt{2}\ , \tag{4.32}$$

$$\mathcal{L}_{\mathrm{dephase}}\rho = A_{\mathrm{d}}\rho A_{\mathrm{d}} - \frac{1}{2}A_{\mathrm{d}}A_{\mathrm{d}}\rho - \frac{1}{2}\rho A_{\mathrm{d}}A_{\mathrm{d}}\ . \tag{4.33}$$

As discussed above, we expect any additional pure dephasing rate to be much smaller than the level of decoherence that is already accounted for. Taking γ_{11} as an indicative comparative measure, we will consider a dephasing rate that is 5-20% of that.

Fig. 4.12 shows the maximum relative enhancement of the different models, for the same parameters as in Fig. 4.5. We find that the asymmetric model is very susceptible to pure dephasing, compared to the symmetric one, especially in the very weak coupling to the reaction centre regime. In some cases pure dephasing even brings the otherwise superior asymmetric model below the symmetric one. We believe this

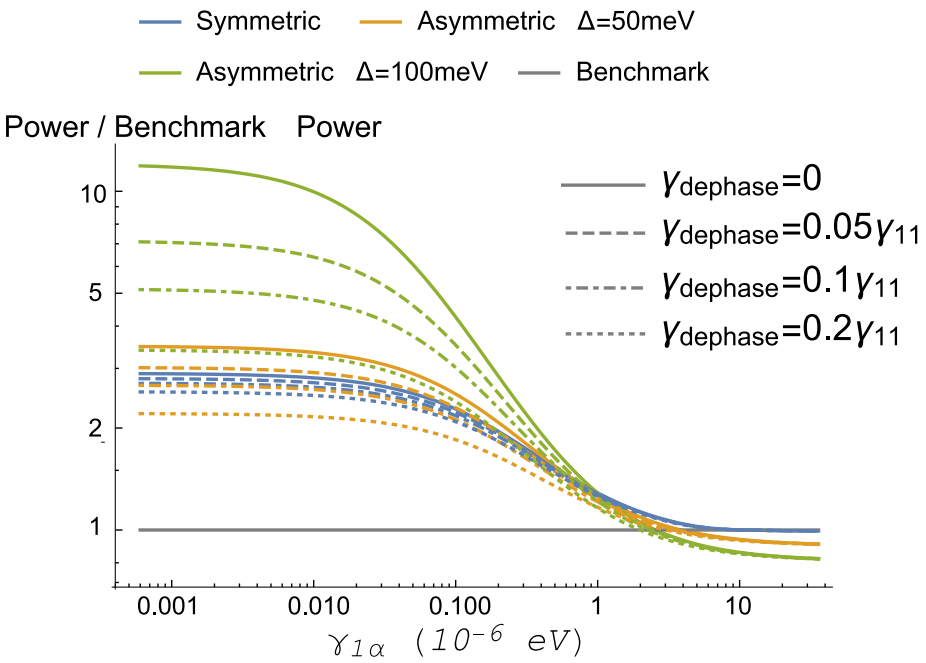

Figure 4.12: The enhancement given by the different models as a function of the rate into the reaction centre $\gamma_{1\alpha}$, with phenomological pure dephasing γ_{dephase}. All other parameters are the same as in Fig. 4.5.

is because such pure dephasing, defined with respect to the site basis, effectively corresponds to a non-directional (or infinite temperature) transition $|-\rangle \leftrightarrow |+\rangle$, thus degrading the protection against exciton recombination given by the $|-\rangle$ state, which is the main advantage of the asymmetric model over the symmetric one.

Figs. 4.13 and 4.14 show the enhancements given by the asymmetric model and symmetric models, respectively, for the same parameters as in Fig. 4.6. We find that for both cases, additional pure dephasing reduces the enhancement by roughly 10% for $\gamma_{\text{dephase}} = 0.1\gamma_{11}$. It is well-known that pure dephasing noise can enhance transport in quantum networks[148,149], and specifically in light-harvesting systems[126,150–153]. In our model, the added dephasing enhances the transfer $|-\rangle \to |+\rangle$, which is the reason for the reduction in the power output.

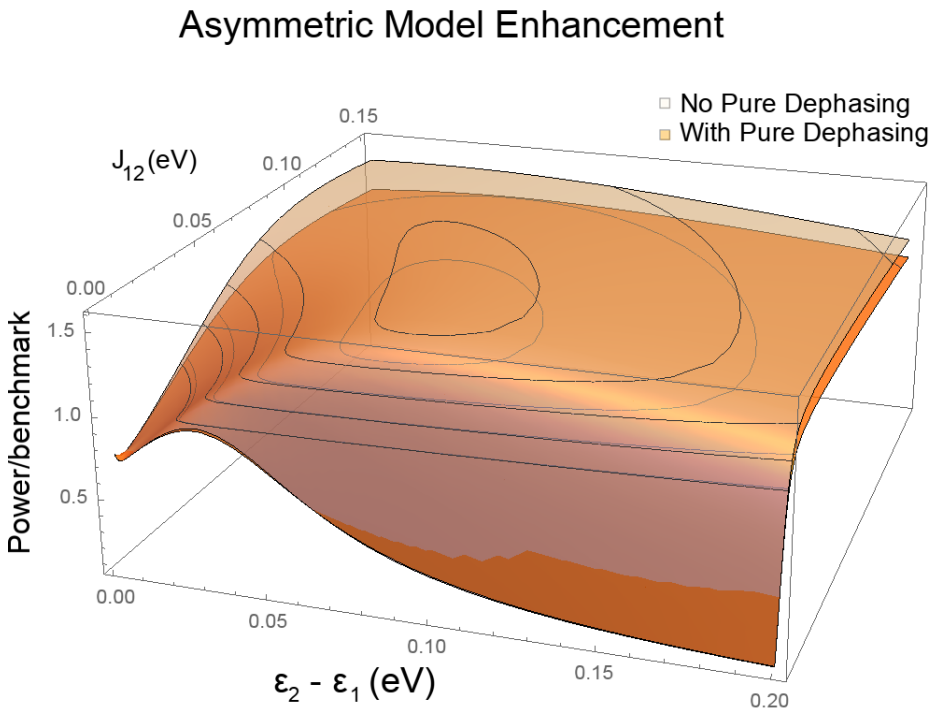

Figure 4.13: The enhancement given by the asymmetric model with and without phenomological pure dephasing. Here, $\gamma_{\text{dephase}} = 0.1\gamma_{11}$ and all other parameters are the same as in Fig. 4.6.

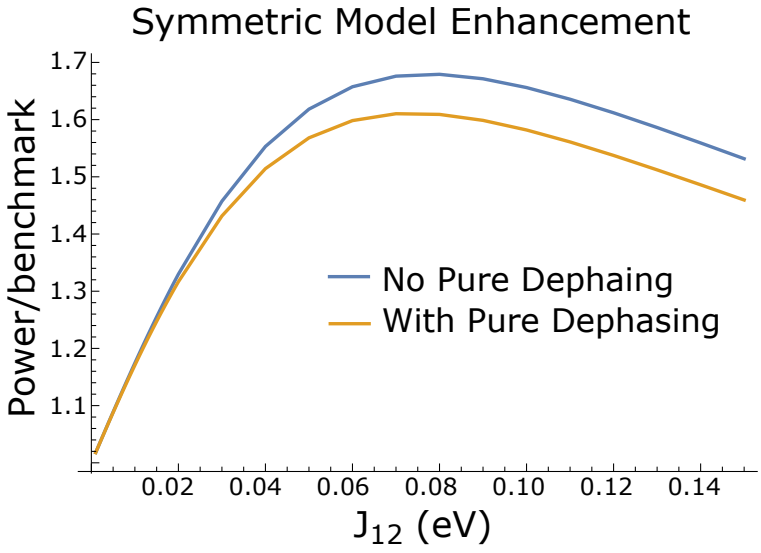

Figure 4.14: The enhancement given by the symmetric model with and without phenomological pure dephasing. Here, $\gamma_{\text{dephase}} = 0.1\gamma_{11}$ and all other parameters are the same as in Fig. 4.6.

Chapter 5

Optimising energy transport down a biased chain

5.1 Introduction

In this chapter we use the same theoretical framework of Chapter 4, but instead of two molecules, we think of a chain of many (non-identical) molecules. One side of the chain is close to the reaction centre, and only the adjacent molecule is coupled to it, while on the far side of the chain there is a molecule which is the source of the initial excitation. A sketch of the system is depicted in Fig. (5.1).

The question we ask is the following: given an initial excitation energy E_0, and excitation energy E_{N+1} at the 'final' site[§], what is the optimal energy configuration for the middle N molecules, which maximises the power output of the reaction centre, assuming equal coherent dipole-dipole interaction between nearest-neighbours, and in the presence of phonons and spontaneous emission.

The inspiration for this question was to find the quantum equivalent of the brachistochrone problem, presented by Johann Bernoulli in 1696, as a challenge to his fellow mathematicians: find the shape of the curve down which a bead sliding from rest and accelerated by gravity will slip (without friction) from one point to another in the least time.

By the expiration date for the challenge, Johann had received 5 (correct) solutions

[§]That is the excitation energy of the molecule that is closest to the reaction centre

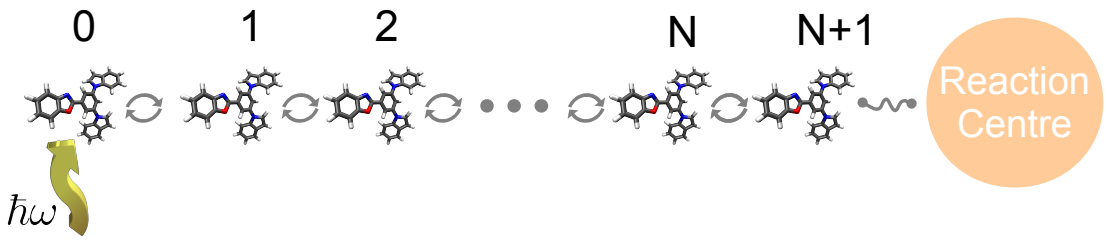

Figure 5.1: A sketch of the model, consists of $N+2$ molecules and a reaction centre. The initial excitation occurs at molecule 0, molecule $N+1$ is coupled to the reaction centre, and we treat the excitation energies of the middle N molecules as free parameters in order to optimise the power output of the reaction centre.

to his problem: his own solution, one from Leibniz, one from his brother Jakob, one from l'Hôpital, and finally, there was an anonymous submission bearing an English postmark. There is a legend saying that Johann, partially chastened, partially in awe, put down the unsigned document and knowingly remarked "I recognise the lion by his paw". Famously, it was Newton's solution, and it took him less than a day to prove that the optimal solution is a segment of a cycloid[154]. For completeness, we include a solution to the brachistochrone problem in Appendix A.

Naturally, the brachistochrone problem has been studied under many different generalisations, including to the relativistic[155–157] and quantum[158–165] theories. The usual formulation of the so-called quantum brachistochrone problem[165] is to find a Hamiltonian that, under the constraint that the difference between the highest and lowest eigenvalues is bounded, evolves an initial state $|i\rangle$ to a final state $|f\rangle$ in the least time. In this chapter we are concerned with a different problem, which is perhaps a more direct analogue to the classical problem.

Our translation of the brachistochrone problem to the quantum world is not perfect: The energy difference $E_0 - E_{N+1}$ could be translated to the potential energy difference between the two points in the classical problem, but it is not quite clear how to translate the vertical distance to the nearest-neighbours coupling, when the picture in mind is one of a chain of sites. Also, a quantum excitation will necessary be localised when $E_0 - E_{N+1} > 0$, and for it not to get 'stuck', we need to add some external environment that allows the system to hop between eigenstates. This envi-

ronment very loosely relates to the gravitational force on a classical bead, in the sense that the bead does not move when no gravitation exists, but that's where the similarity ends. Finally – in this research we are looking to maximise the power output of the reaction centre, which roughly translates to the probability of the excitation reaching the reaction centre, rather than to minimise time it takes to get there.

Because what we optimise is the power output of the reaction centre, we find that an optimal configuration is not necessarily one that transfers the excitation to the reaction centre as fast as possible, but rather one that exhibits many dark states, where an excitation is protected from spontaneous emission. Surprisingly, in such configurations the energy difference between two neighbouring molecules can get substantial, and the excitation seems to tunnel through high-energy molecules, even though we only consider nearest-neighbours coupling. Moreover, this is possible only for coupling constants that are above a certain threshold.

5.2 Model

We consider a model of $N + 2$ molecules, each can be either excited with excitation energy E_n, or in the ground-state, plus a reaction centre having two states. We assume (coherent) nearest-neighbours dipolar coupling between the molecules, where for simplicity, even though we think of molecules with different excitation energies, we take all coupling to be equal in magnitude J.

We study the case where there is no more than a single excitation throughout the entire system, including the reaction centre. We do note that in the case of a long chain it is possible that two excitations might occur, if the excitation takes a long time to reach the reaction centre. Nevertheless we think that adding another excitation to the Hilbert space would (a) make the computation much more involved, and (b) would not change the resulting 'best chain' conclusion, but indeed this is speculative and needs to be checked. We denote by $|n\rangle$ the state where molecule n is excited while all the other molecules are in their electronic ground state, $|g\rangle$ is the zero-excitation state. The reaction centre is modelled by two states $|\alpha\rangle$ and $|\beta\rangle$, in

the same manner as in Chapter 4. The system Hamiltonian is thus given by

$$\mathcal{H}_S = \sum_{n=0}^{N+1} E_n \left|n\right\rangle \left\langle n\right| + \frac{1}{2} J \sum_{n=0}^{N} \Big(\left|n\right\rangle \left\langle n+1\right| + \left|n+1\right\rangle \left\langle n\right| \Big) + \epsilon_g \left|g\right\rangle \left\langle g\right| + \epsilon_\alpha \left|\alpha\right\rangle \left\langle \alpha\right| + \epsilon_\beta \left|\beta\right\rangle \left\langle \beta\right| \ . \tag{5.1}$$

Apart from the bare system, similar to the previous chapter, we also include several environments at different temperatures that induce incoherent energy flow throughout the system. First, we have two kinds of photonic baths: one is the 'excitation' bath, or the sunlight bath, coupled only to the molecule at the far end to the reaction centre, molecule number 0. This bath represents sunlight, and so its effective temperature is chosen to be $T_h = 6000\ K$. Another photonic bath is the ambient electromagnetic environment (EM), coupled to all of the molecules together, and allows for spontaneous emission of the excitation. We think of this electromagnetic environment as not related to the sun, and so it has a temperature of the ambient environment T_c. We assume the long wavelength limit on this radiation bath, so it couples to all of the molecules with the same phase. We also assume that its spectral density is flat around the absorption frequencies of the molecules, so that the emission rate does not depend on the excitation energy. The ambient electromagnetic bath is important for the optimisation process, since it penalises configurations where an excitation takes a long time to reach the reaction centre, and favours configurations where the probability of reaching the reaction centre is high. We also include a local phonon environment to each of the $N+1$ molecules, with temperature T_c. These represent local or internal vibrations of each molecule, that do not directly influence their neighbouring molecules, and for simplicity also do not change the coherent coupling J between them. We take each vibronic environment to have the same Drude-Lorentz spectral density

$$J(\omega) = A \frac{\gamma\omega}{\gamma^2 + (\omega - \omega_0)^2} \ , \tag{5.2}$$

where A is proportional to the reorganisation energy[§], and ω_0, γ define the location and width of the single peak it exhibits. This spectral density is maximal when

[§]The reorganisation energy for this case is $\int_0^\infty d\omega J(\omega)/\omega = A[\pi/2 + \tan^{-1}(\omega_0/\gamma)]$.

$\omega = \omega_{\max} = \sqrt{\omega_0^2 + \gamma^2}$. In a second-order Markovian treatment, the rates induced by the environment are proportional to $J(|\Delta|)$, where Δ is a system energy frequency [c.f Eqn. (1.101)]. For our model, we choose the maximum value $\omega_{\max} = (E_0 - E_{N+1})/(N+1)$, such that the system will see the fastest rates if the eigenenergies of the chain part of $\mathcal{H}_S$ are evenly distributed (up to some boundary effects).

Finally, we include non-local phonons that induce transitions from molecule $N+1$ to the reaction centre $|\alpha\rangle$, inside the reaction centre $|\alpha\rangle \leftrightarrow |\beta\rangle$, and back to the ground state $|\beta\rangle \leftrightarrow |g\rangle$, all at the ambient temperature T_c. The interaction Hamiltonian is thus

$$\mathcal{H}_I = \sum_{n=0}^{N+1} \hat{I}_{nn} + \hat{I}_{\text{collective}} + \hat{I}_{0g} + \hat{I}_{N+1,\alpha} + \hat{I}_{\alpha\beta} + \hat{I}_{\beta g} \ , \tag{5.3}$$

where $\hat{I}_{ab} = \frac{1}{2}(|a\rangle\langle b| + |b\rangle\langle a|)\mu_{ab}$, $\mu_{0g} = \mu_{\text{ex}}$ is the coupling operator of the excitation photon bath, $\mu_{N+1,\alpha}, \mu_{\alpha\beta}, \mu_{\beta}$ generate transfer into and out of the reaction centre. The interaction with the local EM field is given by

$$\hat{I}_{\text{collective}} = \hat{\xi}\mu_{\text{em}} = \sum_{n=0}^{N+1}(|n\rangle\langle g| + |g\rangle\langle n|)\mu_{\text{em}}. \tag{5.4}$$

The operator $\hat{\xi}$ is the source of the spontaneous emission from the chain, since the rate of emission from a system eigenstate $|\varphi_k\rangle$ is proportional to $|\langle g|\hat{\xi}|\varphi_k\rangle|^2 = |\sum_{n=0}^{N+1}\langle n|\varphi_k\rangle|^2$. This defines the "darkness" of the state, and we find that having many dark states is key for optimising the system.

We analyse the system using the Pauli master equation (PME), and compare that to the Redfield equations, as described in Chapter 1.3.2. Apart from the local vibrations which are modelled using the spectral density of Eqn. (5.2), we assume that the Redfield rates (including the Lamb shift which contains the reorganisation energy), are given by [c.f. Eqn. (1.96)]

$$\int_0^\infty d\tau e^{-\mathrm{i}\omega\tau}\alpha_{ab}(\tau) = \begin{cases} \gamma_{ab}N(\omega), & \text{if } \omega > 0 \\ \gamma_{ab}[N(|\omega|)+1], & \text{if } \omega < 0 \\ -0.1\mathrm{i}\gamma_{ab}, & \text{if } \omega = 0 \ , \end{cases} \tag{5.5}$$

where α_{ab} is the response function of each environment, γ_{ab} is a constant not depending on the frequency, and $N(\omega)$ is the thermal occupation at frequency ω and the

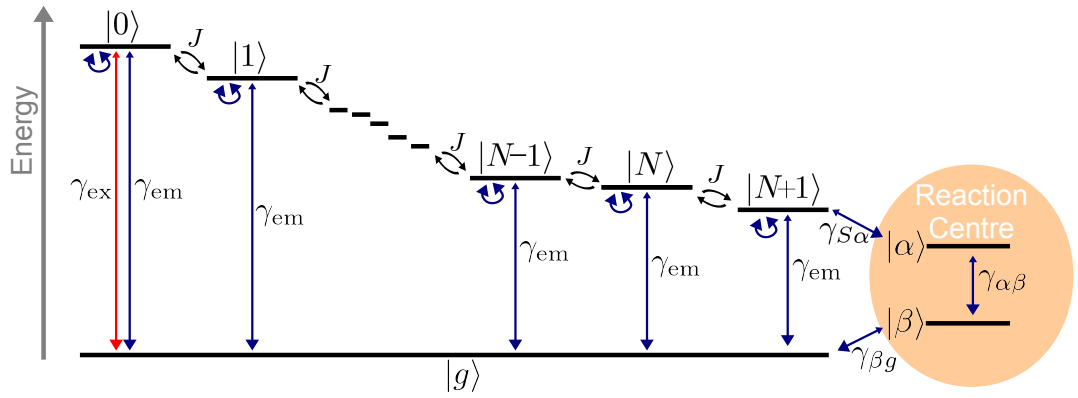

Figure 5.2: Sketch of the system Hamiltonian. The blue arrows represent environments with temperature T_c, while the red arrow represent the excitation photon bath.

temperature of the relevant environment. This means we assume all the environments apart from the local vibrations have flat spectral densities around the relevant transition frequencies, are super-Ohmic, the reorganisation energy is $1/10^{th}$ of the flat rates (in zero temperature), and the Lamb-shifts are negligible at system frequencies. The excitation rate which is derived from $\mu_{\rm ex}$ is denoted $\gamma_{\rm ex}$, and similarly the spontaneous-emission rate is $\gamma_{\rm em}$. For clarity we denote the rate from the chain into the reaction centre as $\gamma_{S\alpha} = \gamma_{N+1,\alpha}$. A sketch of the model is given in Fig. (5.2).

As in Chapter 4, we define the reaction centre current, voltage, and power using Eqns. (4.9 - 4.11), written here again for convenience,

$$I = e\gamma_{\alpha\beta}P_\alpha \ , \tag{5.6}$$

$$V = \epsilon_\alpha - \epsilon_\beta + k_{\rm B}T_c \ln(P_\alpha/P_\beta) \ , \tag{5.7}$$

$$P = IV \ . \tag{5.8}$$

Here $k_{\rm B}$ the Boltzmann constant, e the electron charge, and $P_\alpha = \rho_{\alpha\alpha}, P_\beta = \rho_{\beta\beta}$ are the populations of the reaction centre. We are interested in the steady-state power output, which is found by solving the algebraic equations obtained by demanding no time-dependence in the Redfield or Pauli equations. In the absence of sunlight (in the form of excitation photons $\mu_{\rm ex}$), the system thermalises to equilibrium with the phonon bath temperature, and the voltage vanishes. Thus V is a measure of the deviation from the thermal state with temperature T_c.

We treat the reaction centre as a black box, where the rate $\gamma_{\alpha\beta}$ is chosen to maximise the power output, *i.e.* the power for each configuration is given by the maximum possible power by varying $\gamma_{\alpha\beta}$. We are looking for the energy configuration $E_1, E_2, \cdots, E_N$ that maximises the power of the circuit, while keeping all other parameters constant, including the initial and final excitation energies E_0, E_{N+1}. Formally this is an optimisation problem with $N+1$ parameters (N energy levels plus the rate $\gamma_{\alpha\beta}$).

In Appendix B, we show how to diagonalise the system Hamiltonian analytically, for the case of a *linear configuration*, where the excitation energies of the molecules are given by $E_n = E_0 + n\Delta_L$, for both finite and semi-infinite chains. We note that the transport problem for an Hamiltonian of an *infinite* chain with a linear configuration is related to the problem of electronic transport in the presence of a strong electrical field and phonon interactions. This problem has been studied back in 1970 by Thornber and Feynman[166], and there have been many studies on the subject since[167–172].

5.3 Numerical Results

Here we present numerical results of the optimisation process for the excitation energies E_n. Technically, this is done using a quasi-Newton method of Broyden, Fletcher, Goldfarb, and Shanno (BFGS)[173], applied to an N-dimensional problem, where for each configuration we vary $\gamma_{\alpha\beta}$ to find the (maximum) power output of the circuit, according to the Pauli master equation (PME). Once we have the optimal configuration according to PME, we calculate the power output for the same parameters in full Redfield equations model, which is much more numerically demanding. The Redfield equations can predict higher or lower power outputs, depending on the configuration, and it is hard to find which without actually performing the calculations. We even found configurations for which PME showed an enhancement over the linear configuration, while Redfield showed a lower performance. All the results shown below are for the Redfield equations. We note that there are some configurations for

which the Redfield equations lead to negative eigenvalues of the density matrix in the steady-state. As discussed in Chapter 1.3.2, the Redfield treatment does not guarantee positivity. Such configurations are discarded since we cannot trust the predictions of PME or Redfield for them.

We would like to stress that the optimal configuration we reach is not necessarily the absolute optimal configuration, but rather a local maximum. The local maximum we obtain depends on the initial condition of the optimisation algorithm. The initial condition we choose is either a linear configuration that is equivalent to the straight line in the brachistochrone problem, *i.e.* $E_n = E_0 + \frac{n}{N+1}(E_{N+1} - E_0) = E_0 - n\Delta_L$, or the best configuration found for a system with similar parameters. We define an enhancement of a configuration as its power output over the power output of the linear configuration.

In Fig. 5.3 we plot the optimal configuration for $\Delta_L = 0.05\ eV$ and different values of coupling constants J. We find that for $J < J^*$, with $J^*/\Delta_L \approx 2$, the enhancement is rather modest < 2, and the optimal configuration is very close to the linear configuration, with some boundary effects at the ends of the chain. On the other hand, for $J > J^*$, the enhancements suddenly jumps to values larger than 17, and the optimal configuration exhibits peculiar spikes in the energy landscape. In Fig. 5.4 we plot the power output of the optimal configurations vs the linear ones, and show the point of transition between the two regimes.

We find that for the configurations with coupling constant $J > J^*$, the system exhibits many ($\sim 80\%$) dark states, where the chance of spontaneous emission is very low $\left|\langle g|\,\hat{\xi}\,|\varphi\rangle_k\right|^2 \ll 1$ [c.f. Eqn. (5.4)], and a few very bright states. Note that the total rate is fixed for all configurations or coupling constants. We plot the darkness of the states for $J = 0.08\ eV < J^*$ and $J = 0.1\ eV > J^*$, for both linear and optimal configurations, in Fig. (5.5).

Fig. 5.6 shows the eigenstates of the optimal configuration for $J = 0.1\ eV$, where we also visualise the population of each eigenstate, and the site-population of each site. As expected, the bright states (marked by white squares) are hardly populated,

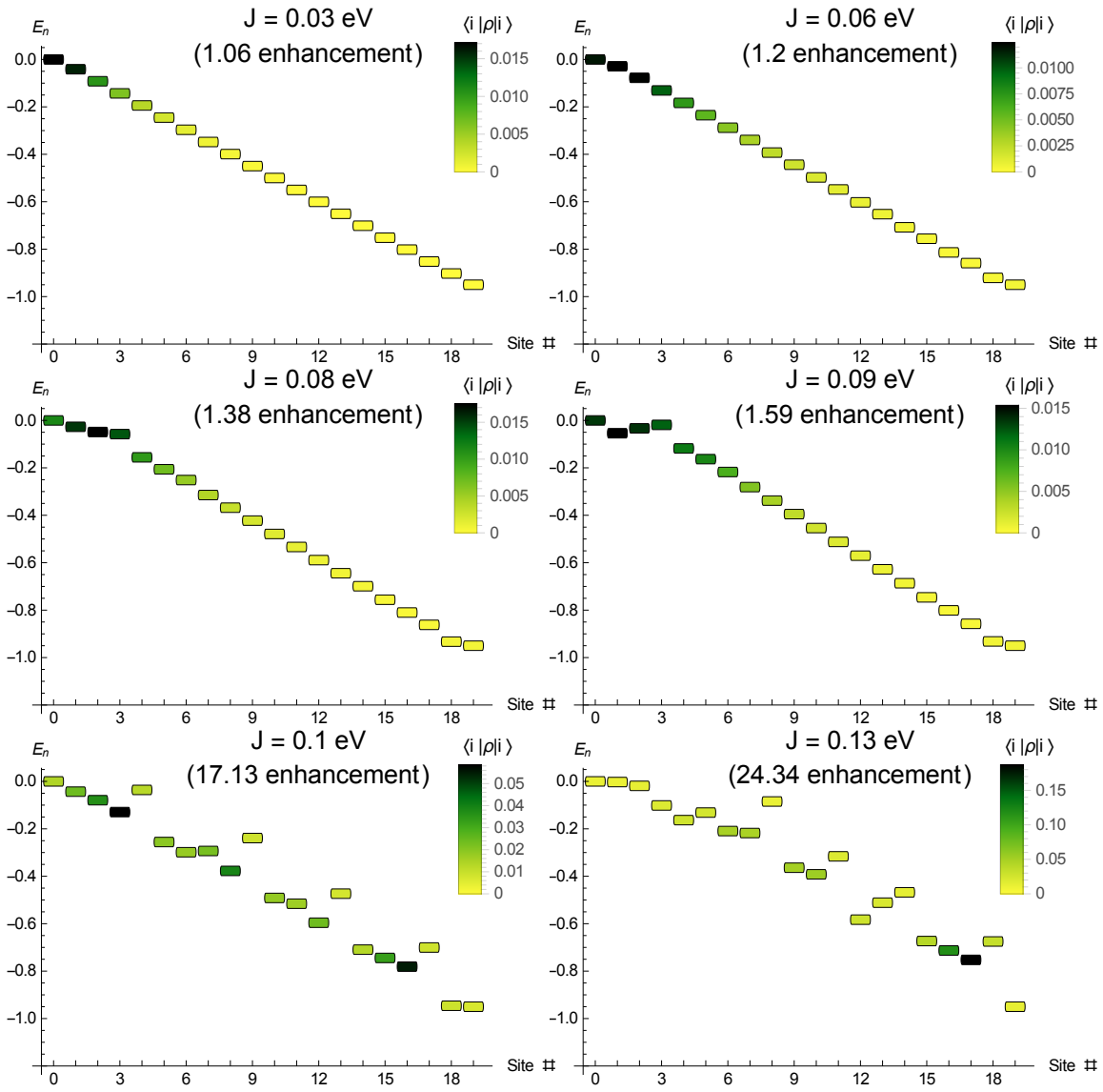

Figure 5.3: The optimal configuration found for different values of J , for chains of 20 sites ($N = 18$), with $E_0 = 0\ eV$, $E_{19} = -0.95\ eV$, $\Delta_L = 0.05\ eV$. The colours represent the site-basis steady-state populations, *i.e.* $\langle i|\,\rho\,|i\rangle$. The enhancement in parenthesis is with respect to a linear configuration. the reaction-centre and ground-state energies are given by $\epsilon_\alpha = -1.1\ eV$, $\epsilon_\beta = -1.4\ eV$, $\epsilon_g = -1.6\ eV$. The rates are given by $\gamma_{S\alpha} = 1.05\ meV$, $\gamma_{\beta g} = 1.3\ meV$, $\gamma_{\rm em} = 1.0\ meV$, $\gamma_{\rm ex} = 2.3\ meV$. The parameters for the spectral function for the phonons [Eqn. (5.2)] are $\omega_{\rm max} = 50meV, \gamma = 20meV$, and $A = 1.4meV$. The excitation temperature is $T_h = 6000\ K$, and the ambient temperature is $T_c = 300\ K$.

probably because they are prone to spontaneous emission, and the states with energies just above a bright state are highly populated.

In Fig. 5.7, we plot the power output of the linear and optimised configurations,

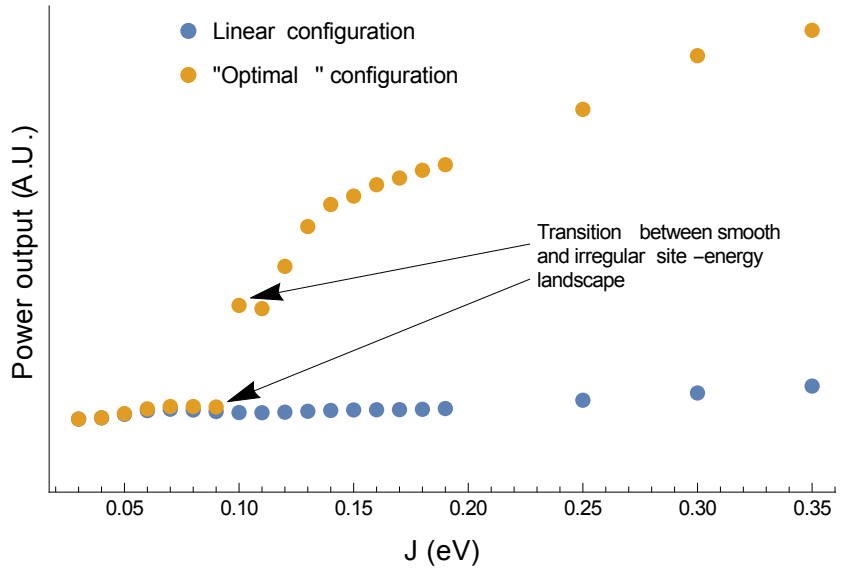

Figure 5.4: Power output of the optimal configurations, vs the linear power output, as a function of the coupling energies J. The parameters here are the same as in Fig. 5.3.

for different lengths of the chain. We find that the transition to an irregular energy landscape occurs roughly at the same value of J^*, where for lengths of $15-19$ sites we find $J^* \approx 0.09\ eV$, and for a 20-site chain it shifts to $J^* \approx 0.1\ eV$. Also, we find that the longer the chain the bigger the enhancement possible by going to the optimal configuration, but overall power output decreases with increasing chain length.

In Fig. 5.8, we plot the power output of the linear and optimised configurations, for different values of E_0, which translates to different values of the neighbouring energy difference in the linear configuration, $\Delta_L = (E_0 - E_{19})/19$. For each case we set the spectral density [Eqn. (5.2)] to be maximal when $\omega_{\max} = \Delta_L$, and normalise it such that the maximal value is the same for all cases. We find that the larger $E_0 - E_{19}$ is, the bigger the enhancement possible by using the optimisation procedure, but the absolute power is lower. We also find that the transition to an irregular energy landscape J^* grows almost linearly with Δ_L, which is to be expected since the system Hamiltonian of the molecules, *i.e.* the first line of Eqn. (5.1) scales with $(\Delta_L, J) \to (\alpha\Delta_L, \alpha J)$.

Fig. (5.9) shows the power output of the linear and optimised configurations, as

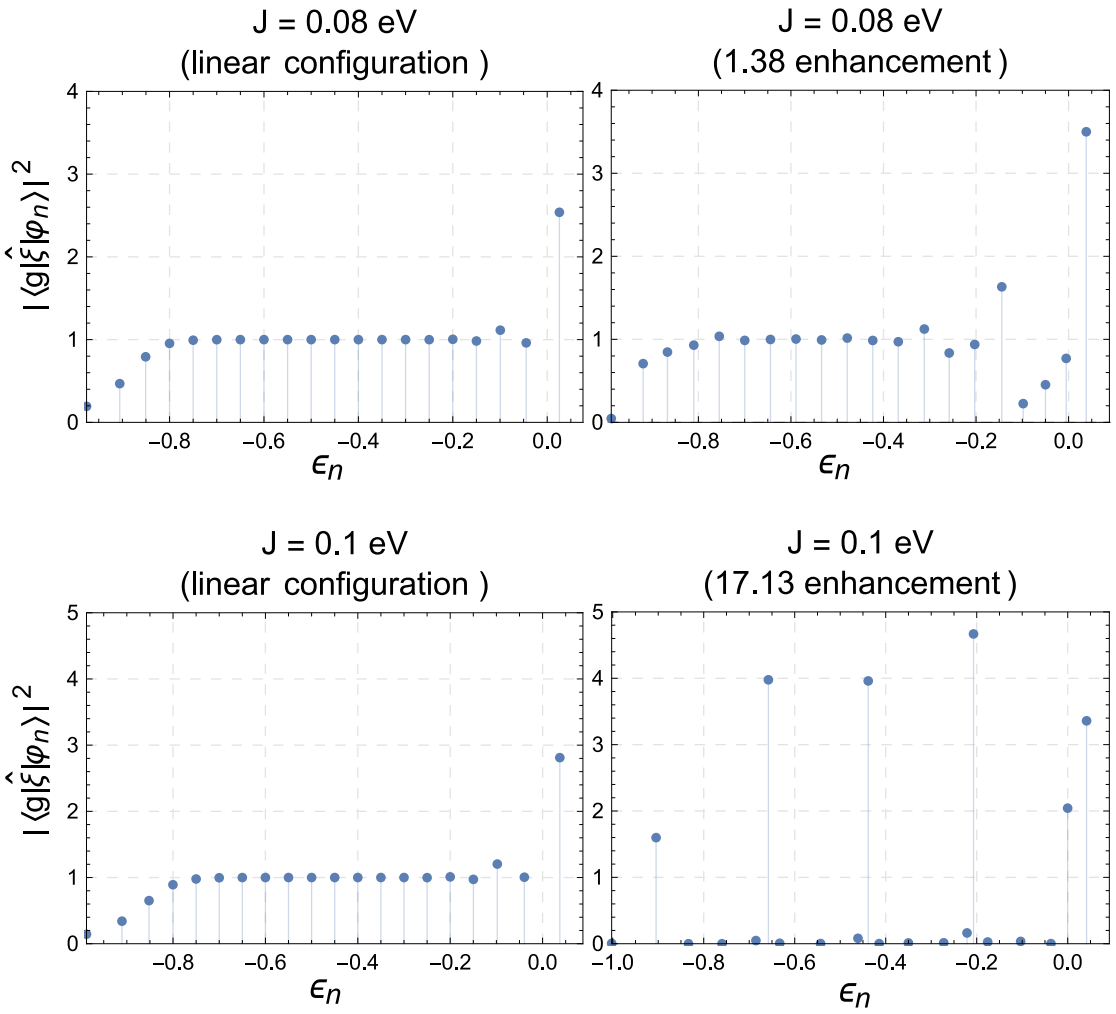

Figure 5.5: Visualisation of the darkness of the eigenstates, $\left|\langle g|\,\hat{\xi}\,|\varphi_n\rangle\right|^2$, of the linear and optimal configurations, for two values of the coupling constant J. The parameters here are the same as in Fig. 5.5.

a function of the local phonon bath strength A [c.f. Eqn (5.2)]. We find that the the power generally grows with stronger coupling to the phonons, but we expect this to maximise for some finite value, above which the the excitation will get localised because of the Zeno effect. We note that the Redfield equations are only suitable for the weak-coupling case, and going to strong coupling one might need to employ a different method.

Fig. (5.10) shows the power output of the linear and optimised configurations, as a function of the spontaneous emission rate γ_{em}. As expected, the system performs better when this rate is lower. We find that the transition coupling constant J^*,

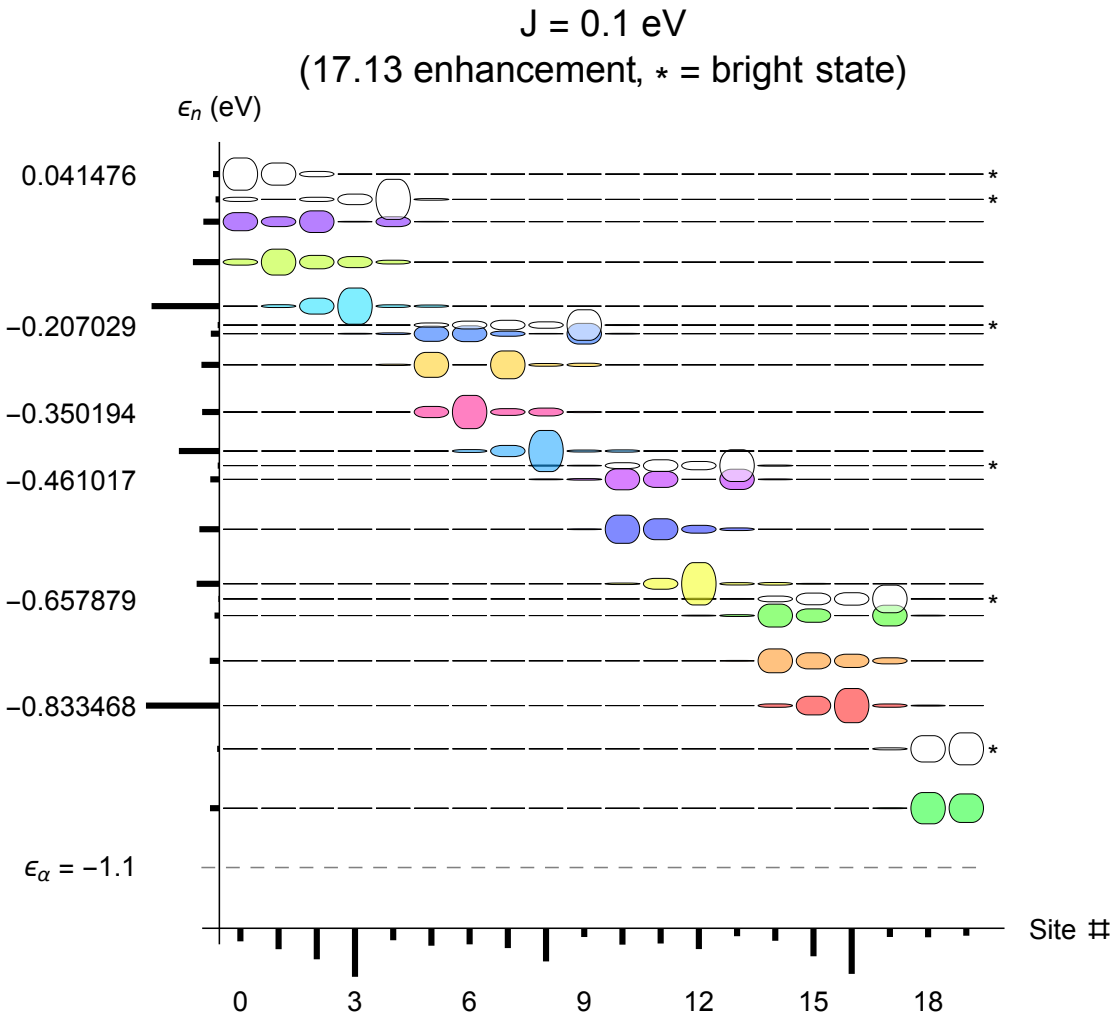

Figure 5.6: Visualisation of the eigenstates of the system, in the optimal configuration for $J = 0.1\ eV$. The height of each (rounded) square is proportional to $|\langle\varphi_n|i\rangle|^2$. The white squares represent the bright states, which are marked with a "*". The ticks length in this plot are proportional to the steady-state population of the different eigenstates / sites. The parameters here are the same as in Fig. 5.3.

between smooth and irregular energy landscape, is also a function of γ_{em}, where $J = 0.1\ eV$ is below the transition for $\gamma_{\text{em}} = 0.2\ meV$, but above for $\gamma_{\text{em}} = 0.3\ meV$. This is a bit surprising because one would expect the system to prefer a configuration with many dark states if possible, regardless of the spontaneous emission rate, which is the main way an excitation is lost in the system. The second way is of course via the excitation photon, which coupled to the initial site. We suspect that for a given J, in the linear configuration the probability for an excitation to return to the

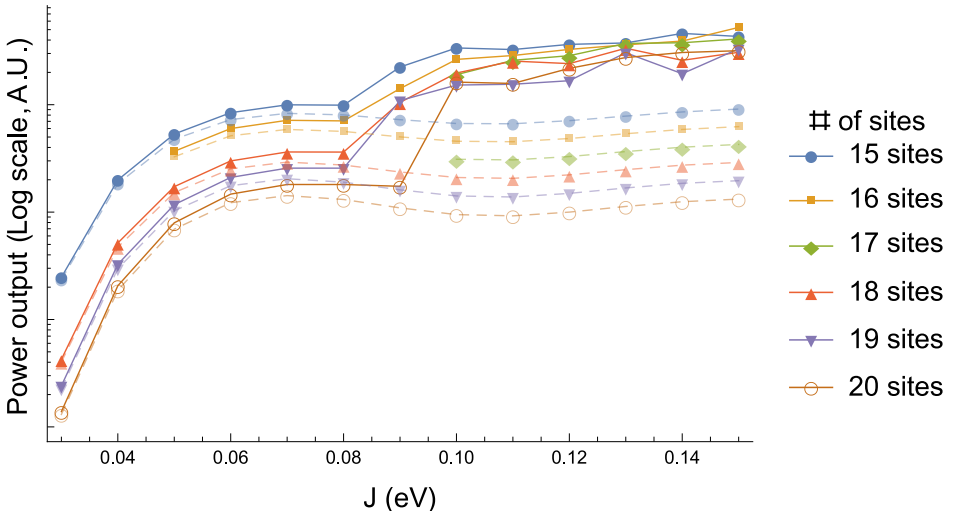

Figure 5.7: Power output (in logarithmic scale) for different lengths of chains, as a function of the coupling J. All of the parameters are the same as in Fig. 5.3, apart from E_0 which is now defined by the length of the chain, with $(E_0 - E_{N+1})/(N+1) = 0.05\ eV$, and $E_{N+1} = -0.95\ eV$. In solid line is the power output for the optimal configurations, while in dashed brighter colours are the linear configuration power outputs.

initial site is vanishingly small, while it is finite for the irregular configurations with many dark states, thus when the spontaneous-emission rate is very small, the latter configuration performs worse.

5.4 Discussion and Conclusion

In conclusion, we have presented a basic model for a problem which could be called the "quantum brachistochrone" problem, based on a model presented in Chapter 4. In contrast to the classical problem, here we optimise the probability for an excitation to get from one end of the chain to the reaction centre, rather than minimising the time it takes to get there. We assume equal nearest-neighbour coupling, and find that very irregular energy configuration of the absorption energies of the molecules can be optimal. This is because they generate many dark states in the system.

In the presence of collective spontaneous emission, for coupling larger than a threshold value J^*, these dark states protect excitations from spontaneous emission, and thus increase the probability that they reach reaction centre, when compared to

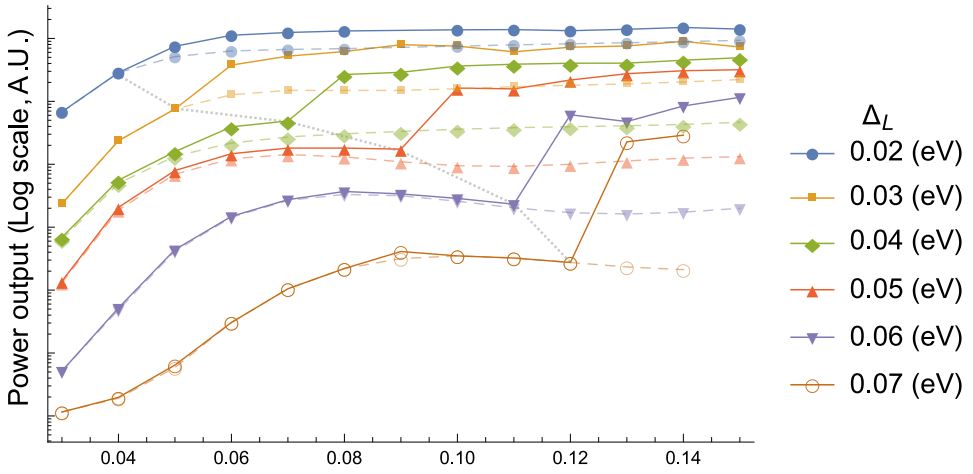

Figure 5.8: Power output (in logarithmic scale) for chains with 20 ($N = 18$) sites, with different E_0, as a function of the coupling J. All of the parameters are the same as in Fig. 5.3, apart from E_0 which is now defined by $E_0 = E_{19} + 19\Delta_L$, and the spectral density is modified such that it maximises for $\omega_{\max} = \Delta_L$, and normalises such that $J(\omega_{\max})$ is equal for all cases. In solid line is the power output for the optimal configurations, while in dashed brighter colours are the linear configuration power outputs. The Dashed gray line represents the data-point with the highest coupling constant J for each case where the optimal energy landscape is smooth. For larger J, the optimal energy landscape exhibits spikes.

a linear "staircase" configuration. This way, depending on the parameters, the power output of the reaction centre can increase by as much as an order of magnitude.

We found that the value of J^* does not depend strongly on the number of sites in the chain, but it is a function of the total energy drop per site (Δ_L). It also depends on the spontaneous emission rate, where for very low rates there is no advantage in going to these exotic configurations.

In our model we assume the long wavelength limit for the electromagnetic environment that induces the spontaneous emission. We note that this assumption only needs to be valid for the localisation length of the systems eigenvectors, which is for example ~ 5 molecules in the case of Fig. (5.6).

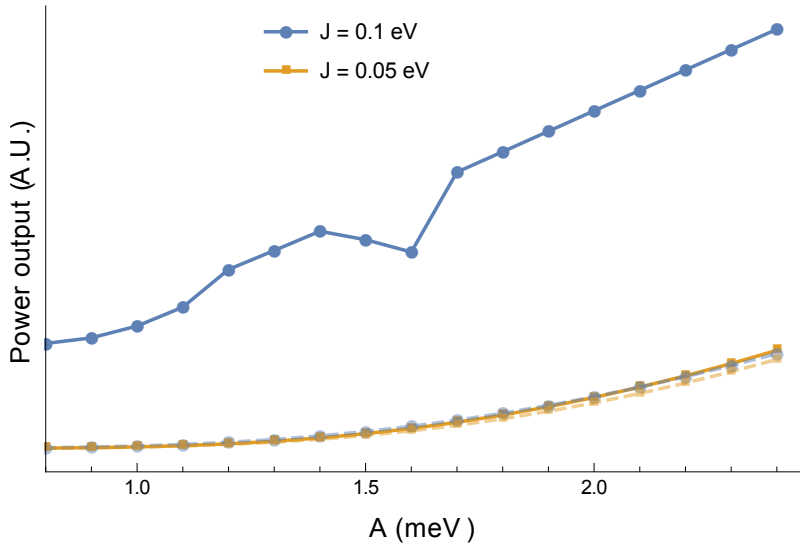

Figure 5.9: Power output for $J = 0.1\ eV > J^*$ and $J = 0.05\ eV < J^*$, as a function of the local phonon bath coupling A. All of the parameters are the same as in Fig. 5.3. In solid line is the power output for the optimal configurations, while in dashed brighter colours are the linear configuration power outputs.

Appendix A: Solution to the classical brachistochrone problem

For completeness, we include a solution to the classical brachistochrone problem, based on the solution published in [174]. We are looking for the curve $y(x)$ that minimises the time it takes a small bead sliding from rest and accelerated by gravity alone, to slip from one point to the other without friction. An illustration of the problem is given in Fig. (5.11).

We denote the start point as $(0, 0)$ and end point as (W, H). Since there is no friction, the energy is conserved and the velocity is given by $v = \sqrt{2gy(x)}$, with g being the gravity constant. On the other hand, we have $v = \frac{\sqrt{dx^2+dy^2}}{dt} = v_x\sqrt{1+y'(x)^2}$. The time it takes a bead to slip along a given curve $y(x)$ with $y(0) = 0, y(W) = H$, is thus

$$T = \int_0^T dt = \int_0^W \frac{1}{v_x}dx = \frac{1}{\sqrt{2g}}\int_0^W dx\frac{\sqrt{1+y'(x)^2}}{\sqrt{y(x)}}\ . \tag{5.9}$$

The curve that minimises the above time is thus not dependent on the constant g, which will be ignored from now. To find the optimal curve we use calculus of

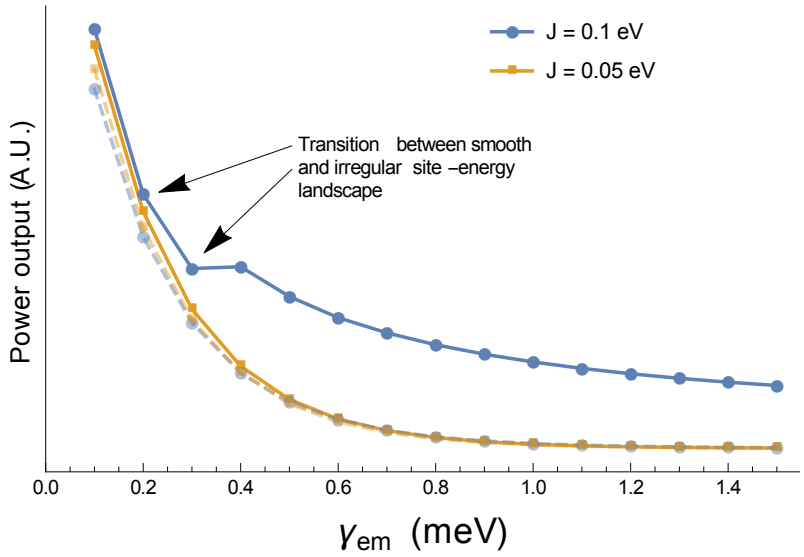

Figure 5.10: Power output for $J = 0.1\ eV$ and $J = 0.05\ eV$, as a function of the spontaneous emission rate γ_{em}. All of the parameters are the same as in Fig. 5.3. In solid line is the power output for the optimal configurations, while in dashed brighter colours are the linear configuration power outputs.

variations, which states that if we define

$$\mathcal{L}(y, y') = \frac{\sqrt{1 + y'^2}}{\sqrt{y}} \ , \tag{5.10}$$

the optimal curve is given by the Euler-Lagrange equation

$$\frac{\partial \mathcal{L}}{\partial y} - \frac{\partial}{\partial x}\frac{\partial \mathcal{L}}{\partial y'} = 0 \ . \tag{5.11}$$

Since $\mathcal{L}$ does not depend explicitly on x, we can use the Beltrami identity $\mathcal{L} - y' \frac{\partial \mathcal{L}}{\partial y'} = C$ with C being a constant. Substituting Eqn. (5.10), we end up with

$$y(x)(1 + y'(x)^2) = 2R \ , \tag{5.12}$$

where R is another constant. The solution to this equation is given in terms of parametric equations

$$x = R(\theta - \sin\theta) \ , \qquad\qquad y = R(1 - \cos\theta) \ , \tag{5.13}$$

which are exactly the equations of a cycloid with radius R. The values of R and θ_{max} which is the value of θ at the end of the curve, are given by solving Eqn. (5.13) for the end point. A sketch of a cycloid is given in Fig. (5.12).

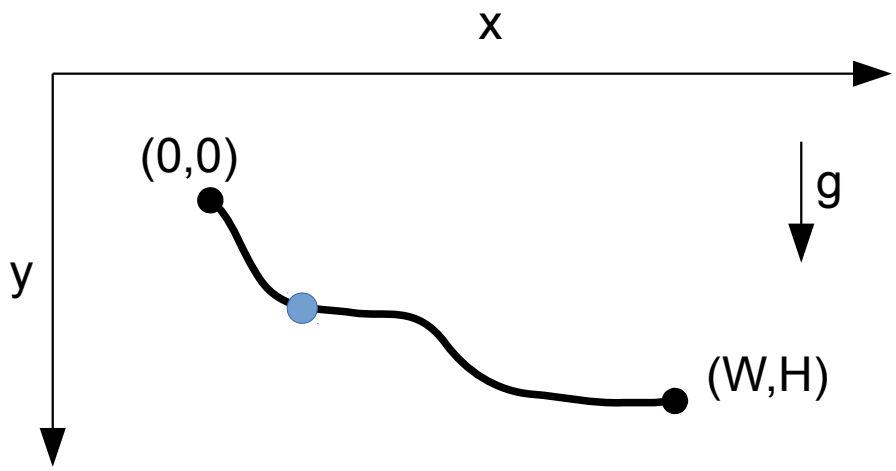

Figure 5.11: An illustration of a the Brachistochrone problem. Find the curve that minimises the time taken for a bead starting from rest to reach the point (W, H), when it is accelerated only by gravity.

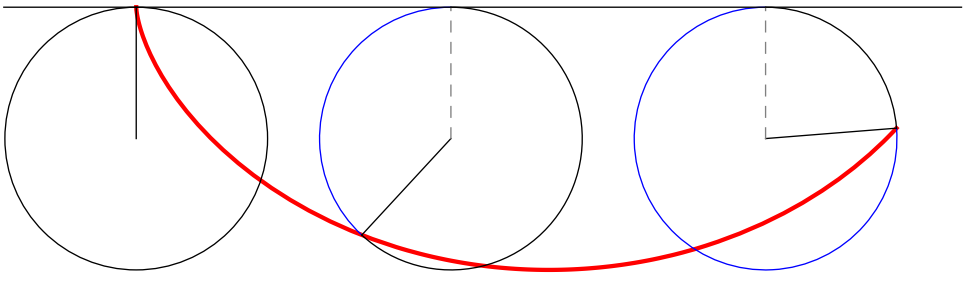

Figure 5.12: An illustration of a cycloid, with $W/H = 44/7$. The red line is the cycloid.

Appendix B: Analytical diagonlisations of a linear chain

In this Appendix we show how to diagonalise a chain of molecules with a linear gradient. We look at a chain of molecules, which is half-infinite, and has an energy difference of Δ between adjacent sites. The Hamiltonian for such a system is

$$\mathcal{H} = \begin{pmatrix} 0 & a/2 & & & & & \cdots \\ a/2 & \Delta & a/2 & & & & \cdots \\ & a/2 & 2\Delta & a/2 & & & \cdots \\ & & a/2 & 3\Delta & a/2 & & \cdots \\ & & & a/2 & 4\Delta & a/2 & \cdots \\ \vdots & \vdots & \vdots & \vdots & \ddots & \ddots & \ddots \end{pmatrix} \tag{5.14}$$

i.e. $\langle n|\,\mathcal{H}\,|n\rangle = n\Delta$, $\langle n+1|\,\mathcal{H}\,|n\rangle = \langle n|\,\mathcal{H}\,|n+1\rangle = a/2$, and all the other elements are zero. Here a is the hopping amplitude, and Δ is the energy gradient.[§]

The recurrence equation for the infinite case is the Bessel recurrence equation, hence the general solution to it is

$$|\varphi_k\rangle = \sum_n \Big(c_1 J_{n-k}(-a/\Delta) + c_2 Y_{n-k}(-a/\Delta)\Big)\,|n\rangle\,, \tag{5.15}$$

Here $J_\nu(x)$ and $Y_\nu(x)$ are the Bessel J and Y functions of order ν, known as Bessel functions of the first and second kind, respectively. c_1 and c_2 are constants which are determined by boundary conditions. The first boundary condition is that there is no site -1, so the eigensystem is given by

$$\begin{aligned} |\varphi_k\rangle = \mathcal{N}_k \sum_n \Big(&J_{n-k}(-a/\Delta)Y_{-1-k}(-a/\Delta) \\ &- Y_{n-k}(-a/\Delta)J_{-1-k}(-a/\Delta)\Big)\,|n\rangle\ , \end{aligned} \tag{5.16}$$

$$E_k = k\Delta\ , \tag{5.17}$$

where $\mathcal{N}_k$ is a normalisation factor. The Bessel Y functions diverge $Y_\nu(x) \underset{\nu\to\infty}{\to} \infty$, while $J_\nu(x) \underset{\nu\to\infty}{\to} 0$ vanishes.[175][§§] This imposes a requirement on the energies $k\Delta$: they

[§] We use a and not J to avoid confusion, because the solutions involve the Bessel J functions.

[§§] Actually J_ν vanishes for $\nu \to \pm\infty$ only when ν is an integer, otherwise it diverges for $\nu \to -\infty$, while still converges for $\nu \to \infty$. This is why the solution for the fully-infinite case only involves integer values of ν.

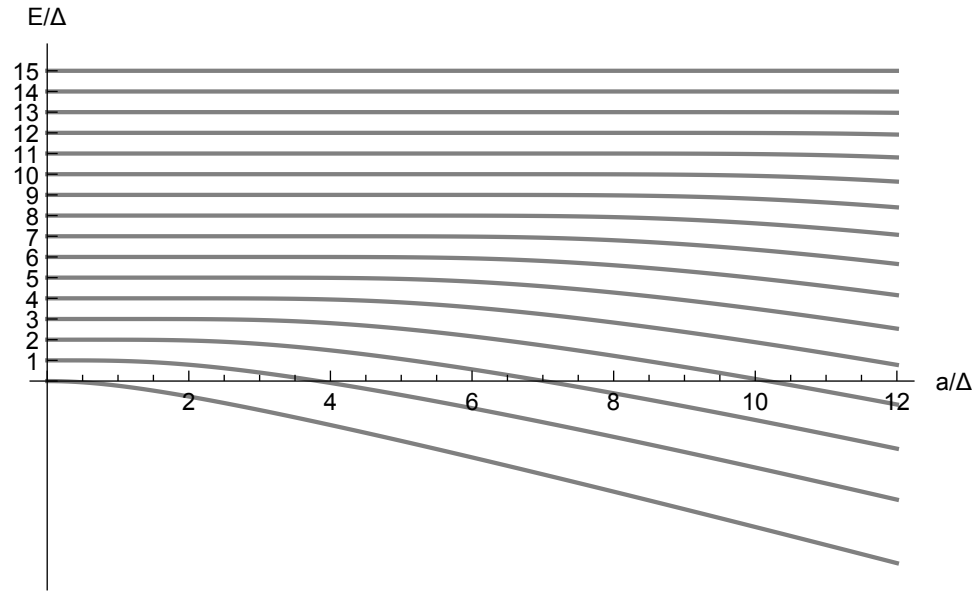

Figure 5.13: The first 16 energies as a function of coupling a/Δ, the energy differences are getting bigger near the end of the chain, while approaching Δ far from it.

must obey

$$J_{-1-k}(a/\Delta) = 0 \ . \tag{5.18}$$

With Eqn. (5.18) the eigensystem is given by:

$$|\varphi_k\rangle = \mathcal{N}_k \sum_n J_{n-k}(-a/\Delta)\,|n\rangle \ , \tag{5.19}$$

$$E_k = k\Delta \ , \tag{5.20}$$

$$J_{-1-k}(a/\Delta) = 0 \ . \tag{5.21}$$

For large $k \gg a/\Delta$, the normalization tends towards $\mathcal{N}_k \to 1$, as known from the infinite case[168]. In the infinite case, we get the so called *Wannier-Stark* states[169,172] or the *Bloch ladder*[176], which leads to the phenomena of *Bloch oscillations* that have been seen experimentally even at room temperature[177]. The first 16 energies are plotted in Fig. 5.13

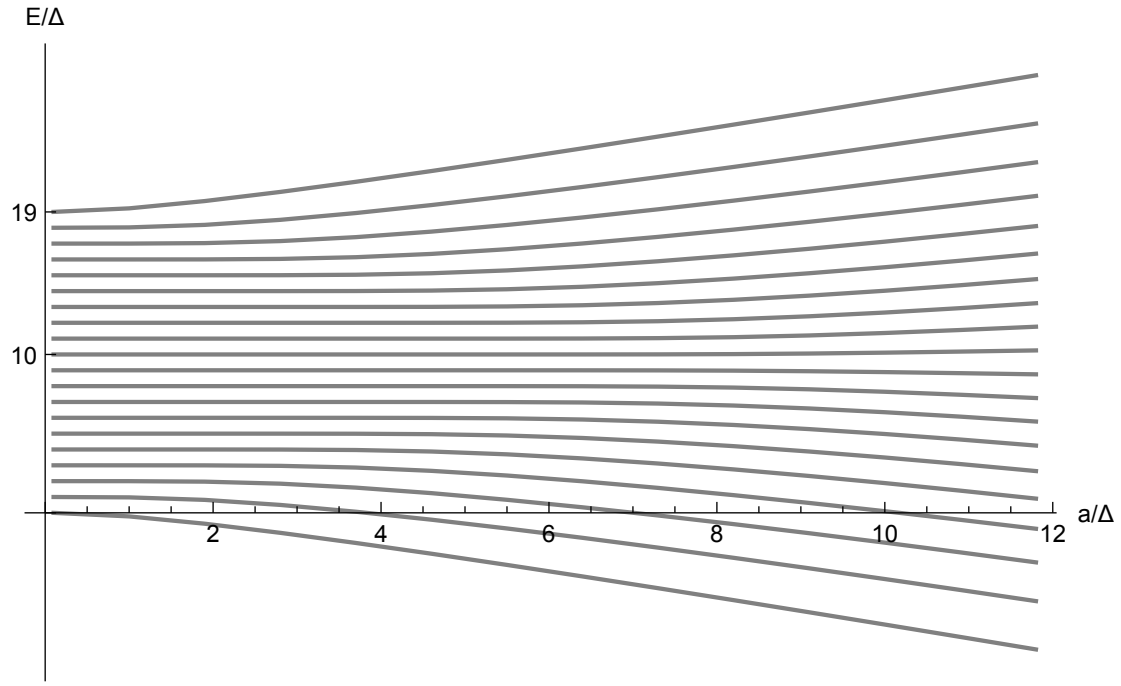

Figure 5.14: The first energies as a function of coupling a/Δ for the case of $N = 20$.

For a finite chain, with N different sites and a linear gradient Δ,

$$\mathcal{H}_s = \begin{pmatrix} 0 & a/2 & & & & \cdots & 0 \\ a/2 & \Delta & a/2 & & & \cdots & 0 \\ & a/2 & 2\Delta & a/2 & & \cdots & 0 \\ & & a/2 & 3\Delta & a/2 & \cdots & 0 \\ & & & a/2 & 4\Delta & a/2 & \cdots & 0 \\ \vdots & \vdots & \vdots & & \ddots & \ddots & \ddots & a/2 \\ 0 & 0 & 0 & \cdots & 0 & 0 & a/2 & (N-1)\Delta \end{pmatrix}, \tag{5.22}$$

the solution is the same as Eqn. (5.16), but now the boundary conditions states that

$$J_{N-k}(-a/\Delta)Y_{-1-k}(-a/\Delta) - Y_{N-k}(-a/\Delta)J_{-1-k}(-a/\Delta) = 0 \ . \tag{5.23}$$

An example of the energies for the case of $N = 20$ is given in Fig. 5.14.

Chapter 6

Conclusion and outlook

We conclude this Thesis with a summary of the main results found for each research chapter, and an outlook for future work that can be based upon them.

In Chapter 2 we were concerned with an open system in a tiered environment, where we have a system of interest that is directly coupled to its environment, which is in turn coupled to a wider universe. The environment is treated in a perturbative but non-Markovian way, while the effect of the universe is approximated by Lindblad rates. We developed a perturbative technique we call "P-mat" to study this case, which also works for the 'standard' case of no wider universe. We found that, at least to second order, the effect of the wider universe can be captured by a simple redefinition of the response function [Eqn. (2.52)]. A natural extension of this scheme is to look at the *exact* dynamics of the joint system and environment, in the presence of a wider universe, using a path-integral formalism. That is, to calculate the effect of the wider universe on the exact influence functional. This could reveal some higher-order processes that are intractable with the method introduced in Chapter 2, but still yield the same result in the weak-coupling regime.

In Chapter 3 we examined two perturbative techniques: the P-mat, and the TCL expansion. We introduced a criterion, which tests under what conditions we are permitted to use these perturbative techniques on open quantum systems. This criterion depends on the temperature and spectral density of the environment, on the system eigenfrequencies, and on the coupling between the two. This is done in a relatively

straight-forward manner, by comparing explicit terms from a second-order expansion to the corresponding fourth-order terms. The criterion we end up with is valid for a system of any (finite) size, which is linearly coupled to a bath of harmonic oscillators. We also found that this criterion is closely related to the known phenomena of the 'slippiage of initial conditions', which in turn is a measure of non-Markovianity. Even though TCL2 is a wildly popular and established method, introduced back in the 70's[178–180], this is, to our knowledge, the first rigorous method to estimate its validity in the general case. We tested our criterion on the canonical spin-Boson model, and on the more complex FMO model. We found that the low temperature case of the FMO, contrary to popular belief, lies well in the perturbative regime and there is no need to employ numerically intensive techniques to simulate its dynamics.

In the FMO example studied, we also found two cases for which the exact dynamics are nearly identical, yet our criterion indicates that the cases are very much different when the perturbative solution is applied. The only difference between the cases is the cut-off frequency of the environment, yet for one case TCL2 is inadequate, while for the other case it yields very good results. Since both have nearly identical dynamics, a perturbative treatment to the *first* case is actually a very good approximation to the *second* case, even though the latter is not in the perturbative regime. This raises the following question: If we were given only the second case, could we have known that a TCL2 treatment on a problem with a different cutoff-frequency is a good approximation? Or more generally, in what case can a system which is not in the perturbative regime, be well approximated by perturbative techniques on a *different* system?

Another interesting study could be finding examples where the criterion fails: It might be possible to engineer environmental coupling such that the fourth-order terms in the perturbative expansion are smaller than second-order ones, but sixth or higher-orders are larger again, and cutting the solution in second order yields wrong results.

In Chapter 4 we presented a simple model of a photocell, based on a formalism suggested by Dorfman *et al*[116]. The main novelty of our model is that we use two

different molecules acting as an antenna, rather than the same one, in an asymmetric configuration. We showed that this configuration, if set up carefully, can exhibit a dark state which is protected from leakage into the bright state due to environmental phonons. This setup thus outperforms the symmetric setup in cases where the probability for an excitation to hop from the antenna to reaction centre is very low. In this way we showed that the quantum enhancement to the power output of a photocell can, in principle, be as high as an order of magnitude. As we describe in the Chapter, we believe there is a plethora of potential molecule pairs that can exhibit a good (asymmetric) dark state, and we are very hopeful and excited to see it implemented in real experiments or even photovoltaic devices in the future.

In Chapter 5 we presented a basic model, which is our interpretation of a direct extension of the classical brachistochrone problem to the quantum regime, using the same formalism studied in Chapter 4. In contrast to the classical problem, here we were looking to optimise the power output of a reaction centre coupled to the end of a chain, rather than minimising the time an excitation takes to get from one side of the chain to the other. Essentially we were preferring configurations with a low chance of spontaneously emitting an excitation into the vacuum. We found that there is a value of the coupling between neighbouring sites, J^*, above which the optimal configuration of the absorption energies in the chain exhibits peaks, *i.e.* some molecules have (much) higher absorption energies than both their neighbours. The excitation thus tunnels through these molecules down the chain and into the reaction centre. This optimal configuration, when looked at in the energy eigenbasis of the chain, shows that most of the eigenstates are very dark, which explains why it can perform even orders of magnitude better than a linear configuration. This was a preliminary study of this model. First it would be interesting to fully understand the nature of J^* using analytical tools. Perhaps a hint for this lies in the form of the eigenstates of the linear chain [Eqn. (5.16)], but as we showed in the chapter, the total rate of spontaneous emission also plays a role here. Second, it is interesting to generalise this setup to different topologies - perhaps 2D structures could also exhibit many dark states using exotic energy landscapes? It has been shown that ring structures also exhibit similar

characteristics[121]. Finally, it would be very interesting to see an experiment trying to realise these peaked configurations. It might be possible to do so using a chain of identical molecules, where the different excitation energies are realised using different environmental coupling, in the same manner that identical BChl units in the FMO complex exhibit different excitation energies[29].

Bibliography

[1] A. Fruchtman, B. W. Lovett, S. C. Benjamin, and E. M. Gauger, "Quantum dynamics in a tiered non-Markovian environment," *New Journal of Physics*, vol. 17, p. 023063, feb 2015.

[2] A. Fruchtman, N. Lambert, and E. M. Gauger, "When do perturbative approaches accurately capture the dynamics of complex quantum systems?," *Scientific Reports*, vol. 6, p. 28204, jun 2016.

[3] A. Fruchtman, R. Gómez-Bombarelli, B. W. Lovett, and E. M. Gauger, "Photocell Optimization Using Dark State Protection," *Physical Review Letters*, vol. 117, p. 203603, nov 2016.

[4] H. P. Breuer and F. Petruccione, *The Theory of Open Quantum Systems*. OUP Oxford, 2007.

[5] J. Von Neumann, "Wahrscheinlichkeitstheoretischer aufbau der quantenmechanik," *Nachrichten von der Gesellschaft der Wissenschaften zu Göttingen, Mathematisch-Physikalische Klasse*, vol. 1927, pp. 245–272, 1927. English title: Probabilistic construction of quantum mechanics.

[6] L. Landau, "Das dämpfungsproblem in der wellenmechanik," *Zeitschrift für Physik*, vol. 45, no. 5-6, pp. 430–441, 1927. English title: The damping problem in wave mechanics.

[7] R. McWeeny, "Some Recent Advances in Density Matrix Theory," *Reviews of Modern Physics*, vol. 32, pp. 335–369, apr 1960.

[8] R. Feynman and F. Vernon, "The theory of a general quantum system interacting with a linear dissipative system," *Annals of Physics*, vol. 173, pp. 118–173, 1963.

[9] K. Kraus, "General state changes in quantum theory," *Annals of Physics*, vol. 64, no. 2, pp. 311 – 335, 1971.

[10] K. Kraus, A. Böhm, J. D. Dollard, and W. H. Wootters, eds., *States, Effects, and Operations Fundamental Notions of Quantum Theory*, vol. 190 of *Lecture Notes in Physics*, (Berlin, Heidelberg), Springer Berlin Heidelberg, 1983.

[11] V. Gorini, A. Kossakowski, and E. C. G. Sudarshan, "Completely positive dynamical semigroups of nlevel systems," *Journal of Mathematical Physics*, vol. 17, no. 5, pp. 821–825, 1976.

[12] G. Lindblad, "On the generators of quantum dynamical semigroups," *Communications in Mathematical Physics*, vol. 48, no. 2, pp. 119–130, 1976.

[13] A. Shaji and E. Sudarshan, "Who's afraid of not completely positive maps?," *Physics Letters A*, vol. 341, no. 14, pp. 48 – 54, 2005.

[14] J. M. Dominy, A. Shabani, and D. A. Lidar, "A general framework for complete positivity," *Quantum Information Processing*, vol. 15, no. 1, pp. 465–494, 2015.

[15] K. M. F. Romero, P. Talkner, and P. Hänggi, "Is the dynamics of open quantum systems always linear?," *Phys. Rev. A*, vol. 69, p. 052109, May 2004.

[16] K. E. Cahill, "Coherent-state representations for the photon density operator," *Physical Review*, vol. 138, no. 6B, p. B1566, 1965.

[17] C. Gardiner and P. Zoller, *Quantum Noise: A Handbook of Markovian and Non-Markovian Quantum Stochastic Methods with Applications to Quantum Optics*. Springer Series in Synergetics, Springer, 2004.

[18] R. J. Glauber, "Coherent and incoherent states of the radiation field," *Physical Review*, vol. 131, no. 6, p. 2766, 1963.

[19] E. Sudarshan, "Equivalence of semiclassical and quantum mechanical descriptions of statistical light beams," *Physical Review Letters*, vol. 10, no. 7, p. 277, 1963.

[20] J. R. Klauder, J. McKenna, and D. G. Currie, "On"diagonal"coherent-state representations for quantum-mechanical density matrices," *Journal of Mathematical Physics*, vol. 6, no. 5, pp. 734–739, 1965.

[21] N. Makri, "The Linear Response Approximation and Its Lowest Order Corrections: An Influence Functional Approach," *The Journal of Physical Chemistry B*, vol. 103, pp. 2823–2829, apr 1999.

[22] N. Makri, "Exploiting classical decoherence in dissipative quantum dynamics: Memory, phonon emission, and the blip sum," *Chemical Physics Letters*, vol. 593, pp. 93–103, feb 2014.

[23] A. O. Caldeira and A. J. Leggett, "Influence of dissipation on quantum tunneling in macroscopic systems," *Physical Review Letters*, vol. 46, no. 4, p. 211, 1981.

[24] M. Pope and C. Swenberg, *Electronic Processes in Organic Crystals and Polymers*. Monographs on the physics and chemistry of materials, Oxford University Press, 1999.

[25] U. Wurfel, M. Thorwart, and E. Weber, *Quantum Efficiency in Complex Systems, Part II: From Molecular Aggregates to Organic Solar Cells: Organic Solar Cells*. Semiconductors and Semimetals, Elsevier Science, 2011.

[26] J. Frenkel, "On the transformation of light into heat in solids. ii," *Phys. Rev.*, vol. 37, pp. 1276–1294, May 1931.

[27] G. H. Wannier, "The structure of electronic excitation levels in insulating crystals," *Phys. Rev.*, vol. 52, pp. 191–197, Aug 1937.

[28] V. May and O. Kühn, *Charge and energy transfer dynamics in molecular systems*. John Wiley & Sons, 2008.

[29] J. Adolphs and T. Renger, "How proteins trigger excitation energy transfer in the FMO complex of green sulfur bacteria.," *Biophysical Journal*, vol. 91, pp. 2778–97, Oct. 2006.

[30] G. Ritschel, J. Roden, W. T. Strunz, and A. Eisfeld, "An efficient method to calculate excitation energy transfer in light-harvesting systems: application to the FennaMatthewsOlson complex," *New Journal of Physics*, vol. 13, p. 113034, Nov. 2011.

[31] G. Panitchayangkoon, D. Hayes, K. a. Fransted, J. R. Caram, E. Harel, J. Wen, R. E. Blankenship, and G. S. Engel, "Long-lived quantum coherence in photosynthetic complexes at physiological temperature.," *Proceedings of the National Academy of Sciences of the United States of America*, vol. 107, pp. 12766–70, July 2010.

[32] A. Ishizaki and G. R. Fleming, "Theoretical examination of quantum coherence in a photosynthetic system at physiological temperature.," *Proceedings of the National Academy of Sciences of the United States of America*, vol. 106, pp. 17255–60, Oct. 2009.

[33] Y.-C. Cheng and G. R. Fleming, "Dynamics of light harvesting in photosynthesis.," *Annual review of physical chemistry*, vol. 60, pp. 241–262, 2009.

[34] A. Ishizaki and G. R. Fleming, "Unified treatment of quantum coherent and incoherent hopping dynamics in electronic energy transfer: reduced hierarchy equation approach.," *The Journal of Chemical Physics*, vol. 130, p. 234111, June 2009.

[35] P. Nalbach, A. Ishizaki, G. R. Fleming, and M. Thorwart, "Iterative path-integral algorithm versus cumulant time-nonlocal master equation approach for dissipative biomolecular exciton transport," *New Journal of Physics*, vol. 13, p. 063040, June 2011.

[36] G. D. Scholes and G. R. Fleming, "Energy transfer and photosynthetic light harvesting," *Adv. Chem. Phys*, vol. 132, pp. 57–130, 2005.

[37] R. Dorner, J. Goold, L. Heaney, T. Farrow, and V. Vedral, "Effects of quantum coherence in metalloprotein electron transfer," *Phys. Rev. E*, vol. 86, p. 031922, Sep 2012.

[38] E. M. Gauger, E. Rieper, J. J. L. Morton, S. C. Benjamin, and V. Vedral, "Sustained Quantum Coherence and Entanglement in the Avian Compass," *Physical Review Letters*, vol. 106, p. 040503, Jan. 2011.

[39] A. Chciska, F. A. Pollock, L. Heaney, and A. Nazir, "Dissipation enhanced vibrational sensing in an olfactory molecular switch," *The Journal of Chemical Physics*, vol. 142, no. 2, 2015.

[40] A. Leggett, S. Chakravarty, A. Dorsey, M. Fisher, A. Garg, and W. Zwerger, "Dynamics of the dissipative two-state system," *Reviews of Modern Physics*, vol. 59, pp. 1–85, Jan. 1987.

[41] S. Jang, J. Cao, and R. J. Silbey, "Fourth-order quantum master equation and its Markovian bath limit," *Journal of Chemical Physics*, vol. 116, no. 7, pp. 2705–2717, 2002.

[42] A. Suárez, R. Silbey, and I. Oppenheim, "Memory effects in the relaxation of quantum open systems," *The Journal of Chemical Physics*, vol. 97, no. 7, p. 5101, 1992.

[43] P. Gaspard and M. Nagaoka, "Slippage of initial conditions for the Redfield master equation," *The Journal of Chemical Physics*, vol. 111, no. 13, p. 5668, 1999.

[44] H. Carmichael, *Statistical Methods in Quantum Optics 1: Master Equations and Fokker-Planck Equations*. Theoretical and Mathematical Physics, Springer Berlin Heidelberg, 2013.

[45] C. Smith and A. Caldeira, "Generalized Feynman-Vernon approach to dissipative quantum systems," *Physical Review A*, vol. 36, no. 7, pp. 1–3, 1987.

[46] H. Grabert, P. Schramm, and G.-L. Ingold, "Quantum Brownian motion: The functional integral approach," *Physics Reports*, vol. 168, pp. 115–207, Oct. 1988.

[47] Y. Tanimura and R. Kubo, "Time evolution of a quantum system in contact with a nearly Gaussian-Markoffian noise bath," *Journal of the Physical Society of Japan*, vol. 58, no. 1, pp. 101–114, 1989.

[48] Y. Tanimura, "Nonperturbative expansion method for a quantum system coupled to a harmonic-oscillator bath," *Physical Review A*, vol. 41, no. 12, pp. 6676–6687, 1990.

[49] Y. Tanimura and P. Wolynes, "Quantum and classical Fokker-Planck equations for a Gaussian-Markovian noise bath," *Physical Review A*, vol. 43, no. 8, pp. 4131–4142, 1991.

[50] Q. Shi, L. Chen, G. Nan, R.-X. Xu, and Y. Yan, "Efficient hierarchical Liouville space propagator to quantum dissipative dynamics.," *The Journal of Chemical Physics*, vol. 130, p. 084105, Feb. 2009.

[51] J. Ma, Z. Sun, X. Wang, and F. Nori, "Entanglement dynamics of two qubits in a common bath," *Phys. Rev. A*, 2012.

[52] Y. Tanimura, "Reduced hierarchy equations of motion approach with drude plus brownian spectral distribution: Probing electron transfer processes by means of two-dimensional correlation spectroscopy," *The Journal of Chemical Physics*, vol. 137, no. 22, pp. –, 2012.

[53] M. Tanaka and Y. Tanimura, "Multistate electron transfer dynamics in the condensed phase: exact calculations from the reduced hierarchy equations of motion approach.," *The Journal of Chemical Physics*, vol. 132, p. 214502, June 2010.

[54] M. Tanaka and Y. Tanimura, "Quantum Dissipative Dynamics of Electron Transfer Reaction System: Nonperturbative Hierarchy Equations Approach," *Journal of the Physical Society of Japan*, vol. 78, p. 073802, July 2009.

[55] A. G. Dijkstra, C. Wang, J. Cao, and G. R. Fleming, "Coherent exciton dynamics in the presence of underdamped vibrations," *The Journal of Physical Chemistry Letters*, vol. 6, no. 4, pp. 627–632, 2015.

[56] C. Meier and D. J. Tannor, "Non-Markovian evolution of the density operator in the presence of strong laser fields," *The Journal of Chemical Physics*, vol. 111, no. 8, p. 3365, 1999.

[57] Y. Tanimura, "Stochastic Liouville, Langevin, Fokker-Planck, and Master Equation Approaches to Quantum Dissipative Systems," *Journal of the Physics Society Japan*, vol. 75, p. 082001, Aug. 2006.

[58] J. Strümpfer and K. Schulten, "Excited state dynamics in photosynthetic reaction center and light harvesting complex 1.," *The Journal of Chemical Physics*, vol. 137, p. 065101, Aug. 2012.

[59] J. Strümpfer and K. Schulten, "Open Quantum Dynamics Calculations with the Hierarchy Equations of Motion on Parallel Computers.," *Journal of Chemical Theory and Computation*, vol. 8, pp. 2808–2816, Aug. 2012.

[60] C. Kreisbeck, T. Kramer, M. Rodríguez, and B. Hein, "High-performance solution of hierarchical equations of motion for studying energy transfer in light-harvesting complexes," *Journal of Chemical Theory and Computation*, vol. 7, no. 7, pp. 2166–2174, 2011.

[61] A. Ishizaki and Y. Tanimura, "Quantum Dynamics of System Strongly Coupled to Low-Temperature Colored Noise Bath: Reduced Hierarchy Equations Approach," *Journal of the Physics Society Japan*, vol. 74, pp. 3131–3134, Dec. 2005.

[62] N. Makri, "Improved Feynman propagators on a grid and non-adiabatic corrections within the path integral framework," *Chemical Physics Letters*, vol. 193, pp. 435–445, 1992.

[63] N. Makri and D. E. Makarov, "Tensor propagator for iterative quantum time evolution of reduced density matrices. I. Theory," *The Journal of Chemical Physics*, vol. 102, no. 11, p. 4600, 1995.

[64] N. Makri and D. E. Makarov, "Tensor propagator for iterative quantum time evolution of reduced density matrices. II. Numerical methodology," *The Journal of Chemical Physics*, vol. 102, no. 11, p. 4611, 1995.

[65] P. Nalbach, J. Eckel, and M. Thorwart, "Quantum coherent biomolecular energy transfer with spatially correlated fluctuations," *New Journal of Physics*, vol. 12, p. 065043, June 2010.

[66] P. Nalbach, D. Braun, and M. Thorwart, "Exciton transfer dynamics and quantumness of energy transfer in the Fenna-Matthews-Olson complex," *Physical Review E*, vol. 84, p. 041926, Oct. 2011.

[67] N. Makri, "Path integral renormalization for quantum dissipative dynamics with multiple timescales," *Molecular Physics*, vol. 110, pp. 1001–1007, May 2012.

[68] R. Lambert and N. Makri, "Memory propagator matrix for long-time dissipative charge transfer dynamics," *Molecular Physics*, vol. 110, pp. 1967–1975, Aug. 2012.

[69] N. Makri, "Blip decomposition of the path integral: Exponential acceleration of real-time calculations on quantum dissipative systems," *The Journal of Chemical Physics*, vol. 141, no. 13, 2014.

[70] M. J. Burek, D. Ramos, P. Patel, I. W. Frank, and M. Lonar, "Nanomechanical resonant structures in single-crystal diamond," *Applied Physics Letters*, vol. 103, no. 13, pp. –, 2013.

[71] M. D. LaHaye, J. Suh, P. M. Echternach, K. C. Schwab, and M. L. Roukes, "Nanomechanical measurements of a superconducting qubit.," *Nature*, vol. 459, pp. 960–4, June 2009.

[72] C. Eichler, C. Lang, J. M. Fink, J. Govenius, S. Filipp, and A. Wallraff, "Observation of entanglement between itinerant microwave photons and a superconducting qubit," *Phys. Rev. Lett.*, vol. 109, p. 240501, Dec 2012.

[73] J. M. Pirkkalainen, S. U. Cho, J. Li, G. S. Paraoanu, P. J. Hakonen, and M. A. Sillanpää, "Hybrid circuit cavity quantum electrodynamics with a micromechanical resonator.," *Nature*, vol. 494, pp. 211–5, Feb. 2013.

[74] M. Ganzhorn, S. Klyatskaya, M. Ruben, and W. Wernsdorfer, "Strong spin-phonon coupling between a single-molecule magnet and a carbon nanotube nanoelectromechanical system.," *Nature nanotechnology*, vol. 8, pp. 165–9, Mar. 2013.

[75] A. Pályi, P. R. Struck, M. Rudner, K. Flensberg, and G. Burkard, "Spin-Orbit-Induced Strong Coupling of a Single Spin to a Nanomechanical Resonator," *Physical Review Letters*, vol. 108, p. 206811, May 2012.

[76] A. Mavalankar, T. Pei, E. M. Gauger, J. H. Warner, G. A. D. Briggs, and E. A. Laird, "Photon-assisted tunneling and charge dephasing in a carbon nanotube double quantum dot," *Phys. Rev. B*, vol. 93, p. 235428, Jun 2016.

[77] G. S. Engel, T. R. Calhoun, E. L. Read, T.-K. Ahn, T. Mancal, Y.-C. Cheng, R. E. Blankenship, and G. R. Fleming, "Evidence for wavelike energy transfer through quantum coherence in photosynthetic systems.," *Nature*, vol. 446, pp. 782–6, Apr. 2007.

[78] E. J. O'Reilly and A. Olaya-Castro, "Non-classicality of the molecular vibrations assisting exciton energy transfer at room temperature.," *Nature communications*, vol. 5, p. 3012, Jan. 2014.

[79] J. Prior, A. W. Chin, S. F. Huelga, and M. B. Plenio, "Efficient Simulation of Strong System-Environment Interactions," *Physical Review Letters*, vol. 105, p. 050404, July 2010.

[80] J. Iles-Smith, N. Lambert, and A. Nazir, "Environmental dynamics, correlations, and the emergence of noncanonical equilibrium states in open quantum systems," *Physical Review A*, vol. 90, p. 032114, sep 2014.

[81] H. P. Breuer, "Genuine quantum trajectories for non-Markovian processes," *Physical Review A*, vol. 70, no. July, p. 012106, 2004.

[82] A. Imamoglu, "Stochastic wave-function approach to non-Markovian systems," *Physical Review A*, vol. 50, pp. 3650–3653, Nov. 1994.

[83] H. Gassmann, F. Marquardt, and C. Bruder, "Non-Markoffian effects of a simple nonlinear bath," *Physical Review E*, vol. 66, p. 041111, Oct. 2002.

[84] M. Scala, B. Militello, A. Messina, J. Piilo, and S. Maniscalco, "Microscopic derivation of the Jaynes-Cummings model with cavity losses," *Physical Review A*, vol. 75, p. 013811, Jan. 2007.

[85] M. M. Wolf and J. I. Cirac, "Dividing quantum channels," *Communications in Mathematical Physics*, vol. 168, pp. 147–168, 2008.

[86] B. J. Dalton, S. M. Barnett, and B. M. Garraway, "Theory of pseudomodes in quantum optical processes," *Physical Review A*, vol. 64, p. 053813, 2001.

[87] A. Garg, J. N. Onuchic, and V. Ambegaokar, "Effect of friction on electron transfer in biomolecules," *The Journal of Chemical Physics*, vol. 83, no. 9, p. 4491, 1985.

[88] M. Thorwart, L. Hartmann, I. Goychuk, and P. Hänggi, "Controlling decoherence of a two-level-atom in a lossy cavity," *Journal of Modern Optics*, vol. 47:14-15, pp. 2905–2919, Mar. 2000, 0003029.

[89] K. H. Hughes, C. D. Christ, and I. Burghardt, "Effective-mode representation of non-Markovian dynamics: a hierarchical approximation of the spectral density. II. Application to environment-induced nonadiabatic dynamics.," *The Journal of chemical physics*, vol. 131, p. 124108, Sept. 2009.

[90] M. Thorwart, E. Paladino, and M. Grifoni, "Dynamics of the spin-boson model with a structured environment," *Chemical Physics*, vol. 296, pp. 333–344, Jan. 2004.

[91] M. Goorden, M. Thorwart, and M. Grifoni, "Entanglement Spectroscopy of a Driven Solid-State Qubit and Its Detector," *Physical Review Letters*, vol. 93, p. 267005, Dec. 2004.

[92] M. C. Goorden, M. Thorwart, and M. Grifoni, "Spectroscopy of a driven solid-state qubit coupled to a structured environment," *The European Physical Journal B*, vol. 45, pp. 405–417, July 2005.

[93] P. Huang and H. Zheng, "Quantum dynamics of a qubit coupled with a structured bath," *Journal of Physics: Condensed Matter*, vol. 20, p. 395233, Oct. 2008.

[94] H. J. Carmichael and D. F. Walls, "Master equation for strongly interacting systems," *Journal of Physics A: Mathematical, Nuclear and General*, vol. 6, no. 10, p. 1552, 1973.

[95] U. Weiss, *Quantum Dissipative Systems*, vol. 13. World Scientific, 2012.

[96] D. P. S. McCutcheon, N. S. Dattani, E. M. Gauger, B. W. Lovett, and A. Nazir, "A general approach to quantum dynamics using a variational master equation: Application to phonon-damped Rabi rotations in quantum dots," *Physical Review B*, vol. 84, p. 081305, Aug. 2011.

[97] C. Kreisbeck and T. Kramer, "Long-Lived Electronic Coherence in Dissipative Exciton Dynamics of Light-Harvesting Complexes," *The Journal of Physical Chemistry Letters*, vol. 3, no. 19, pp. 2828–2833, 2012.

[98] R. Graham and M. Höhnerbach, "Two-state system coupled to a boson mode: quantum dynamics and classical approximations," *Zeitschrift für Physik B Condensed Matter*, vol. 248, pp. 233–248, 1984.

[99] F. A. Pollock, D. P. S. McCutcheon, B. W. Lovett, E. M. Gauger, and A. Nazir, "A multi-site variational master equation approach to dissipative energy transfer," *New Journal of Physics*, vol. 15, p. 075018, July 2013.

[100] K. D. B. Higgins, B. W. Lovett, and E. M. Gauger, "Quantum thermometry using the ac Stark shift within the Rabi model," *Phys. Rev. B*, vol. 88, p. 155409, Oct 2013.

[101] M. P. Woods, R. Groux, A. W. Chin, S. F. Huelga, and M. B. Plenio, "Mappings of open quantum systems onto chain representations and Markovian embeddings," *Journal of Mathematical Physics*, vol. 55, p. 032101, Mar. 2014.

[102] M. Mohseni, P. Rebentrost, S. Lloyd, and A. Aspuru-Guzik, "Environment-assisted quantum walks in photosynthetic energy transfer," *Journal of Chemical Physics*, vol. 129, no. 17, 2008, 0805.2741.

[103] N. Lambert, Y.-N. Chen, Y.-C. Cheng, C.-M. Li, G.-Y. Chen, and F. Nori, "Quantum biology," *Nature Physics*, vol. 9, pp. 10–18, Dec. 2012.

[104] L. a. Pachón and P. Brumer, "Computational methodologies and physical insights into electronic energy transfer in photosynthetic light-harvesting complexes.," *Physical Chemistry Chemical Physics*, vol. 14, pp. 10094–108, Aug. 2012.

[105] A. Ishizaki, T. R. Calhoun, G. S. Schlau-Cohen, and G. R. Fleming, "Quantum coherence and its interplay with protein environments in photosynthetic electronic energy transfer," *Physical Chemistry Chemical Physics*, vol. 12, no. 27, pp. 7319–7337, 2010.

[106] a. Shabani, M. Mohseni, H. Rabitz, and S. Lloyd, "Efficient estimation of energy transfer efficiency in light-harvesting complexes," *Physical Review E*, vol. 86, p. 011915, July 2012.

[107] A. Shabani, M. Mohseni, H. Rabitz, and S. Lloyd, "Numerical evidence for robustness of environment-assisted quantum transport," *Physical Review E - Statistical, Nonlinear, and Soft Matter Physics*, vol. 89, no. 4, pp. 1–7, 2014.

[108] J. Jeske, D. J. Ing, M. B. Plenio, S. F. Huelga, and J. H. Cole, "Bloch-Redfield equations for modeling light-harvesting complexes," *The Journal of Chemical Physics*, vol. 142, p. 064104, feb 2015, 1408.2726.

[109] G. Mahan, *Many-Particle Physics*. Physics of Solids and Liquids, Springer, 2000.

[110] D. P. S. McCutcheon and A. Nazir, "Quantum dot Rabi rotations beyond the weak excitonphonon coupling regime," *New Journal of Physics*, vol. 12, p. 113042, Nov. 2010.

[111] J. L. Skinner and D. Hsu, "Pure dephasing of a two-level system," *The Journal of Physical Chemistry*, vol. 90, pp. 4931–4938, Oct. 1986.

[112] S. Barnett, *Quantum Information*. Oxford Master Series in Physics, OUP Oxford, 2009.

[113] D. M. Wilkins and N. S. Dattani, "Why quantum coherence is not important in the fenna-matthews-olsen complex," *Journal of Chemical Theory and Computation*, vol. 11, no. 7, pp. 3411–3419, 2015. PMID: 26575775.

[114] A. Aharony, S. Gurvitz, Y. Tokura, O. Entin-Wohlman, and S. Dattagupta, "Partial decoherence in mesoscopic systems," *Physica Scripta*, vol. T151, p. 014018, nov 2012, 1205.5622.

[115] N. Dattani, F. Pollock, and D. Wilkins, "Analytic influence functionals for numerical Feynman integrals in most open quantum systems," *arXiv preprint arXiv:1203.4551*, pp. 1–11, 2012, arXiv:1203.4551v1.

[116] K. E. Dorfman, D. V. Voronine, S. Mukamel, and M. O. Scully, "Photosynthetic reaction center as a quantum heat engine," *Proc. Natl. Acad. Sci.*, vol. 110, no. 8, pp. 2746–2751, 2012.

[117] T. Tokihiro, Y. Manabe, and E. Hanamura, "Superradiance of Frenkel excitons in linear systems," *Physical Review B*, vol. 47, pp. 2019–2030, jan 1993.

[118] C. Creatore, M. a. Parker, S. Emmott, and a. W. Chin, "Efficient biologically inspired photocell enhanced by delocalized quantum states," *Physical Review Letters*, vol. 111, no. 25, pp. 1–5, 2013.

[119] N. Killoran, S. F. Huelga, and M. B. Plenio, "Enhancing light-harvesting power with coherent vibrational interactions: A quantum heat engine picture," *The Journal of Chemical Physics*, vol. 143, no. 15, 2015.

[120] Y. Zhang, S. Oh, F. H. Alharbi, G. S. Engel, and S. Kais, "Delocalized quantum states enhance photocell efficiency," *Phys. Chem. Chem. Phys.*, vol. 17, no. 8, pp. 5743–5750, 2015.

[121] K. D. B. Higgins, B. W. Lovett, and E. M. Gauger, "Quantum-enhanced capture of photons using optical ratchet states," *arXiv preprint arXiv:1504.05849*, 2015, arXiv:1504.05849.

[122] K. Mukai, S. Abe, and H. Sumi, "Theory of Rapid Excitation-Energy Transfer from B800 to Optically-Forbidden Exciton States of B850 in the Antenna System LH2 of Photosynthetic Purple Bacteria," *The Journal of Physical Chemistry B*, vol. 103, pp. 6096–6102, jul 1999.

[123] R. E. Fenna and B. W. Matthews, "Chlorophyll arrangement in a bacteriochlorophyll protein from Chlorobium limicola," *Nature*, vol. 258, no. 5536, pp. 573–577, 1975.

[124] J. Moix, J. Wu, P. Huo, D. Coker, and J. Cao, "Efficient Energy Transfer in Light-Harvesting Systems, III: The Influence of the Eighth Bacteriochlorophyll on the Dynamics and Efficiency in FMO," *The Journal of Physical Chemistry Letters*, vol. 2, no. 24, pp. 3045–3052, 2011.

[125] T. Ritz, S. Park, and K. Schulten, "Kinetics of Excitation Migration and Trapping in the Photosynthetic Unit of Purple Bacteria," *The Journal of Physical Chemistry B*, vol. 105, pp. 8259–8267, aug 2001.

[126] A. Olaya-Castro, C. F. Lee, F. F. Olsen, and N. F. Johnson, "Efficiency of energy transfer in a light-harvesting system under quantum coherence," *Physical Review B - Condensed Matter and Materials Physics*, vol. 78, pp. 1–7, aug 2008, 0708.1159.

[127] A. Y. Smirnov, L. G. Mourokh, P. K. Ghosh, and F. Nori, "High-Efficiency Energy Conversion in a Molecular Triad Connected to Conducting Leads," *The Journal of Physical Chemistry C*, vol. 113, pp. 21218–21224, dec 2009.

[128] M. Einax, M. Dierl, and A. Nitzan, "Heterojunction Organic Photovoltaic Cells as Molecular Heat Engines: A Simple Model for the Performance Analysis," *The Journal of Physical Chemistry C*, vol. 115, pp. 21396–21401, nov 2011, 1107.0924.

[129] M. Einax, M. Dierl, P. R. Schiff, and A. Nitzan, "Multiple state representation scheme for organic bulk heterojunction solar cells: A novel analysis perspective," *EPL (Europhysics Letters)*, vol. 104, p. 40002, nov 2013, arXiv:1311.6495v2.

[130] S. Ajisaka, B. Žunkovič, and Y. Dubi, "The Molecular Photo-Cell: Quantum Transport and Energy Conversion at Strong Non-Equilibrium," *Scientific Reports*, vol. 5, p. 8312, feb 2015.

[131] M. Kasha, "Characterization of electronic transitions in complex molecules," *Discussions of the Faraday society*, vol. 9, pp. 14–19, 1950.

[132] J.-L. Brédas, J. E. Norton, J. Cornil, and V. Coropceanu, "Molecular Understanding of Organic Solar Cells: The Challenges," *Accounts of Chemical Research*, vol. 42, pp. 1691–1699, nov 2009.

[133] R. A. J. Janssen and J. Nelson, "Factors Limiting Device Efficiency in Organic Photovoltaics," *Advanced Materials*, vol. 25, pp. 1847–1858, apr 2013.

[134] R. T. Ross, "Some thermodynamics of photochemical systems," *The Journal of Chemical Physics*, vol. 46, no. 12, pp. 4590–4593, 1967.

[135] W. Niedenzu, D. Gelbwaser-Klimovsky, and G. Kurizki, "Performance limits of multilevel and multipartite quantum heat machines," *Phys. Rev. E*, vol. 92, p. 042123, Oct 2015.

[136] R. Uzdin, A. Levy, and R. Kosloff, "Equivalence of Quantum Heat Machines, and Quantum-Thermodynamic Signatures," *Physical Review X*, vol. 5, p. 031044, sep 2015.

[137] D. Gelbwaser-Klimovsky, W. Niedenzu, and G. Kurizki, "Chapter twelve - thermodynamics of quantum systems under dynamical control," vol. 64 of *Advances In Atomic, Molecular, and Optical Physics*, pp. 329 – 407, Academic Press, 2015.

[138] E. a. Martinez and J. P. Paz, "Dynamics and Thermodynamics of Linear Quantum Open Systems," *Physical Review Letters*, vol. 110, p. 130406, mar 2013, 1207.4256.

[139] R. Kosloff and A. Levy, "Quantum Heat Engines and Refrigerators: Continuous Devices," *Annual Review of Physical Chemistry*, vol. 65, pp. 365–393, apr 2014.

[140] A. Levy and R. Kosloff, "The local approach to quantum transport may violate the second law of thermodynamics," *EPL (Europhysics Letters)*, vol. 107, no. 2, p. 20004, 2014.

[141] D. M. Bierman, A. Lenert, W. R. Chan, B. Bhatia, I. Celanović, M. Soljačić, and E. N. Wang, "Enhanced photovoltaic energy conversion using thermally based spectral shaping," *Nature Energy*, vol. 1, p. 16068, may 2016.

[142] O. Nicolet and E. Vauthey, "Ultrafast Nonequilibrium Charge Recombination Dynamics of Excited DonorAcceptor Complexes," *The Journal of Physical Chemistry A*, vol. 106, pp. 5553–5562, jun 2002.

[143] A. C. Stuart, J. R. Tumbleston, H. Zhou, W. Li, S. Liu, H. Ade, and W. You, "Fluorine Substituents Reduce Charge Recombination and Drive Structure and Morphology Development in Polymer Solar Cells," *Journal of the American Chemical Society*, vol. 135, pp. 1806–1815, feb 2013.

[144] R. W. Munn and R. Silbey, "Theory of electronic transport in molecular crystals. II. Zeroth order states incorporating nonlocal linear electronphonon coupling," *The Journal of Chemical Physics*, vol. 83, no. 4, p. 1843, 1985.

[145] R. W. Munn and R. Silbey, "Theory of electronic transport in molecular crystals. III. Diffusion coefficient incorporating nonlocal linear electronphonon coupling," *The Journal of Chemical Physics*, vol. 83, no. 4, p. 1854, 1985.

[146] Y. Zhao, D. W. Brown, and K. Lindenberg, "On the MunnSilbey approach to nonlocal excitonphonon coupling," *The Journal of Chemical Physics*, vol. 100, no. 3, p. 2335, 1994.

[147] S. Mukamel and D. Abramavicius, "Many-Body Approaches for Simulating Coherent Nonlinear Spectroscopies of Electronic and Vibrational Excitons," *Chemical Reviews*, vol. 104, pp. 2073–2098, apr 2004.

[148] Y. Li, F. Caruso, E. Gauger, and S. C. Benjamin, "Momentum rejuvenation underlies the phenomenon of noise-assisted quantum energy flow," *New Journal of Physics*, vol. 17, no. 1, p. 13057, 2015.

[149] F. Caruso, "Universally optimal noisy quantum walks on complex networks," *New Journal of Physics*, vol. 16, 2014, 1312.1832.

[150] P. Rebentrost, M. Mohseni, I. Kassal, S. Lloyd, and A. Aspuru-Guzik, "Environment-assisted quantum transport," *New Journal of Physics*, vol. 11, 2009, 0807.0929.

[151] Y. Dubi, "Interplay between Dephasing and Geometry and Directed Heat Flow in Exciton Transfer Complexes," *Journal of Physical Chemistry C*, vol. 119, no. 45, pp. 25252–25259, 2015, 1510.03026.

[152] M. Mohseni, P. Rebentrost, S. Lloyd, and A. Aspuru-Guzik, "Environment-assisted quantum walks in photosynthetic energy transfer," *Journal of Chemical Physics*, vol. 129, no. 17, pp. 0–9, 2008, 0805.2741.

[153] A. W. Chin, A. Datta, F. Caruso, S. F. Huelga, and M. B. Plenio, "Noise-assisted energy transfer in quantum networks and light-harvesting complexes," *New Journal of Physics*, vol. 12, 2010, 0910.4153.

[154] W. Dunham, *Journey through genius: the great theorems of mathematics*. Wiley science editions, Wiley, 1990.

[155] V. Perlick, "The brachistochrone problem in a stationary space-time," *Journal of Mathematical Physics*, vol. 32, no. 11, pp. 3148–3157, 1991.

[156] F. Giannoni, P. Piccione, and J. A. Verderesi, "An approach to the relativistic brachistochrone problem by sub-Riemannian geometry," *Journal of Mathematical Physics*, vol. 38, no. 12, p. 6367, 1997.

[157] F. Giannoni and P. Piccione, "An existence theory for relativistic brachistochrones in stationary spacetimes," *Journal of Mathematical Physics*, vol. 39, no. 11, p. 6137, 1998.

[158] A. Carlini, A. Hosoya, T. Koike, and Y. Okudaira, "Time-optimal quantum evolution," *Physical Review Letters*, vol. 96, no. 6, pp. 1–4, 2006, 0511039v1.

[159] C. M. Bender, D. C. Brody, H. F. Jones, and B. K. Meister, "Faster than Hermitian quantum mechanics," *Physical Review Letters*, vol. 98, no. 4, pp. 2–5, 2007, 0609032.

[160] A. Carlini, A. Hosoya, T. Koike, and Y. Okudaira, "Time-optimal unitary operations," *Physical Review A - Atomic, Molecular, and Optical Physics*, vol. 75, no. 4, pp. 1–8, 2007, 0608039.

[161] A. Mostafazadeh, "Quantum brachistochrone problem and the geometry of the state space in Pseudo-Hermitian quantum mechanics," *Physical Review Letters*, vol. 99, no. 13, pp. 1–4, 2007, 0706.3844.

[162] A. M. Frydryszak and V. M. Tkachuk, "Quantum brachistochrone problem for a spin-1 system in a magnetic field," *Physical Review A - Atomic, Molecular, and Optical Physics*, vol. 77, no. 1, pp. 1–4, 2008, 0709.0931.

[163] A. T. Rezakhani, W. J. Kuo, A. Hamma, D. A. Lidar, and P. Zanardi, "Quantum adiabatic brachistochrone," *Physical Review Letters*, vol. 103, no. 8, pp. 2–5, 2009, 0905.2376.

[164] A. Kuzmak and V. Tkachuk, "The quantum brachistochrone problem for an arbitrary spin in a magnetic field," *Physics Letters A*, vol. 379, no. 1819, pp. 1233 – 1239, 2015.

[165] X. Wang, M. Allegra, K. Jacobs, S. Lloyd, C. Lupo, and M. Mohseni, "Quantum Brachistochrone Curves as Geodesics: Obtaining Accurate Minimum-Time Protocols for the Control of Quantum Systems," *Physical Review Letters*, vol. 114, no. 17, p. 170501, 2015, 1408.2465.

[166] K. K. Thornber and R. P. Feynman, "Velocity Acquired by an Electron in a Finite Electric Field in a Polar Crystal," *Physical Review B*, vol. 1, pp. 4099–4114, may 1970.

[167] F. S. Khan, J. H. Davies, and J. W. Wilkins, "Quantum transport equations for high electric fields," *Physical Review B*, vol. 36, no. 5, pp. 2578–2597, 1987.

[168] D. Emin and C. F. Hart, "Phonon-assisted hopping of an electron on a Wannier-Stark ladder in a strong electric field," *Physical Review B*, vol. 36, no. 5, pp. 2530–2546, 1987.

[169] S. Rott, N. Linder, and G. Döhler, "Field dependence of the hopping drift velocity in semiconductor superlattices," *Physical Review B*, vol. 65, no. 19, pp. 1–12, 2002.

[170] L. Vidmar, J. Bonča, M. Mierzejewski, P. Prelovšek, and S. A. Trugman, "Nonequilibrium dynamics of the Holstein polaron driven by an external electric field," *Physical Review B*, vol. 83, p. 134301, apr 2011, 1012.1716.

[171] D. Golež, J. Bonča, L. Vidmar, and S. A. Trugman, "Relaxation Dynamics of the Holstein Polaron," *Physical Review Letters*, vol. 109, p. 236402, dec 2012, /arxiv.org/abs/1209.2586.

[172] A. K. C. Cheung and M. Berciu, "Phonon-assisted carrier motion on the Wannier-Stark ladder," *Physical Review B - Condensed Matter and Materials Physics*, vol. 88, no. 3, pp. 1–9, 2013, arXiv:1412.3202v1.

[173] J. Nocedal and S. Wright, *Numerical Optimization*. Springer Series in Operations Research and Financial Engineering, Springer New York, 2006.

[174] E. W. Weisstein, "Brachistochrone problem." MathWorld–A Wolfram Web Resource, http://mathworld.wolfram.com/BrachistochroneProblem.html.

[175] "NIST Digital Library of Mathematical Functions." http://dlmf.nist.gov/, Release 1.0.11 of 2016-06-08.

[176] N. Ashcroft and N. Mermin, *Solid State Physics*. HRW international editions, Holt, Rinehart and Winston, 1976.

[177] T. Dekorsy, R. Ott, H. Kurz, and K. Köhler, "Bloch oscillations at room temperature," *Phys. Rev. B*, vol. 51, no. 23, pp. 275–278, 1995.

[178] F. Shibata, Y. Takahashi, and N. Hashitsume, "A generalized stochastic liouville equation. Non-Markovian versus memoryless master equations," *Journal of Statistical Physics*, vol. 17, pp. 171–187, oct 1977.

[179] S. Chaturvedi and F. Shibata, "Time-convolutionless projection operator formalism for elimination of fast variables. Applications to Brownian motion," *Zeitschrift fr Physik B Condensed Matter and Quanta*, vol. 35, pp. 297–308, sep 1979.

[180] M. Tokuyama and H. Mori, "Statistical-Mechanical Theory of Random Frequency Modulations and Generalized Brownian Motions," *Progress of Theoretical Physics*, vol. 55, pp. 411–429, feb 1976.